GEOLOGICA ULTRAIECTINA

Mededelingen van het
Instituut voor Aardwetenschappen der
Rijksuniversiteit te Utrecht

No. 56

INTRACRYSTALLINE DEFORMATION AND SLATY CLEAVAGE DEVELOPMENT IN VERY LOW-GRADE SLATES FROM THE CENTRAL PYRENEES

ANTON-JAN BONS

GEOLOGICA ULTRAIECTINA

Mededelingen van het
Instituut voor Aardwetenschappen der
Rijksuniversiteit te Utrecht

No. 56

INTRACRYSTALLINE DEFORMATION AND SLATY CLEAVAGE DEVELOPMENT IN VERY LOW-GRADE SLATES FROM THE CENTRAL PYRENEES

ISBN 90-71577-09-0

INTRACRYSTALLINE DEFORMATION AND SLATY CLEAVAGE DEVELOPMENT IN VERY LOW-GRADE SLATES FROM THE CENTRAL PYRENEES

INTRAKRISTALLIJNE DEFORMATIE EN DE ONTWIKKELING VAN LEISPLIJTING IN ZEER LAAGGRADIGE LEISTEEN VAN DE CENTRALE PYRENEEËN

(Met een samenvatting in het Nederlands)

PROEFSCHRIFT

TER VERKRIJGING VAN DE GRAAD VAN DOCTOR
AAN DE RIJKSUNIVERSITEIT TE UTRECHT, OP GEZAG VAN
DE RECTOR MAGNIFICUS PROF. DR. J.A. VAN GINKEL,
VOLGENS BESLUIT VAN HET COLLEGE VAN DEKANEN
IN HET OPENBAAR TE VERDEDIGEN OP MAANDAG
21 NOVEMBER 1988 DES NAMIDDAGS TE 4.15 UUR

DOOR

ANTONIE JAN BONS

GEBOREN OP 8 JULI 1959 TE LEMSTERLAND

1988
OFFSETDRUKKERIJ HAVEKA B.V., ALBLASSERDAM

PROMOTOR: PROF. DR. H.J. ZWART
CO-PROMOTOR: DR. M.R. DRURY

CIP-GEGEVENS KONINKLIJKE BIBLIOTHEEK, DEN HAAG

Bons, Anton Jan

Intracrystalline deformation and slaty cleavage development in very low-grade slates from the central Pyrenees, Spain / Anton Jan Bons. - [Utrecht : Instituut voor Aardwetenschappen der Rijksuniversiteit Utrecht]. - (Geologica Ultraiectina ; no. 56)
Proefschrift Utrecht. - Met lit. opg. - Met samenvatting in het Nederlands.
ISBN 90-71577-09-0
SISO eu-span 565 UDC 552.52(234.12)(043.3)
Trefw.: Pyreneeën ; geologie.

aan Iris
en Laura

CONTENTS

VOORWOORD

Dit proefschrift is geheel anders geworden dan ik mij vier jaar geleden had voorgesteld. Mijn oorspronkelijke plan, een regionale studie naar de leisplijtingen in de Liguride Apennijnen, werd door mijn promotor Prof. Dr. H.J. Zwart bijgestuurd in de richting van meer fundamenteel onderzoek naar de ontwikkeling van leisplijting; ook was het zijn idee om daarvoor de leien van de Orri Dome te bestuderen met de electronenmicroscoop. Ik ben hem daar bijzonder dankbaar voor. Zijn leiding tijdens het onderzoek en bij het schrijven van het proefschrift was onmisbaar. Mijn co-promotor Dr. M.R. Drury wil ik bedanken voor zijn zeer concrete hulp bij het electronenmicroscopisch onderzoek en zijn gedetailleerde kritiek op verschillende versies van het manuscript. Martyn, thanks for everything!

Mijn paranymfen ben ik ook veel dank verschuldigd. Iris Steen, mijn vrouw, las steeds alle teksten voor ze de deur uitgingen en spoorde vele onlogische redeneringen vroegtijdig op. Vooral de laatste weken zat zij vaak tot diep in de nacht te corrigeren. Zonder haar praktische en morele steun had ik dit werk niet kunnen doen. Met Raymond Franssen, studievriend sinds mij eerste jaar, heb ik eindeloze diskussies gevoerd over geologie, het leven van een promovendus, en vele andere zaken. Zijn hulp in de laatste fase van het schrijven van het proefschrift was onmisbaar.

In de loop van mijn onderzoek heb ik vele zijstappen gedaan naar andere vakgebieden, en velen hebben mij daarbij geholpen. Arie Speksnijder introduceerde mij in de geologie van de Orri Dome. Het onderzoek naar de illietkristalliniteit heb ik kunnen doen dankzij de deskundige adviezen en praktische hulp van Prof. Dr. H.J. Kisch van de Ben Gurion University of the Negev (Beer-Sheva, Israel). Ton Zalm, Peter van Krieken en Marjan Reith hielpen bij de monsterpreparatie, Charl Laman deed het röntgendiffractiewerk. Het geochemische zeldzame-aarden onderzoek deed ik samen met Gert-Jan de Haas, Marc Hollanders en Simon Vriend, die zelf nog naar de Pyreneeën zijn gegaan om nieuwe monsters te halen; Ben Jansen gaf deskundige adviezen. Boorkernen van Noordzee-sedimenten, die ik als referentiemateriaal gebruikte voor de illietkristalliniteit en voor het microstructurele onderzoek, kreeg ik van

de British Petroleum Exploratie Maatschappij Nederland B.V. en van Mobil Producing Netherlands Inc.

Joop Pieters van de vakgroep Moleculaire Celbiologie van de Rijksuniversiteit Utrecht leerde mij de electronenmicroscopen, zowel TEM als SEM, te bedienen. Bij de electronenmicroscopie heb ik verder veel hulp gehad van Herman van Roermund. Het weloverwogen commentaar en de opbouwende kritiek van Prof. Dr. P. Hartman hebben mij veel geholpen. De chlorieten uit het Traversella-gebied kreeg ik van Dr. R.J. Felius, met wie ik ook vele leerzame gesprekken heb gevoerd over phyllosilicaten. De microanalyse op SEM en microprobe had ik niet kunnen doen zonder de hulp van René Poorter, Manfred van Bergen en Pieter Kleingeld. Het HRTEM onderzoek heb ik gedaan in samenwerking met Nick Schryvers, Prof. Dr. J. van Landuyt, Wim Coene (allen verbonden aan het Rijksuniversitair Centrum te Antwerpen) en Cees Woensdregt.

Hans Schiet deed een groot deel van het fotowerk en maakte de figuren en foto's offsetgereed.

De vakgroep Structurele en Toegepaste Geologie (thans opgenomen in de Vakgroep Geologie) financierde het grootste deel van het onderzoek. De JEM-200C TEM en de JXA-8600 microprobe zijn gefinancierd door de Nederlandse Organisatie voor Wetenschappelijk Onderzoek (N.W.O.). De faciliteiten op de 1MV HVTEM in Apeldoorn werden ter beschikking gesteld door de Stichting Geavanceerde Metaalkunde, de bijkomende kosten werden deels betaald uit een gift van Mobil Producing Netherlands Inc.

Ik wil alle personen en instanties die hebben bijgedragen aan dit werk van harte bedanken.

Anton-Jan Bons
september 1988

SAMENVATTING

In dit proefschrift worden de resultaten gepresenteerd van een studie naar de rol van intrakristallijne deformatie (de vervorming van het kristalrooster in de korrels) van phyllosilicaten in de ontwikkeling van leisplijting. Het eerste hoofdstuk vat de probleemstelling samen. Leisplijting wordt al meer dan 150 jaar bestudeerd en er is reeds veel bekend omtrent de processen die de splijting vormen. Hoewel vele auteurs hebben aangetoond dat tijdens de ontwikkeling van de leisplijting belangrijke intrakristallijne deformatie plaatsvindt, concentreren de meeste studies zich op andere processen. De laatste tijd zijn er technieken ontwikkeld, zoals transmissie electronen microscopie (TEM), die bijzonder geschikt zijn om intrakristallijne deformatie verschijnselen te bestuderen. In deze studie wordt TEM gebruikt om deze verschijnselen te bestuderen in leistenen uit de Cambro-Ordovicische Seo-Formatie van de Orri Dome en omgeving, Centrale Pyreneeën, Spanje.

Het tweede hoofdstuk geeft een overzicht van eerdere onderzoeken naar de ontwikkeling van leisplijting. Leisplijting is het gevolg van afplatting van het gesteente loodrecht op de splijtvlakken; zij wordt gewoonlijk gevormd na verharding van het sediment. De belangrijkste stappen in de ontwikkeling van leisplijting zijn: (1) korte, onderbroken, onregelmatige splijtvlakjes (*rough cleavage*), (2) gespatieerde splijting met of zonder microplooien tussen de splijtvlakken (*crenulation/disjunctive cleavage*), en (3) continue splijting, d.w.z. alle korrels zijn evenwijdig aan de splijting gerangschikt (*continuous cleavage*). De belangrijkste processen bij de vorming van splijting zijn: (1) mechanische rotatie van bestaande korrels, (2) drukoplossing, (3) microplooiing van een bestaande foliatie, (4) korrelgroei en rekristallisatie en (5) intrakristallijne deformatie.

De geologie van de Orri Dome wordt samengevat in hoofdstuk drie. Tijdens minstens twee gebergtevormingen (Varistisch en Alpien) hebben vele deformatiefasen plaatsgevonden, waarbij verschillende splijtingen zijn gevormd. Gelukkig is de geologie van de Orri Dome goed bekend en kunnen er gebieden worden geselecteerd die geschikt zijn voor het onderzoek van de leisplijting.

Omdat de graad van metamorfose van de Seo Formatie tot nu toe nog niet in detail bestudeerd was, wordt dit onderwerp in hoofstuk vier behandeld. Zowel mineraalparagenese als illietkristalliniteit wijzen erop dat de leistenen van de Seo Formatie gemetamorfoseerd zijn in het hooggradige deel van de anchizone. In de aangrenzende Massana Anticline en het Pallaresa Anticlinorium heeft lagere groenschist-metamorfose plaatsgevonden.

In vele monsters zijn poikiloblastische monazietporfyroblasten gevonden, varirend in grootte van 10 tot 400 μm. De porfyroblasten zijn gegroeid tijdens een hydrothermale metamorfose die plaatsvond vóór de belangrijkste Varistische deformatiefase. De Seo Formatie in de Massana Anticline bevat allanietporfyroblasten rijk aan zeldzame aarden, in plaats van monaziet. Voor de metamorfose van de zeldzame-aarden-mineralen wordt het volgende model voorgesteld: tijdens de hydrothermale metamorfose in de anchizone worden de monazietporfyroblasten gevormd. Bij voortschrijdende metamorfose worden de monazieten weer afgebroken en in de lagere groenschistfacies worden allaniet-profyroblasten gevormd rijk aan zeldzame aarden.

De microstructuur van de leisplijting wordt beschreven in hoofdstuk vijf. In de Orri Dome is de leisplijting een anastomoserende *zonal disjunctive cleavage* met een gemiddelde spatiëring van 20 μm. Een ouder sedimentair maaksel is plaatselijk bewaard gebleven. De fyllieten van het Pallaresa Anticlinorium vertonen een continue splijting.

De ontwikkeling van de leispleiting in de Seo Formatie wordt als volgt voorgesteld. Bij kleine vervormingen ontwikkelt zich een *rough cleavage*; de splijtingsdomeinen beginnen te groeien aan de randen van korrels. De domeinen groeien vervolgens in lengte en breedte door rotatie en buiging van bestaande korrels, en door nieuwgroei en rekristallisatie. Het oudere maaksel in de microlithons wordt geleidelijk afgebroken door het verwijderen van materiaal (drukoplossing), reori ntatie van korrels, korrelgoei en rekristallisatie. In de lagere groenschistfaciës worden de laatste resten van de microlithons vernietigd door de groei van de korrels in de splijtingsdomeinen.

Hoofdstuk zes beschrijft het TEM onderzoek aan de intrakristallijne deformatie van chloriet en muscoviet tijdens de ontwikkeling van de leisplijting. Een hoog oplossend vermogen TEM onderzoek aan de chlorieten heeft verschillende onregelmatigheden in

de stapeling van de kristallagen aangetoond, zoals: (1) verschuivingen van de lagen ten opzichte van elkaar; de verschuivingen kunnen optreden in de bruciet-laag, maar ook binnen de 2:1-laag; (2) tussengeschakelde lagen met een talk- structuur; en (3) lagen met een 1:1 phyllosilicaatstructuur. De vervorming van chloriet tijdens splijtingsontwikkeling gaat gepaard met polygonisatie: het kristal wordt opgedeeld in cellen met grenzen ongeveer loodrecht en ongeveer evenwijdig aan de (001) vlakken. Plastische vervorming van chloriet is mogelijk door een combinatie van het glijden van dislocaties langs het (001) vlak, klimmen van [00w] dislocaties en lokaal geactiveerd glijden van [00*w*] dislocaties langs (*hk*0) vlakken. Er zijn enige aanwijzingen gevonden dat polygonizatie ook optreedt in muscoviet, maar korrelgrensmigratie domineert de vervorming van muscoviet.

Op korrelgrenzen in kwarts zijn aanwijzingen gevonden een vloeibare fase aanwezig is geweest; grensvlakken in de phyllosilicaten tonen zulke resten niet. De struktuur van de semi-coherente korrelgrenzen in de phyllosilicaten suggereert dat diffusie door het kristal belangrijk kan zijn geweest tijdens splijtingsontwikkeling, omdat de diffusiesnelheden zeer groot waren door de aanwezigheid van dislocaties.

In hoofdstuk zeven wordt de samenhang tussen de verschillende mechanismen die verantwoordelijk zijn voor de ontwikkeling van de leisplijting besproken. Drukoplossing en plastische vervorming zijn de belangrijkste processen die het gesteente vervormen. Deze processen leiden ook tot de vorming van het nieuwe maaksel, samen met rotatie en rekristallisatie. Het nieuwe maaksel benvloedt op zijn beurt weer de vervormingsmechanismen. Intrakristallijne deformatie speelt een essentiële rol in de vroege stadia van de splijtings-ontwikkeling. In latere stadia, wanneer de meeste phyllosilicaten een stabiele oriëntatie hebben evenwijdig aan de splijting, neemt de rol van intrakristallijne deformatie af, en worden drukoplossing en rekristallisatie belangrijker.

ABSTRACT

This thesis presents the results of a study on the role of intracrystalline deformation of phyllosilicates during slaty cleavage development. Chapter one gives an introduction to the problem being investigated. Slaty cleavage has been studied for over 150 years, and much is already known about the cleavage forming processes. Although many authors have shown that significant intracrystalline deformation of phyllosilicates occurs during cleavage development, most studies have concentrated on other processes. Recently new techniques have become available, like transmission electron microscopy (TEM), which are particularly suited for the study of intracrystalline deformation phenomena. In the present study TEM has been used to study these phenomena in Cambro-Ordovician slates from the Central Pyrenees, Spain.

Chapter two reviews previous research into slaty cleavage development. Slaty cleavage is the product of flattening perpendicular to the cleavage planes, and it is usually formed after lithification of the sediment. The main steps in the development of slaty cleavage are: (1) rough cleavage; (2) disjunctive or crenulation cleavage; (3) truly continuous cleavage. The main cleavage forming processes are: (1) mechanical rotation of existing grains; (2) pressure solution; (3) microfolding of an existing foliation; (4) recrystallisation and (5) intracrystalline deformation.

The geology of the Orri Dome is summarized in chapter three. During at least two orogenies (Variscan and Alpine) many deformational events have ocurred. Fortunately the geology of the Orri Dome is well documented in the literature, and suitable areas for microstructural investigations of the mainphase cleavage can be selected.

Because the metamorphic grade of the Seo Slates had not yet been studied in detail, this subject is treated in chapter four. Both mineral paragenesis and illite crystallinity measurements indicate that the slates of the Seo Formation in the Orri Dome have been metamorphosed in the high- grade part of the anchizone. In the Massana Anticline and the Pallaresa Anticlinorium lower greenschist facies metamorphism has occurred.

Poikiloblastic monazite porphyroblasts were encountered in most of the samples, varying in size from 10 to 400 μm. The porphyroblasts grew early in the metamorphic history, during a hydrothermal metamorphic event that predates the Variscan mainphase deformation in the Orri Dome. The Seo Formation in the Massana Anticline shows no monazite, but contains REE-rich allanite porphyroblasts. The following model is proposed for the metamorphic evolution of REE minerals in the Seo Formation: During a hydrothermal metamorphic event in the anchizone monazite porphyroblasts were formed. With prograde metamorphism the monazites break down and REE-rich allanite porphyroblasts ar formed in the lower greenschist facies.

The microstructure of the slaty cleavage is described in chapter five. In the Orri Dome it is an anastomosing zonal disjunctive cleavage with a spacing of 10-40 μm. A pre-cleavage bedding fabric is preserved locally. The phyllites of the Pallaresa Anticlinorium have a continuous cleavage *s.s.*

The development of the slaty cleavage in the Seo Formation is envisaged as follows. At low strains a rough cleavage is developed; cleavage domains nucleate at the edges of grains. The cleavage domains grow in length and in width by rotation and bending of existing grains and by recrystallisation. The pre-cleavage fabric in the microlithons is gradually destroyed by removal of material (pressure solution), rotation of grains, bending, folding, kinking and recrystallisation. In the lower greenschist facies the last remnants of the microlithons are removed by growth of the cleavage grains.

Chapter six reports the transmission electron microscope study into the intracrystalline deformation of chlorite and muscovite during cleavage development. A HRTEM study of chlorite has revealed several stacking irregularities which are already present before deformation. These irregularities include (1) semi-random stacking of the chlorite layers, associated with shifts of the layers parallel to (001) which occur both at the brucite sheet and inside the 2:1 layer, (2) intercalations with a talc structure, and (3) intercalations of 1:1 phyllosilicate. Deformation of chlorite during cleavage development is associated with polygonization. The crystal is divided into subgrains with boundaries subnormal and subvertical to (001). Chlorite can deform

plastically by a combination of basal slip, climb of [00w] dislocations and locally activated non-basal slip of [00w] dislocations. Some evidence of rotation recrystallisation has been observed in muscovite, but recrystallisation dominates during the deformation of muscovite.

Grain boundaries in quartz show indications that a fluid phase has been present; no such remnants have been preserved on the phyllosilicate interfaces. The structure of semi-coherent grain boundaries in phyllosilicates suggest that dislocation enhanced solid-state diffusion may have been significant during cleavage development.

In chapter seven the interaction between various cleavage forming mechanisms is discussed. Pressure solution and plastic deformation are the main processes in the deformation of the rock. They also lead to the formation of the new fabric, together with rotation processes and recrystallisation. The new fabric in turn influences the deformation mechanisms. Intracrystalline deformation plays an essential role in the early stages of cleavage development. In later stages, when most of the phyllosilicates have a stable orientation parallel to the cleavage, its role diminishes, and pressure solution and recrystallisation become increasingly important.

LIST OF ABBREVIATIONS

ab	albite
AEM	Analytical Electron Microscopy
b	Burgers vector
BF	Bright Field
BSE	Back-Scattered Electrons
CD	Cleavage Domain
chl, chlor	Chlorite
DF	Dark Field
EDS	Energy Dispersive Spectrometer
ep	Epidote
g	reciprocal lattice vector of operating reflection
HRTEM	High-Resolution Transmission Electron Microscope
HVTEM	High-Voltage Transmission Electron Microscope
IC	Illite Crystallinity
ML	Microlithon
mu, musc	Muscovite
SE	Secondary Electrons
SEM	Scanning Electron Microscope
TEM	Transmission Electron Microscope
q	Quartz
WB	Weak Beam

Chapter 1
INTRODUCTION

Geologists have studied slates and slaty cleavage ever since the beginning of the nineteenth century. It was soon understood that slaty cleavage is not an original feature of the rock, but that it has been formed after deposition of the sediment (e.g. Bakewell, 1815, see Siddans, 1972). At the end of the nineteenth century the main processes of cleavage formation, as well as the relationships between cleavage and strain, and cleavage and folds, had been recognised (e.g. Sorby, 1853; Harker, 1886). During the last 100 years the discussion on slaty cleavage has concentrated on a few issues, such as the exact orientation of cleavage with respect to stress and strain, the timing of cleavage formation, and the main cleavage forming processes (see Chapter 2). It became clear that slaty cleavage is the product of a complex interaction of several processes. Recent research on cleavage formation has concentrated on describing the contribution of one or more processes to cleavage formation, without trying to attribute cleavage formation to one single process (e.g. Wood 1974; Williams, 1977; Engelder and Marshak, 1985).

Many studies have shown that significant intracrystalline deformation of phyllosilicates, particularly chlorite, occurs during cleavage development (e.g Van der Pluijm and Kaars-Sijpesteijn, 1984; Dimberline, 1986; Gregg, 1986). However, most studies have concentrated on the role of rigid body rotation, mass transfer processes (Engelder and Marshak, 1985) and the growth of new phyllosilicates (Lee et al., 1986). As intracrystalline deformation is involved both in rotation processes and in the development and growth of new grains it is important that its role in cleavage development is assessed.

In addition, little is known about the plastic deformation processes in phyllosilicates in general, and of chlorite in particular. Plastic deformation of micas has been investigated by a number of authors (e.g. Etheridge et al., 1973; Wilson and Bell, 1979; Bell and Wilson, 1981; Bell et al., 1986), but there is no detailed study available on the deformation of chlorite. It is important to establish the deformation processes of chlorite, as these will influence the rheology of chlorite bearing rocks such as slates, chlorite schists, chloritized ultramafic

rocks, and shearzones in mantle peridotites (Miller, 1988; Drury et al., 1988).

In the last twenty years new techniques from metallurgy and materials science have been applied to the study of natural rocks. One of these techniques is transmission electron microscopy. The transmission electron microscope (TEM) is a very versatile instrument: its high resolution allows very high magnifications, and thus it can be used as an extension of light microscopy. The X-rays, generated in the specimen by the electron beam, can be used for microchemical analyses. Electron diffraction provides detailed information about the crystal structure and crystal defects. The first two techniques have been applied to slaty cleavage by previous authors: Knipe and White (1977) and White and Knipe (1978) investigated the cleavage microstructure on a very small scale (< 1 μm), while Knipe (1979, 1981) studied small-scale chemical variations. The third technique, the imaging of crystal defects by the means of electron diffraction contrast, is particularly useful to study intracrystalline deformation phenomena, but has not yet been applied to slaty cleavage. Therefore a TEM study on slaty cleavage is needed, which uses electron diffraction contrast techniques. This can give information about the deformation mechanisms of the components of slates (mainly phyllosilicates) and about the role of intracrystalline deformation in the development of slaty cleavage.

The present study aims to describe the role of intracrystalline deformation during slaty cleavage development in the Seo Formation of the Orri Dome, central Pyrenees, Spain (see Fig. 3.2), with special emphasis on the deformation mechanisms in chlorite, based on a detailed TEM study. The slates of the Seo Formation of the Orri Dome have been selected for a number of reasons:

- the geology of the Orri Dome is known in great detail (Hartevelt, 1970; Speksnijder, 1986, 1987a,b);
- the Seo Formation has a very homogeneous lithology and a very simple mineralogy (muscovite + chlorite + quartz + albite);
- areas can be selected where the slaty cleavage is the only deformation structure of the rocks;
- the Orri Dome shows an intermediate stage of slaty cleavage development, the end member can be found in the adjoining Pallaresa Anticlinorium;
- various stages in the development of slaty cleavage as a function of strain

can be studied in a small volume of rock (<1 mm^3) due to the presence of strain shadows around pre- kinematic porphyroblasts and other rigid objects;
- signs of intracrystalline deformation related to the slaty cleavage microstructure are obvious.

This thesis is divided broadly into four parts. The first part gives an introduction into slaty cleavage in general (chapter 2). The second part describes the rocks which were used for this study. It gives an overview of the geologic setting (chapter 3) and of the conditions under which the rocks were deformed (chapter 4). The third part describes the slaty cleavage in detail (chapter 5) and includes the TEM study on intracrystalline deformation of the phyllosilicates (chapter 6). In the final part (chapter 7) the role of intracrystalline deformation during slaty cleavage formation in general is discussed.

Chapter 2
SLATY CLEAVAGE: A REVIEW

2.1 CLEAVAGE MORPHOLOGY

2.1.1 Terminology

Slates and slaty cleavage have been studied for over 150 years. During these years a complex and often contradictory and confusing terminology has developed. Many authors introduced their own terminology independently of others, or misused an existing terminology. Powell (1979) clearly showed the necessity of a new consistent terminology, which uses morphological terms only and avoids all references to cleavage forming processes. He proposed a morphological classification of rock cleavage based on geometrical parameters such as cleavage spacing, shape and width of cleavage planes, etc. (Powell, 1979). This classification, which was elaborated in Borradaile et al. (1982), is summarised in Fig. 2.1.

An important element in Powell's classification is the *fabric element.* Fabric elements are those parts of a rock which contribute to the fabric, e.g. elongated grains, microfractures or films of opaque material. A subdivision is made, based on the spatial distribution of fabric elements in the rock. If there are domains rich in fabric elements *(cleavage lamellae)* and domains poor in fabric elements *(microlithons)* the fabric is called a *spaced cleavage.* If no microlithons are visible, one speaks of a *continuous cleavage.* The spaced cleavages are divided into cleavages which are systematically related to microfolds in the microlithons *(crenulation cleavages)* and cleavages which show no systematic microfolds in the microlithons *(disjunctive cleavages).* Further description of the cleavage is based on the shape and width of the cleavage lamellae, etc. (see Fig. 2.1). In the case that no microlithons are visible (continuous cleavage), there are two possibilities: *Continuous cleavage, sense (1)*: the rock is too fine-grained to see the individual fabric elements at the present scale of observation, and it is possible that microlithons would be visible at a higher magnification; and *continuous cleavage, sense (2)*: the individual fabric elements are resolved at the present scale of observation and the fabric is truly continuous.

FIGURE 2.1. Morphological classification of rocks cleavage, after Powell (1979) and Borradaile et al. (1982). a. Main cleavage types

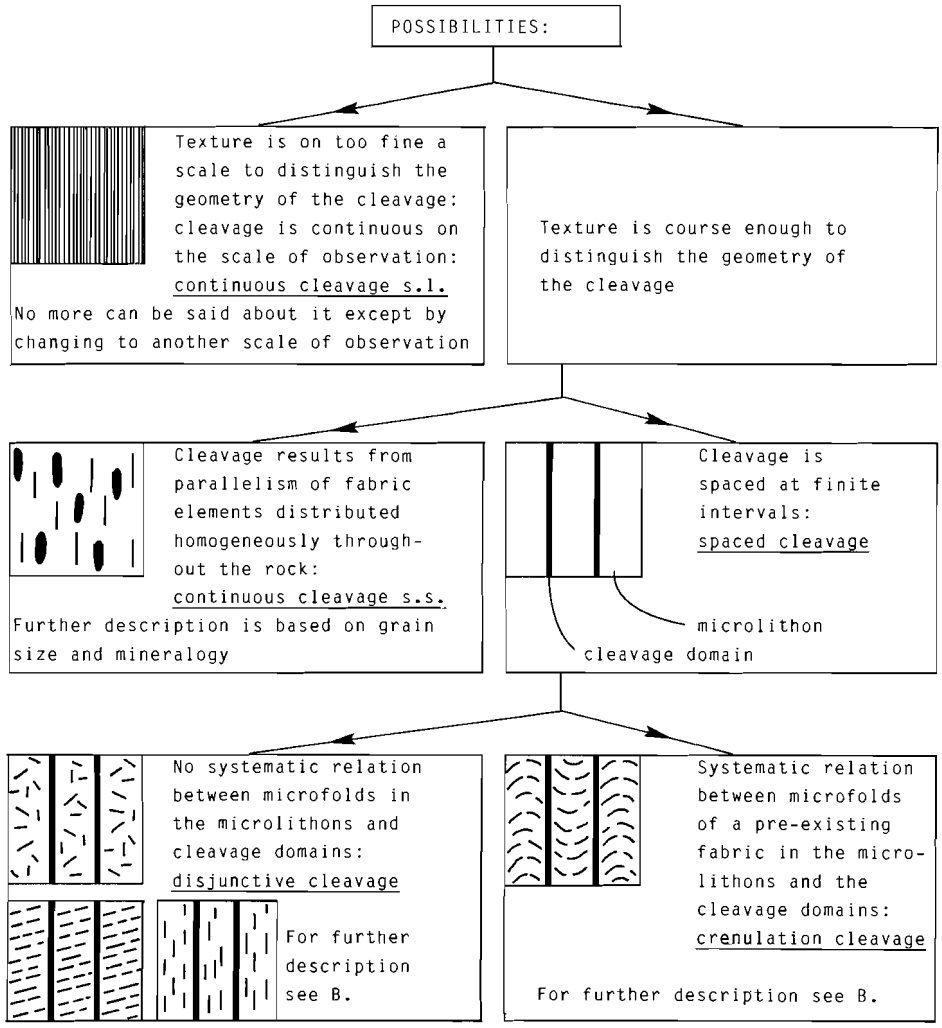

FIGURE 2.1 (continued) b. Description of spaced cleavages

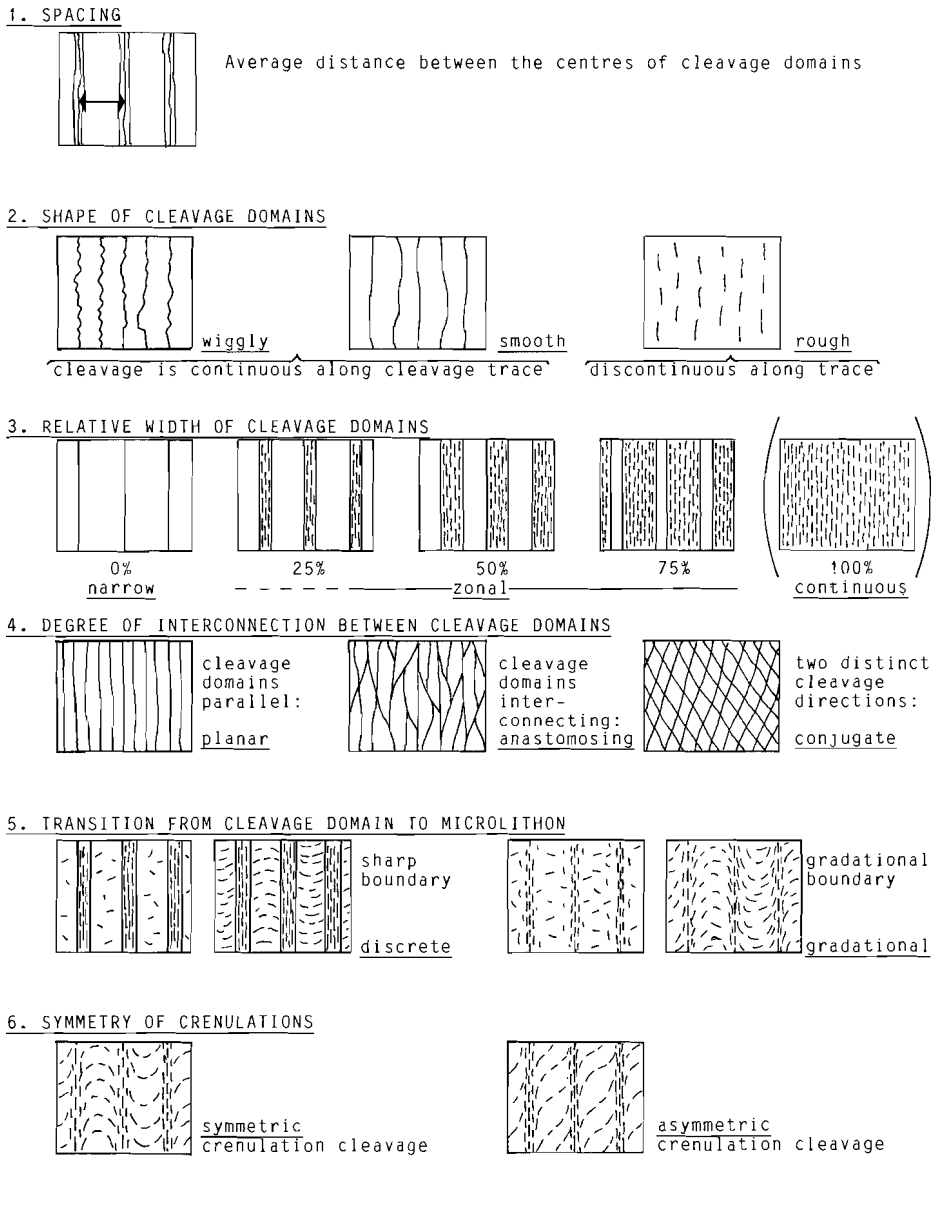

One drawback of Powell's classification is that rock cleavage itself is defined as a secondary structure (Powell, 1979, p.33; Borredaile et al., 1982, p. 6), which is in conflict with the original aim of avoiding genetic implications. Another problem is the confusion caused by the dual meaning of "continuous cleavage", depending on the scale of observation. Although it is clear that this system is not perfect, it is by far the best available in the view of the present author, and therefore it will be used in this thesis. One slight modification is the use of the term "continuous cleavage *sensu strictu (s.s.)*" instead of "continuous cleavage, sense (2)", and "continuous cleavage *sensu lato (s.l.)*" instead of "continuous cleavage, sense (1)".

The term "slaty cleavage" is used here as a field term for a continuous fabric *s.l.*, where the fabric elements can not be distinguished with the naked eye or with a hand lens (grainsize smaller than ca. 100 μm). When the fabric elements (e.g. mica flakes) are large enough to be seen by the naked eye (on the order of 1 mm) the rock is called a *schist*; the term *phyllite* is used for rocks with grain size characteristics intermediate between those of slates and schists (Ramsay and Huber, 1983).

2.1.2 Slaty cleavage microstructure

Slaty cleavage, in the sense of a continuous fabric at the scale of the naked eye or the hand lens, appears to have a wide range of microstructures at a microscopic or sub-microscopic scale. Many slaty cleavages which appear to be continuous even at high magnifications in the optical microscope, are shown to be spaced cleavages by electron microscope observations, either crenulation cleavages (Knipe and White, 1977; Weber, 1976, 1981) or disjunctive cleavages (e.g. Lee et al., 1986). In this context the distinction between continuous cleavage *s.l.* and *s.s.*, which might seem futile at first sight, is very useful.

Many well developed slates show a truly continuous fabric, formed by a preferred orientation of phyllosilicates and elongated quartz grains (e.g. Hobbs et al., 1976, fig 5.8b; Le Corre, 1979, fig. 2D). Due to the relation between crystal shape and crystal axes in phyllosilicates, there is a very strong crystallographic preferred orientation of the phyllosilicicates. However, there is usually no detectable crystallographic quartz fabric, despite the strong shape fabric (Siddans, 1980).

When observed in a powerful optical microscope, or in an electron microscope, many slaty cleavages appear to be spaced (e.g. Knipe and White, 1977; White and Knipe, 1978; Weber, 1976, 1981; Lee et al. 1986; Southwick, 1987). The main groups of spaced slaty cleavage microstructures described in the literature are:
1) *crenulation cleavage.* At high magnifications systematic microfolds are visible in the microlithons (Knipe and White, 1977; Weber, 1976, 1981).
2) *disjunctive cleavage.* Many slates show microlithons without systematic crenulations. Very often the phyllosilicates inside the microlithons are folded (e.g. White and Knipe, 1978) but the folds are too chaotic for the fabric to be called a crenulation cleavage. Sometimes there is no trace of deformation inside the microlithons (Lee et al., 1986). Usually the cleavage domains are not straight and parallel, but more or less sinuous, or the cleavage lamellae are anastomosing or reticulate, a fabric that has previously been termed a "domainal slaty cleavage" (e.g. Woodland, 1982).

Many authors have decribed a mineralogical difference between cleavage domains and microlithons: the cleavage domains consist almost entirely of phyllosilicates, while the microlithons contain some quartz and feldspar (e.g. Williams, 1972; Southwick, 1987). Some authors have incorporated this mineralogical difference in their terminology: P-domains for the phyllosilicate-rich cleavage domains, and Q-domains for the quartz-rich microlithons (Knipe, 1981; Waldron and Sandiford, 1988).

2.2 SLATY CLEAVAGE DEVELOPMENT

2.2.1 Introduction

More than one and a half century of research on slaty cleavage development has resulted in a vast amount of literature. Fortunately, some good reviews are available (Siddans, 1972; Wood, 1974; Williams, 1977), while Engelder and Marshak (1985) give an overview of some recent developments. Therefore, this section will only describe the main trends and achievements of research on slaty cleavage; for detailed information the reader is referred to the literature.

As early as the beginning of the nineteenth century it became clear that slaty cleavage was formed by a preferred orientation of crystals,

which developed after deposition of the sediment (Bakewell, 1815, see Siddans, 1972). Sorby suggested that slaty cleavage developed by re-alignment of the platy grains in a plane perpendicular to the direction of compression (Sorby, 1853). Sharpe (1846) had already mentioned recrystallisation as a possible cleavage forming process. By the end of the nineteenth century, the relationship between slaty cleavage and flattening was well established, and the geometrical relation to folds had been demonstrated (see Siddans, 1972, for references). The cleavage forming processes known at that time (e.g. Sorby, 1879, see Ramsay and Huber, 1983) were:

- mechanical re-orientation of detrital grains and of grains formed during metamorphic reactions
- preferred growth of new minerals in orientations controlled by the stress field or by an anisotropy in the rock caused by the deformation
- plastic flow of individual grains
- pressure solution.

Subsequent research mainly concerned the relative importance of these processes, or added detailed knowledge about one of the processes (Siddans, 1972; Ramsay and Huber, 1983).

2.2.2 The relation between cleavage and strain

Many authors have studied the relation between cleavage and strain in slates. In first instance only well developed slates were analysed, in order to answer the question whether or not slaty cleavage is exactly parallel to the XY-principal plane of the finite strain ellipsoid. During the last decades the emphasis has shifted towards the relationship between regional strain gradients and fabric development (e.g. Siddans, 1979, 1980).

The idea that cleavage forms along planes of high shearing strain was first stated by Laugel (1855). Harker (1885) showed that this was totally incompatible with the observed strain states in slates. In a simple-shear model the XY-plane of the finite strain ellipsoid is always inclined to the shear plane, while circular markers on the shear plane remain circular. This was in contradiction with numerous strain analyses, which had shown that slaty cleavage is always parallel to the XY-plane of the finite strain ellipsoid, and also that there was a component of

deformation in the shear plane (e.g. Sorby, 1853). Nevertheless, the concept of "shear-of-cleavage folding" was followed by a number of authors (e.g. Becker, 1896; Wunderlich, 1959; Voll, 1960).

The controversy between those who believe cleavage to be a shearing phenomenon and those who believe it to be the result of flattening led to a large number of strain analyses in slates (see Wood, 1974, for references). The vast amount of evidence led Wood to state that slaty cleavage develops *exactly* parallel to the XY-plane of the finite strain ellipsoid (Wood, 1974, p. 398). However, some shearing along cleavage planes cannot always be excluded (Hills, 1945; Naha and Ray, 1972; Hobbs et al. 1976). In the course of the deformation history the cleavage plane may have been inclined to the XY-plane of the incremental strain ellipsoid, and some shear along the cleavage planes may have occurred. Progressive deformation would rotate the cleavage plane towards the XY-plane of the finite strain ellipsoid, and the resulting angle between cleavage and XY-plane may be only a few degrees (Ghosh, 1982). Therefore, it is perhaps better to state that slaty cleavage is generally parallel to the XY-plane of the finite strain ellipsoid *within the accuracy of measurement* (Williams, 1977).

Figure 2.2 shows a summary of over 5000 strain analyses of cleaved Cambro-Ordovician slates (Wood, 1974). It is clear that all slates fall in the flattening field. The shortening perpendicular to the cleavage ranges from 50% to 80% and averages about 70% (assuming no significant volume loss); the mean finite strain ellipsoid of slates with a well-defined cleavage has the form 1.76/1/0.24 (Wood, 1974).

Strain states in intermediate stages of cleavage development have been analysed by various authors (Siddans, 1977, 1979, 1980; Kligfield et al, 1981; Reks and Gray, 1982). In general it seems that the first signs of a secondary fabric become visible as a pencil cleavage at a shortening of 10-20% (Reks and Gray, 1982; Ramsay and Huber, 1983), while at 25-35% shortening the cleavage becomes the main anisotropy of the rock (Cloos, 1947; Reks and Gray, 1982). Most good-quality roofing slates have undergone more than 70% flattening (Wood, 1974).

Several authors have studied the relationship between regional strain gradients and cleavage intensity, using either reduction spots (Siddans, 1977, 1979, 1980; Kligfield et al., 1981) or lapilli tuffs (Bell, 1985) as strain markers. Most tectonically unaffected shales have been compacted normal to the bedding, and originally spherical strain

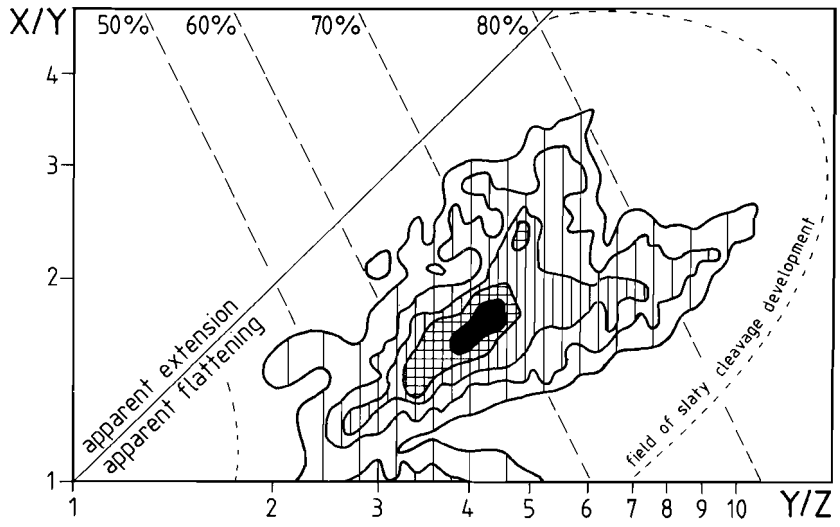

FIGURE 2.2. Contoured logarithmic deformation plot of the strain states of 5200 slates. Contours at 0.5, 1, 2, 3 and 5% of 1% area of "field of slaty cleavage development". Apparent shortening percentages perpendicular to the cleavage, assuming constant volume, are also given (After Wood, 1974).

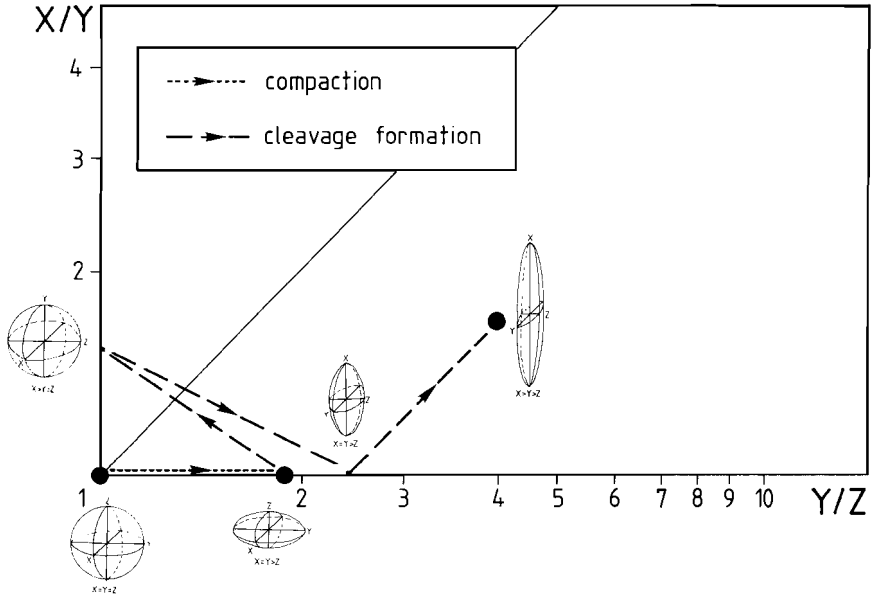

FIGURE 2.3. Logarithmic deformation plot, showing various strain states during the deformation of shales into slates.

markers have an oblate shape parallel to bedding. With increasing cleavage intensity the strain markers can change to prolate, after which the principal axes X and Z switch orientation and the shape changes into oblate again, this time parallel to the cleavage (Siddans, 1980; Bell, 1985). This complex strain path during compaction and cleavage development is sketched in Fig. 2.3. The actual strain path is influenced by the angle between cleavage and bedding, and by the amount of volume loss (Bell, 1985).

Slaty cleavage development usually involves some loss of volume. Estimation of the amount is very difficult, and reported values range from <10% to >50% (e.g. Wood, 1974; Bell, 1985; Engelder & Marshak, 1985; Boulter, 1986). One method to estimate the amount of volume loss is based on the comparison of the specific gravities of deformed and undeformed rocks. Volume reduction can arise from the reduction of the porosity of the rock, expelling the pore fluids, or from dehydration of clay minerals. These two processes lead to an increase in specific gravity of the rock, from 1.9-2.0 g/cm^3 for unconsolidated shales to 2.7-2.85 g/cm^3 for well-developed slates, corresponding to ca. 30% volume loss (Wood, 1974). However, most cleavages have developed after lithification (Wood, 1974; Ramsay and Huber, 1983; Engelder and Marshak, 1985; this study), and therefore specific gravity is not a reliable indicator for the volume changes which are due to the development of cleavage.

Another process which leads to a reduction of volume is the removal of solid material from the local rock system, by dissolution or other differentiation processes. Usually there is a selective removal of one or more phases, e.g. quartz is removed by pressure solution, while opaque minerals are insoluble. The relative concentration of the mobile and immobile phases can be used as a measure for the change in volume (Gratier, 1983; see section 5.3.5). This approach leads to estimated volume losses up to 50% (Gratier, 1983).

Bell (1985) tried to explain the wide range of shape factors he found in deformed lapilli in terms of a superposition of plane strain and volume loss. The best fit to the observed strain states was achieved by a model which involves compaction, followed by pure volume loss (up to 40%) during the initial stage of cleavage development, while further deformation is pure plane strain. Boulter (1986) argues that the wide range in shapes could also be explained by a model of plane strain

associated with moderate volume loss (<20%) superimposed on variable compaction strains.

2.2.3 Geometric relationship between cleavage and folds

In most cases cleavage shows a simple geometrical relationship with the axial surfaces of folds. The cleavage planes are often not exactly parallel to the axial surface, but form a cleavage fan (Fig. 2.4 a); nevertheless, the line of intersection between the folded plane and the cleavage (δ-lineation) is usually parallel to the fold axis, and the

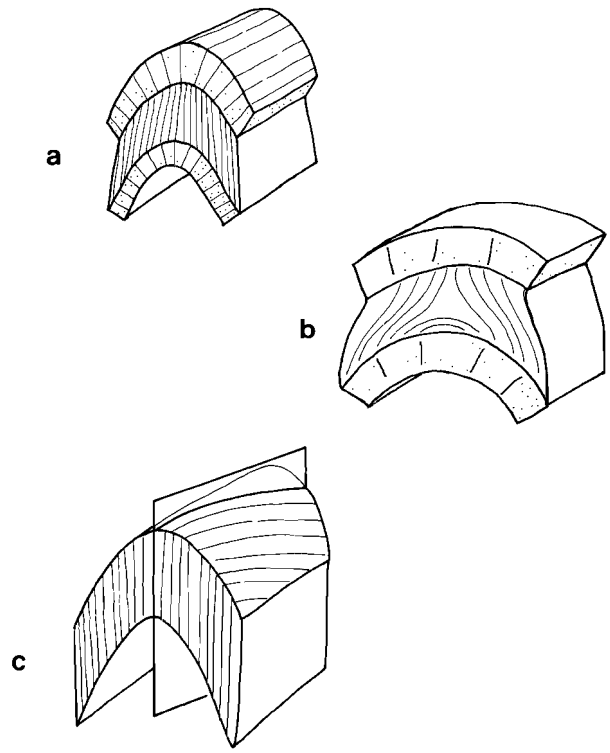

FIGURE 2.4. Geometric relation between cleavage and folds: a. axial plane cleavage, showing refraction, normal fanning and reversed fanning; b. arcuate hinge cleavage in the outer arc of a folded competent layer; c. transected fold.

cleavage plane cuts a folded plane only once. Cleavages which show this systematic relationship to folds are called *axial plane cleavages* (e.g. Hobbs et al, 1976; Williams, 1977).

The angle between the axial plane cleavage and the axial surface may change through a fold. *Divergent* cleavage fans are characteristic for the more competent layers in a folded sequence, while*convergent* fans are found in the less competent layers (Fig. 2.4 a). At the interface between a competent and an incompetent layer, the orientation of the cleavage changes, a phenomenon called cleavage *refraction*. The variations in cleavage orientation can be explained by variations in shape and orientation of the finite strain ellipsoid; this has been supported by theory and experiment (e.g. Ramsay, 1967; Hobbs et al., 1976; Ramsay and Huber, 1983, 1987). However, there are many examples of non-axial plane cleavages, some of which will be discussed below.

Many pelitic rocks show a fabric parallel to the sedimentary layering. Very often it is clear that this fabric is related to the bedding only and not to any tectonic deformation, and it may be explained in terms of sedimentary and diagenetic processes. The fabric develops first from the stable hydrodynamic orientation of platy minerals (Heling, 1970), and secondly by compaction of the sediment perpendicular to bedding (Heling, 1970; O'Brien, 1970). Such a fabric is often called a *fissility* (e.g. Ramsay and Huber, 1983).

Not all bedding-parallel fabrics are clearly unrelated to tectonic deformation. Some are only locally parallel to the bedding, e.g. the arcuate hinge cleavages described below. Others are exactly parallel to bedding, but are interpreted as tectonic foliations (e.g. Holst, 1985). Such folations are clearly secondary foliations and are called *cleavages* in Powell's terminology (see section 2.1). The present author believes that all foliations, whether parallel to bedding or not, should be termed *cleavages*, irrespective of their origin; they can be described using Powell's geometrical classification.

Some folds show a localised bedding-parallel cleavage in the fold hinge (Fig. 2.4 b), termed arcuate hinge cleavage (Savage, 1965; Roberts, 1971; Hobbs et al., 1976; Eichentopf and Greiling, 1987). It is usually restricted to multilayered sequences with considerable competence contrast. Theory and experiments have shown that the outer arc of concentric folds is being stretched, so locally the XY-plane of the

strain ellipsoid is parallel to bedding (e.g. Ramsay, 1967; Hobbs et al., 1976), which explains the local deviation of the cleavage orientation.

Some non-axial plane cleavages seem to have developed contemporaneous with folding. Often such a cleavage seems to be axial planar to the folds when viewed on a section perpendicular to the fold axes, but, when viewed on the folded surfaces, the δ-lineation is slightly inclined to the fold axis (Fig. 2.4 c). Such folds are called *transected folds* (Powell, 1974; Borradaile, 1978; Duncan, 1985).

When the angle of deviation is small, the relationship is easily explained in terms of pre-folding irregularities in the folded surface, or a local heterogeneity of strain (Williams, 1977). However, at larger deviations, the question arises whether the fold and the cleavage represent different phases of deformation. Even the synchronicity of cleavage and folds in the "type area" in Tasmania (Powell, 1974) has been disputed (Duncan, 1985).

2.2.4 Cleavage forming processes

All slaty cleavages are characterised by a preferred orientation of platy grains, and/or a preferred orientation of discontinuities in the rock. A number of processes is involved in the formation of slaty cleavage.

When a rock containing elongated or platy grains is deformed, the grains will rotate. In the extreme case where the grains originally have a random orientation and rotate passively in a homogeneously deforming matrix, the resulting degree of preferred orientation can be calculated using the method of March (1932). There are several studies comparing measured and predicted preferred orientations (Oertel, 1970; Siddans, 1979, 1977; Tullis and Wood, 1972, 1975). Usually the measured degree of preferred orientation deviates from the predictions, either being too low (Tullis and Wood, 1972) or too high (Oertel, 1970), or there is a discrepancy between preferred orientations of various platy minerals in the same rock (e.g. chlorite and muscovite, Le Corre, 1979). There are several explanations for the deviations: the original orientation distribution of inequant grains is usually far from random, the deformation of the matrix is not homogeneous, and other processes than passive rotation play a role in the development of preferred orientation (see below). Nevertheless, passive rotation of platy grains will at least contribute to the development of preferred orientation.

Rotation of grains can also be caused by the removal of framework grains, e.g. by pressure solution, followed by compaction of the rock matrix; inequant grains would then be plastered either against cleavage domains or against relicts of framework grains (Gray, 1981; Engelder and Marshak, 1985). When the shape of the inequant grains is related to the crystallographic axes, as is the case for phyllosilicates, the shape preferred orientation will also be a crystallographic preferred orientation.

If an existing fabric is shortened in a direction inclined to the cleavage plane, buckling may lead to the formation of microfolds or *crenulations*. This may also apply to individual platy grains or grains with a strong crystallographic anisotropy, such as micas (e.g. Gregg, 1986). This results in a re-orientation of a part of the pre-existing fabric. There are several examples of slaty cleavages which developed from crenulation cleavages (Weber, 1976, 1981; Knipe and White, 1977). The initial slaty cleavage anisotropy is developed by alignment of grains in the limbs of the microfolds. Further cleavage development obliterates the microfolds by recrystallisation and grain growth (see below).

Recrystallisation is the formation and/or migration of grain boundaries, often resulting in the development of new grains at the cost of old ones (Urai et al., 1986). The formation of new grain boundaries can occur by the generation and accumulation of dislocations in dislocation walls, caused by a progressive misorientation of adjoining parts of the crystal. This mechanism is called *polygonization*. Recrystallisation can also occur by the movement of grain boundaries, separating regions with different orientation, composition or defect densities.

The recrystallisation process which is most frequently described in slates is the migration of existing grain boundaries separating regions with different composition, e.g. the growth of phyllosilicates in the cleavage lamellae at the expense of those in the microlithons (Weber, 1976, 1981; Knipe and White, 1977; White and Knipe, 1978), where phengitic mica replaces illite (Knipe, 1979, 1981). In the literature on slaty cleavage the meaning of the term *recrystallization* is usually restricted to this mechanism of grain boundary migration and grain growth (e.g. Lee et al. 1986). To avoid confusion, the term *recrystallization* will also be used in this limited meaning in the present thesis.

Several driving forces for recrystallisation during cleavage development have been proposed. Due to its high elastic anisotropy the thermodynamically most stable orientation of mica is the orientation with the (001) planes perpendicular to the maximum compressive stress σ_1 (Kamb, 1959). Therefore a re-orientation of the crystal lattice perpendicular to σ_1 will decrease the energy of the system. This driving force will result in a crystallographic preferred orientation of micas perpendicular to the average direction of σ_1, which will generally coincide with the XY-plane of the finite strain ellipsoid.

Microchemical changes can also be a driving force for recrystallisation (Etheridge and Hobbs, 1974). In general cleavage formation is associated with prograde metamorphism and some phases will be unstable at increasing pressure and temperature. Other phases with a stable chemistry will start to grow at the expense of the unstable phases. Evidence for chemical changes during cleavage development have been found by various authors (e.g. Knipe, 1979, 1981; White and Johnston, 1981).

Another possible driving force is the strain energy stored in the crystals during deformation. Etheridge and Hobbs (1974) suggest that the stored plastic strain energy in mica is of minor importance relative to the energy due to chemical differences. However, White and Knipe (1978) note that cleavage lamellae initiate in regions where the phyllosilicates are most intensely deformed, i.e. where the stored strain energy is highest. It should be noted that the latter two driving forces will not necessarily result in a crystallographic preferred orientation.

In many slates there are examples of truncated grains and fossils in association with cleavage domains (Holeywell and Tullis, 1975; Beutner, 1978; White and Knipe 1978; Gray, 1981; Borradaile et al. 1982; Marshak and Engelder, 1985), indicating that there has been transport of material associated with cleavage development, a process generally called *mass transfer*. The process of mass transfer involves the removal of material from one region, subsequent transport and deposition elsewhere. When the transport takes place through a fluid, either by movement of the fluid or by diffusion through the fluid, the process is called *solution transfer*. *Pressure solution* is the process where dissolution takes place at interfaces with a high normal stress, transport through a fluid and redeposition at interfaces of low normal stress. The driving force for this process is the chemical potential gradient created

by variations in the magnitude of the normal stress (De Boer, 1977; Rutter, 1976, 1983). Pressure solution is the main mass transfer process in slates, although free-face dissolution into an undersaturated fluid may also play a role (Engelder and Marshak, 1985).

It has been argued that huge amounts of moving fluid have been necessary to account for the pressure solution phenomena in slates (e.g. Williams, 1972). Although diffusive mass transfer through a stationary fluid can account for transport of material over short distances, e.g. from the one face of a grain to the other (Rutter, 1976, 1983) or within a small volume of rock (Waldron and Sandiford, 1988), moving fluids may be important for solution transfer over longer distances, e.g. transport of quartz from the slate to veins.

Many authors have mentioned intracrystalline deformation as one of the processes active during cleavage development (Sander, 1930; Fairbairn, 1949; Van der Pluijm and Kaars Sijpesteijn, 1984; Dimberline, 1986). The role of stored strain energy as a driving force for recrystallisation has already been mentioned above. Intracrystalline deformation can also lead to a change in grain shape or to re-orientation of the crystal lattice. These effects have been described mainly in the literature on chlorite-mica aggregates (Craig et al, 1982; Van der Pluijm and Kaars Sijpesteijn, 1984; Gregg, 1986; Dimberline, 1986). Typical deformation structures include bending, kinking, severe undulose extinction, micro-crenulation and displacement of grain segments by rotation or by slip parallel to the basal planes (e.g. Gregg, 1986).

2.2.5 Chlorite-mica aggregates

Almost all slates contain aggregates of chlorite and mica. Many different terms have been employed to describe these aggregates, e.g. chlorite stacks, chlorite-muscovite porphyroblasts, chlorite-rich pods, etc. (see Craig et al., 1982, and Van der Pluijm and Kaars Sijpesteijn, 1984). In this thesis the term *chlorite-mica aggregates* (Weber, 1981; Van der Pluijm and Kaars Sijpesteijn, 1984) will be used.

Chlorite-mica aggregates are usually found in the microlithons, they are barrel-shaped and their basal planes are at a high angle to the cleavage lamellae (see e.g. Fig. 5.19). Occasionally aggregates occur in the cleavage lamellae; in that case both the basal planes and the

long axes of the aggregates are parallel to the cleavage planes (e.g. Beutner, 1978; see also Fig. 5.7).

The theories for the origin of chlorite-mica aggregates can be divided into three groups:

1. the aggregates are of sedimentary origin, and they have not been altered by diagenesis, metamorphism or cleavage development (Beutner, 1978)
2. the aggregates are porphyroblasts which grew during slaty cleavage development (Roy, 1978; Weber, 1981)
3. the aggregates have been formed prior to cleavage development, and have been modified during cleavage development (e.g. Van der Pluijm and Kaars Sijpesteijn, 1984).

In the recent literature it is generally accepted that the aggregates are formed prior to cleavage development and subsequently strongly modified (theory 3; Craig et al. 1982; Woodland, 1982, 1985; Van der Pluijm and Kaars Sijpesteijn, 1984; Gregg, 1986; Dimberline, 1986).

The aggregates can form during early diagenesis and incipient metamorphism (Craig et al., 1982; Van der Pluijm and Kaars Sijpesteijn, 1984), either by prograde alteration of clay minerals (Craig et al., 1982) or as breakdown products of detrital biotite (White et al., 1985; Dimberline, 1986; Morad and AlDahan, 1986).

During cleavage development the aggregates are deformed by kinking and folding (Van der Pluijm and Kaars Sijpesteijn, 1984; Gregg, 1986; Dimberline, 1986) and by solution transfer (Woodland, 1985). The mobile phase during pressure solution can be either chlorite (Van der Pluijm and Kaars Sijpesteijn, 1984; Woodland, 1985) or mica (Gregg, 1986).

2.2.6 Slaty cleavage and metamorphism

Kubler (1967b) noted that the initiation of slaty cleavage in Paleozoic rocks from northern France and southern Belgium coincided with the onset of anchizone metamorphism. The same has been observed in other areas (Dunoyer de Segonzac and Heddebaut, 1971; Weber, 1972b, 1976, 1981; Teichmüller et al., 1979; Piqué, 1982). However, the concurrence of slaty cleavage initiation and anchizone metamorphism does not seem te be a general rule, because in some cases slaty cleavage

has been observed in diagenetic rocks (Kubler, 1967b; Dunoyer de Segonzac, 1970; Artru et al. 1969).

The metamorphic grade influences the cleavage forming processes. In general it seems that purely mechanical re-orientation of existing grains dominates in the low-grade part of the anchizone, while crystallisation processes become important in the high-grade part of the anchizone (Weber, 1976, 1981; Teichmüller et al.; 1979).

2.2.7 Slaty cleavage formation

The idea that slaty cleavage develops in unconsolidated sediments, by passive rotation of grains after the pore water is expelled (dewatering hypothesis) was first proposed by Maxwell (1962). This led to considerable discussion about the timing of slaty cleavage development relative to lithification. Although there are some examples of cleavage-like structures in unlithified sediments or partially lithified rocks (Williams et al., 1969; Moore and Geigle, 1984), it seems that in general slaty cleavage develops after total lithification of the rock (Wood, 1974; Beutner, 1980; Woodland, 1985).

The first stage of cleavage formation seems to be the development of short irregular narrow cleavage domains, resulting in a rough disjunctive cleavage (Piqué, 1981; Norris and Rupke, 1986). Usually slaty cleavage develops first in fine-grained quartz-poor pelitic rocks (Teichmüller et al., 1979, Norris and Rupke, 1986). If a strong pre-cleavage fabric exists, a crenulation cleavage may develop (Woodland, 1982). After a shortening of 10-20% the secondary fabric becomes visible in the outcrop as a pencil cleavage (Reks and Gray, 1982; Ramsay and Huber, 1983).

Subsequently the cleavage domains grow in length and width and an anastomosing or planar spaced cleavage develops, either a disjunctive cleavage (Woodland, 1982; Norris and Rupke, 1986) or a crenulation cleavage (Weber, 1981). In this stage the cleavage planes and the intersection lineations are still quite irregular. In the final stage of cleavage development the cleavage domains grow at the expense of the microlithons, and a continuous cleavage *s.s.* is the result. The cleavage is now very straight and regular in the outcrop, and eventually a stretching lineation can develop (Ramsay and Huber, 1983).

2.2.8 TEM research on slates

A number of TEM techniques has already been applied to the study of slates, and the main results will be summarised in this section. The general changes in mineralogy at the transition from shale to slate has been studied by analytical electron microscopy (AEM) and lattice fringe imaging (Lee and Peacor, 1983, 1985; Lee et al., 1984, 1986). These studies have shown that the phyllosilicates in shales are often irregular interstratifications of illite, chlorite and other clay minerals. Upon the transition to slate the interstratifications become more regular, and 1Md-illite transforms into 2M-muscovite.

High-voltage TEM (HVTEM) has been used to study very small scale structures within individual cleavage domains and microlithons (Knipe and White, 1977; White and Knipe, 1978). These authors described phyllosilicates which can be traced from a bedding-parallel orientation in the microlithons into a cleavage-parallel orientation in the cleavage domains. They also observed recrystallisation of phyllosilicates in sites of high strain within old phyllosilicates, suggesting that this recrystallisation is driven by stored strain energy.

Knipe (1979, 1981) studied the chemical differences between cleavage grains and microlithons with AEM. He found evidence of prograde metamorphic reaction accompanying the formation of cleavage domains, e.g. illite → phengite + paragonite, and Fe-rich chlorite → Fe-poor chlorite. This suggests that chemical potential may also play a role in recrystallisation of phyllosilicates in slates.

No study on intracrystalline deformation phenomena in slates, e.g. using electron diffraction contrast, is available as yet.

2.3 CONCLUSIONS

It is recommended that a consistent geometrical classification is used to describe cleavage, e.g. the system proposed by Powell (1979) and Borradaile et al., (1982).

The structure generally referred to as slaty cleavage is continuous at the scale of the hand specimen, but at suitable magnifications most slaty cleavages show a spaced fabric, either a crenulation cleavage or an anastomosing disjunctive cleavage. Usually, the

fabric elements are individual grains (phyllosilicates, elongated quartz grains) or films of phyllosilicates and/or opaque minerals.

Slaty cleavage is a flattening phenomenon which develops more or less perpendicular to the XY-principal plane of the finite strain ellipsoid. Therefore it is usually axial planar to folds, but as the orientation of the finite strain ellipsoid can vary through a fold, so can the orientation of the cleavage.

The formation of slaty cleavage is usually associated with some loss of volume, although the amount of volume reduction is still under discussion.

Slaty cleavage development has been attributed to the following processes:

1. mechanical rotation of grains
2. folding, kinking and internal deformation of grains
3. mass transfer, mainly by pressure solution
4. grain boundary sliding
5. recrystallisation

Slaty cleavage is always the result of one or more of the above processes; at low temperatures mechanical re-orientation may dominate, at higher temperatures recrystallisation processes gain in importance.

The main steps in the development of slaty cleavage are:

1. rough cleavage
2. narrow disjunctive cleavage, or a crenulation cleavage when a strong pre-cleavage fabric is present
3. zonal disjunctive (or crenulation) cleavage
4. continuous cleavage *s.s.*

Previous TEM studies on slaty cleavage have concentrated on microchemical and small-scale morphological changes during cleavage development.

Chapter 3
THE ORRI DOME

3.1 INTRODUCTION

The Pyrenees can be subdivided into a series of WNW-ESE trending zones, distributed in a more or less symmetric pattern (Fig. 3.1). The central zone, often called the *Axial Zone*, consists almost entirely of Paleozoic sediments, metamorphic rocks and igneous rocks. The internal structure of the axial zone is characterised by large open dome-like anticlinoria (Aston-Hospitalet Massifs, Orri Dome; see fig. 3.2) and narrow tight synclinoria (Llavorsi Syncline, Tor Syncline). To the north and south the Axial Zone is flanked by zones of allochthonous rocks, mainly of Mesozoic age, the detached *North-* and *South Pyrenean Zones*. These zones in turn are bordered by a *Folded Foreland*, which grades into zones of undeformed flatlying sediments of the Aquitanian Basin to the north and the Ebro Basin to the South (e.g. Mattauer and Henry, 1974; Zwart, 1979).

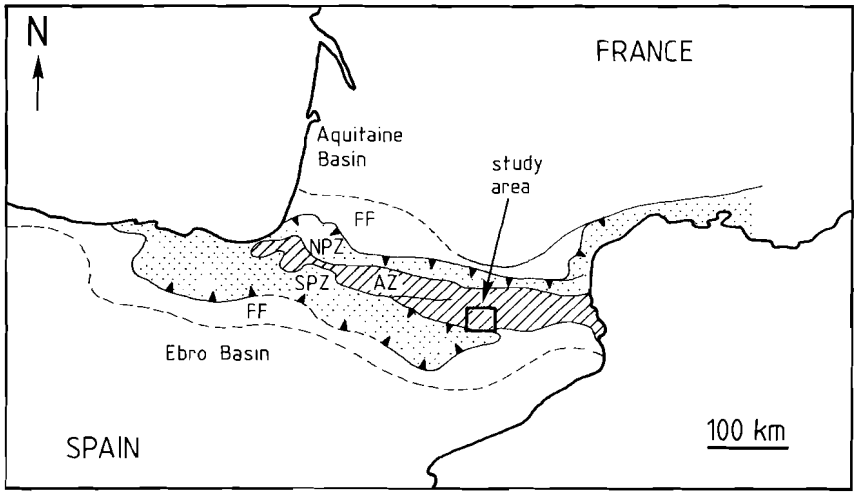

FIGURE 3.1. Schematic map of the Pyrenees. AZ = Axial Zone, NPZ = North Pyrenean Zone, SPZ = South Pyrenean Zone, FF = Folded Foreland. The area of the map of Fig. 3.2 is indicated. After Van den Eeckhout (1986) and Mattauer and Henry (1974).

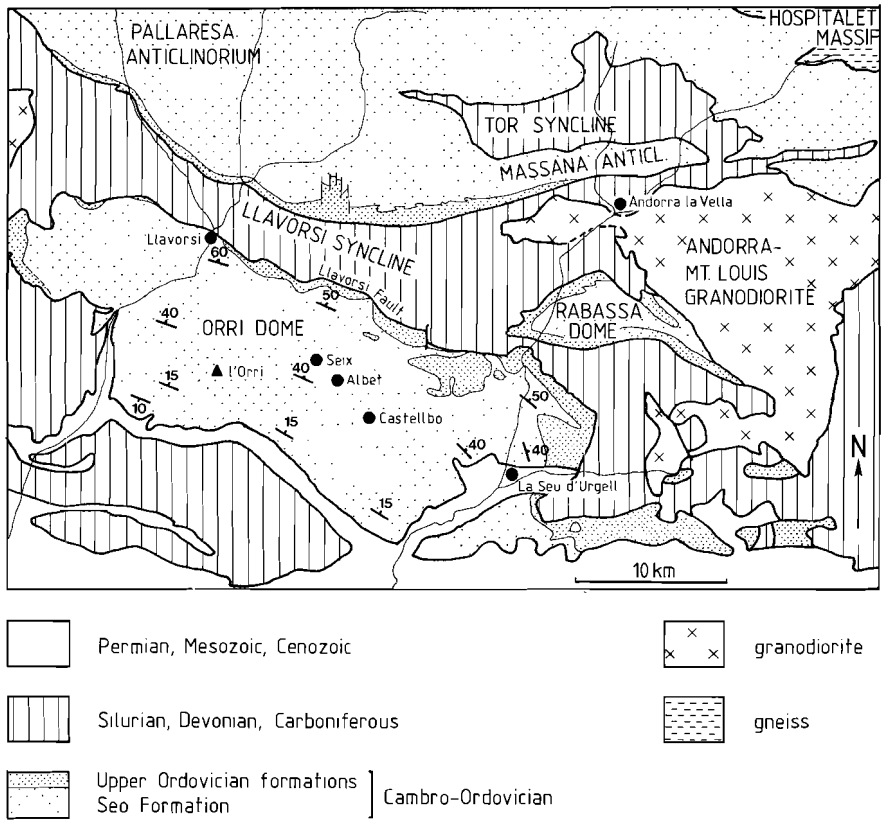

FIGURE 3.2. Geological map of the study area. The orientation of the mainphase cleavage (S_{V3}) in the Orri Dome is also shown.

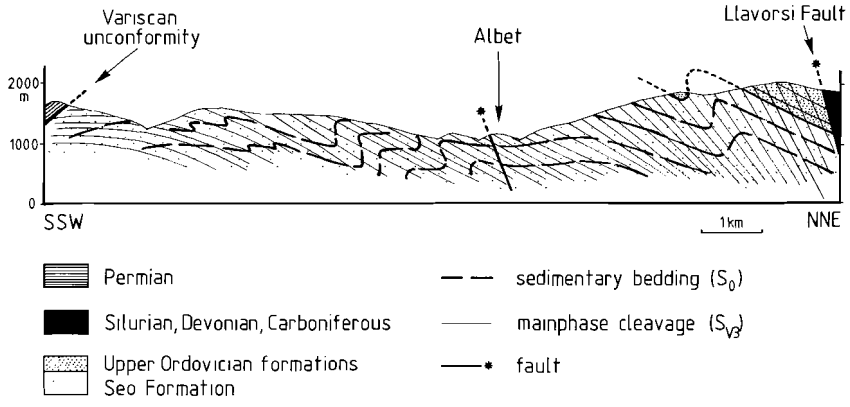

FIGURE 3.3. Schematic cross-section through the central part of the Orri Dome.

At least two orogenies have ocurred in the Pyrenees: the *Variscan Orogeny*, which affected the Paleozoic rocks of the Axial Zone, and the *Alpine Orogeny*, which deformed the Mesozoic rocks in the North- and South Pyrenean zones and the Folded Foreland, and overprinted the Variscan structures in the Axial Zone. This resulted in a complex structure and history of the Axial Zone, including the Orri Dome. This chapter gives a short introduction to the geology of the Orri Dome; for more information about the geology of the Pyrenees in general the reader is referred to the literature (e.g. Mattauer and Henry, 1974; Zwart, 1979, 1981, 1986).

3.2 THE ORRI DOME

The Orri Dome, called after the Orri Mountain in the centre of the structure, is one of the large anticlinoria in the Axial Zone. To the North the Orri Dome is bounded by the Llavorsi Syncline and the Llavorsi Fault. To the south the boundary is formed by the unconformable contact with Permian sediments (Speksnijder, 1985). An excellent map and a general description of the Orri Dome and surrounding structures have been presented by Hartevelt (1970). The structural geology has been studied in detail by Speksnijder (1986, 1987a,b).

3.2.1 Stratigraphy and metamorphism

The Orri Dome is formed mainly by Cambro-Ordovician rocks. Hartevelt (1970) describes several formations within the Cambro-Ordovician. The lowest rock unit is formed by an unfossiliferous sequence of thin-bedded slates and siltstones of at least 2 km thickness, the Seo Formation. An internal subdivision is not possible. Elsewhere, e.g. in the Pallaresa Anticlinorium, several quartzite and limestone levels are recogniseable, which are grouped in the Ransol Member (Zwart, 1965; Hartevelt, 1970). Quartzites do occur in the Seo Formation of the Orri Dome, but they cannot be traced as mappable units. The Seo Formation is probably deposited in a shallow marine environment (Hartevelt, 1970).

TABLE 3-I Deformation generations in the Orri Dome

Hartevelt (1970)	Zwart (1979)	Speksnijder (1986, 1987a,b)	Description (after Speksnijder, 1986, 1987a,b)
F_1*)	F_0	D_{V1}	First pre-mainphase folding. Very open folds, vertical N-S trending axial planes, horizontal foldaxes.
		D_{V2}	Second pre-mainphase folding. Very open folds, vertical E-W trending axial planes, horizontal fold axes.
F_2	F_1	D_{V3}	Mainphase folding. Relatively tight asymmetric south vergent folds, with an axial plane cleavage (slaty cleavage or spaced cleavage). Developed on any scale throughout the Dome.
	(F_3)		(Not recognized in the Orri Dome)
F_4	F_4	D_{V4}	First Variscan refolding. Small-scale folds (m-dm) with a steep E-W trending axial plane. Well-developed axial plane cleavage (usually a crenulation cleavage).
(F_3?)		D_{V5}	Second Variscan refolding. Locally developed asymmetric folds with steep N-S trending axial planes. The folds often have a kink-like appearance. Sometimes a weak (crenulation) cleavage is developed.
		D_{V6}	Kinkbands probably of Variscan age.
		D_{PV1}	Post-Variscan shearing, leading to a large-scale redistribution of older cleavage orientations.
		D_{PV2}	Post-Variscan extensional cleavage fanning.
		D_{PV3}	Kinkbands, probably of post-Variscan age.
		D_{A1}	Alpine thrusting, causing further cleavage fanning.
		D_{PA1}	Post-Alpine extensional faulting.

*) Hartevelt's F_1 applies to *all* premainphase deformation structures and is not strictly equivalent to F_0 of Zwart and D_{v1} and D_{v2} of Speksnijder.

The formations overlying the Seo Formation are found along the northern border of the Orri Dome. The top of the Seo Formation is marked by a sharp contact with mudflow conglomerates of the Rabassa Conglomerate Formation of Caradoc age. The other overlying Ordovician formations are the Cava Formation (mainly fluviatile and shallow marine sandstones), the Estana Formation (shallow marine marls and limestones), the Ansobell Formation (lagoonal black slates) and the Bar Quartzite (coastal barrier sands). These formations wedge out towards the north, and Hartevelt (1970) postulated that the sediments have a source area in the south. Carbonaceous slates, marls and limestones of Silurian to Carboniferous age are found in the synclinal structures such as the Llavorsi Syncline. The next unit in the stratigraphy of this area is formed by the post-Variscan tuffs and redbeds. The youngest rocks are Tertiary sandstones and shales, which are found around La Seu d'Urgell.

The rocks of the Orri Dome are assumed to be non-metamorphic to very low-grade metamorphic (Hartevelt, 1970; Zwart, 1979; Speksnijder, 1986), based on general macroscopic observations. However, this assumption has not yet been supported by any mineralogical data (Zwart, 1979).

3.2.2 Structural geology

Several generations of deformation structures have been described in the Orri Dome, and various notations for these generations have been used in the literature (see Table 3-I). The most recent and most elaborate study is that of Speksnijder (1986, 1987a,b), and his notations will be used in this thesis. The deposition of sediments in the Pyrenees, from Cambro-Ordovician to Carboniferous, without any significant disconformities, indicates that no major Caledonian deformation took place (Speksnijder, 1986). The most evident deformation structures in the Orri Dome are south-facing folds, developed on various scales from centimetres to kilometres, associated with a north-dipping axial plane cleavage. These have been termed *mainphase folds* and *-cleavage* (Speksnijder, 1986, 1987a,b).

Pre-mainphase folds have been described in regions with clear marker horizons, where these folds are overprinted by the mainphase cleavage (e.g. Mey, 1967). No marker beds are available in the

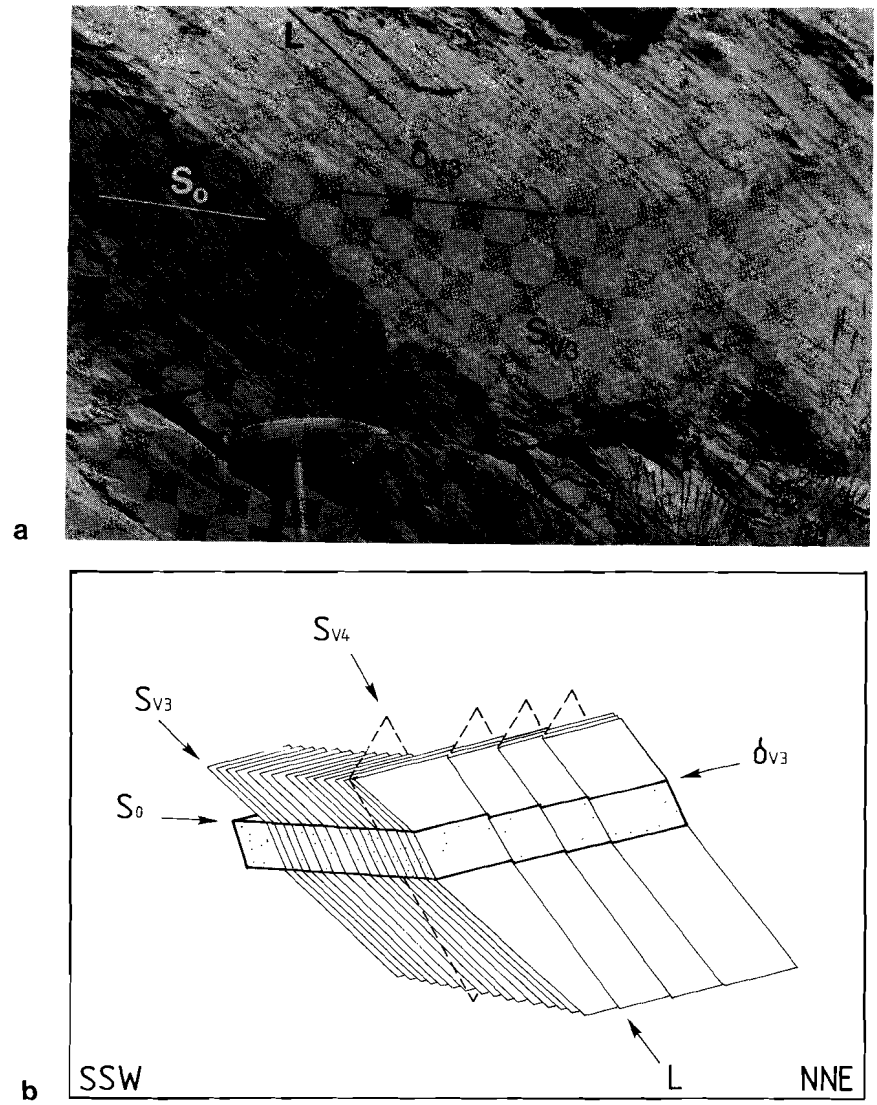

FIGURE 3.4 a. Overprinting relationship between mainphase slaty cleavage (S_{v3}) and a crenulation cleavage (Sv4) in an outcrop W of La Seu d'Urgell. The intersection between bedding and mainphase cleavage (δ_{V3}) is horizontal, the intersection between the two cleavages is indicated by L. b. Schematic sketch of the outcrop, showing the geometric relationships between the structures.

Orri Dome. Based on detailed statistical analysis of cleavage-bedding intersections and other orientation data, Speksnijder (1987a) has demonstrated the existence of pre-mainphase folds in the Orri Dome. These folds are very open and have subvertical axial planes; the fold axes are subhorizontal. Two generations of pre-mainphase folds can be distinguished in the northern part of the Orri Dome: the oldest generation has N-S trending axial planes, the younger one has E-W trending axial planes (D_{V1} and D_{V2} respectively, Speksnijder, 1987a,b). No small-scale pre-mainphase folds have been observed in the field, and the only indication of their presence is the variation in orientation of the mainphase lineations.

The *mainphase folds* (D_{V3}) in the Orri Dome are asymmetrical south-facing folds; the long flatlying limbs usually dip slightly to the north, while the short steep limbs are overturned and dip steeply to the north (Fig. 3.3). There is a N-dipping axial plane cleavage (Fig. 3.4), which is usually described in the field as a slaty cleavage in the fine-grained rocks, and as a spaced cleavage in the sandstones (Speksnijder, 1987b).

The mainphase folds are developed on a kilometre scale, but small-scale folds (cm-m scale) also occur. The orientation of the folds and associated cleavage is not constant through the Orri Dome. In general there is a fanning of the cleavage, from steeply N-dipping in the north of the Orri Dome, to horizontal or even S-dipping in the south. In addition, the strike of the mainphase cleavage changes from approximately WNW-ESE in the central part of the Dome to almost N-S in the east near La Seu d'Urgell (Hartevelt, 1970; Speksnijder, 1987b).

Several generations of *post-mainphase* kinks and folds, sometimes associated with axial plane cleavages (Fig. 3.4), have been described (Hartevelt, 1970; Zwart, 1979; Speksnijder, 1987b); they are summarised in Table 3-I. In general these folds and kinks are developed on a small scale (dm-m, see Fig. 3.5, 3.6) and do not affect the enveloping surface of the mainphase folds. The Alpine deformation was limited to faulting and thrusting.

Some large-scale structures have been attributed to post-mainphase deformation. The large-scale cleavage fanning is attributed to post-Variscan, and probably mainly Alpine, thrusting (Speksnijder, 1987b). The cleavage rotation can be explained by the

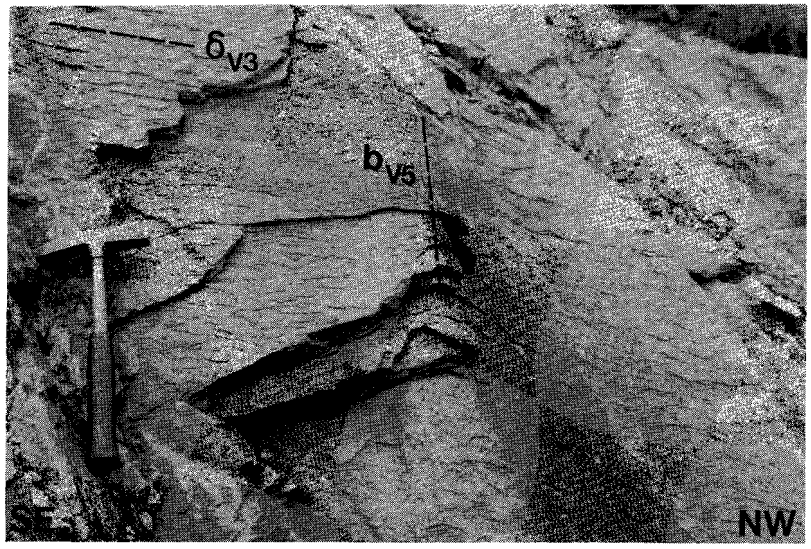

FIGURE 3.5. D_{V5} folds W of Albet. The folded surface is the sedimentary layering; the fold axis b_{V5} plunges towards the north. The mainphase cleavage/ bedding intersection δ_{V3} is folded.

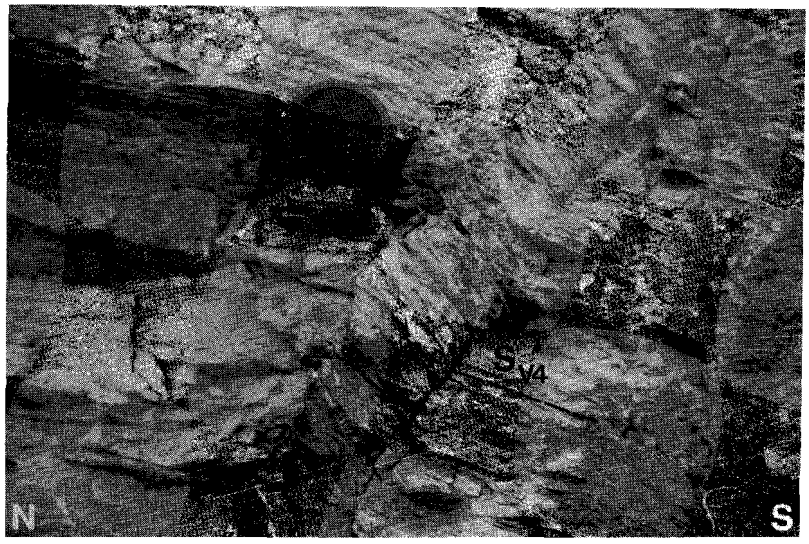

FIGURE 3.6. Kinkbands, probably of Variscan age (D_{V6}). The kinked surface is a post-mainphase foliation (S_{V4}).

combined effect of the Variscan post-mainphase folding and post-Variscan folding (D_{V4} and D_{PV1}; Speksnijder, 1987b).

The intensity of the post-mainphase deformation varies through the Orri Dome. The first post-mainphase folding (Dv4) is developed in almost the entire Orri Dome, except the area around Seix and Albet, in the north-central part of the dome. The small-scale D_{V5}-folds and the D_{V6}-kinks are only locally developed.

3.3 OTHER OUTCROPS OF THE SEO FORMATION

Outside the Orri Dome the Seo Formation crops out in a number of anticlinoria, such as the Rabassa Dome, the Pallaresa Anticlinorium and the Massana Anticline. The metamorphic grade of the rocks of the Massana Anticline and the Pallaresa Anticlinorium is lower greenschist (Zwart, 1959, 1979); the metamorphic grade of the Rabassa Dome is yet unknown.

The mainphase cleavage is developed everywhere, but it is always overprinted by one or more post-mainphase cleavages. The mainphase cleavage in the Seo Formation of the Pallaresa Anticlinorium and the Massana Anticline is a continuous cleavage *s.s.*; these rocks are phyllites rather than slates. The rocks of the Seo Formation in the Rabassa Dome should still be termed slates. The mainphase cleavage in the Rabassa Dome varies from a zonal disjunctive cleavage to a continuous cleavage *s.s.* However, because this cleavage is always overprinted by later cleavages, the situation is too complex for a detailed study of the mainphase cleavage microstructure.

3.4 IMPLICATIONS FOR THE MICROSTRUCTURAL STUDY OF SLATY CLEAVAGE DEVELOPMENT

Many generations of deformation structures have been recognised in the Orri Dome. For example, Speksnijder (1987a,b) distinguishes six Variscan deformation generations and five post-Variscan generations. Fortunately these phases have not affected the rocks of the Orri Dome on every scale and in every outcrop. The north-central part of the Orri Dome has only suffered very open pre-mainphase folding and the

mainphase deformation (Speksnijder, 1986). On the scale of the outcrop the only deformation structures are the mainphase folds and cleavage. Therefore this area is suitable for a microstructural study of the slaty cleavage. Other areas, e.g. the region SE of La Seu d'Urgell and the Rabassa Dome, are so complex, and show so many overprinting cleavages, that a detailed study of the mainphase slaty cleavage is not possible. The microstructure of a continuous cleavage *s.s.*, developed in the same type of rocks, can be studied in the Pallaresa Anticlinorium and the Massana Anticline.

As information on the metamorphic grade of the rocks of the Orri Dome is lacking in the literature, this topic will be treated in detail in chapter 4.

Chapter 4.
METAMORPHISM AND THE OCCURRENCE OF MONAZITE PORPHYROBLASTS

4.1 INTRODUCTION

The Seo Formation in the Orri Dome is assumed to be non-metamorphic to very low-grade metamorphic (Hartevelt 1970; Zwart, 1979; Speksnijder 1986). This assumption is based on the relatively poorly developed cleavages, but has not yet been supported by any mineralogical data (Zwart, 1979).

The determination of the metamorphic grade in very low-grade pelitic and quartzitic rock presents some special problems. In meta-grauwackes and meta-volcanic rocks a metamorphic zonation can be made, based on the occurrence of metamorphic minerals such as zeolites, pumpellyite, prehnite, lawsonite, etc. (e.g. Winkler, 1979). However, such minerals rarely occur in pelitic and quartzitic rocks. Therefore the determination of metamorphic grade in pelitic and quartzitic rocks between diagenesis and the middle greenschist facies can be quite difficult and other indicators than mineral assemblage must often be used.

This chapter reports the results of a detailed study on the metamorphism of the Seo Formation in the Orri Dome and some of the surrounding structures (Pallaresa Anticlinorium, Massana Anticline; see Fig. 4.1).

A striking feature of the rocks of the Seo Formation in the Orri Dome is the occurrence of monazite porphyroblasts (Fig. 4.2). Although monazite is quite common in metamorphic rocks as an accessory mineral, monazite porphyroblasts have not yet been described in very low-grade rocks. Furthermore, the internal fabric of these porphyroblasts is essential to the discussion on slaty cleavage development (see chapter 5). Therefore its occurrence will be described in detail and its origin will be discussed.

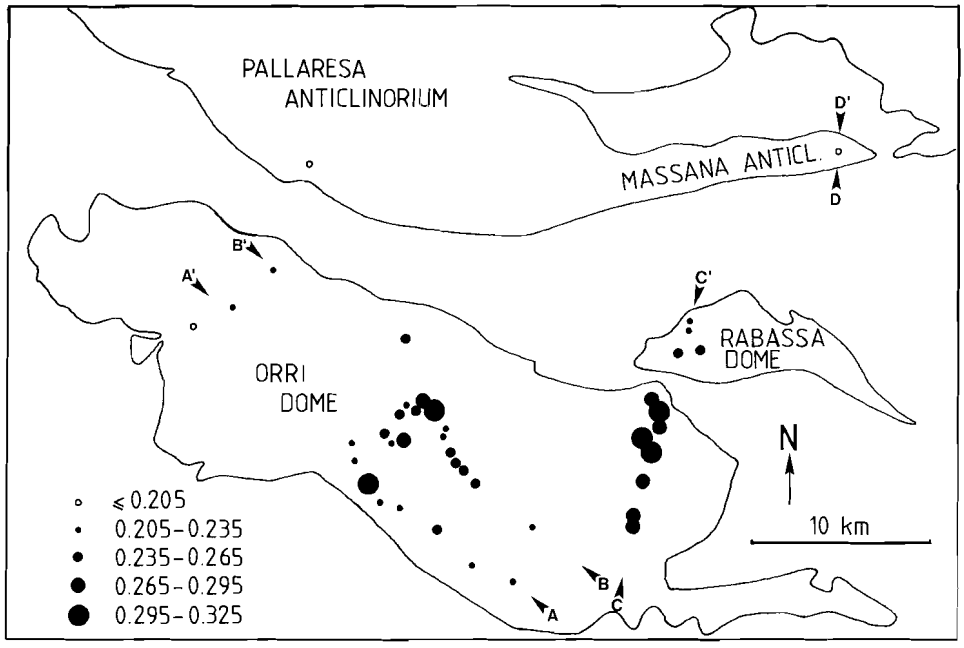

FIGURE 4.1. Schematic map of the Cambro-Ordovician outcrops in the study area, with the illite crystallinity indices (in °2Θ) measured on the K^+-saturated fraction <2μm. More data on the samples taken along the sections A-A', B-B', and C-C' are given in Table 4-V.

TABLE 4-I. Metamorphic zonation in non-metamorphic to low-grade metamorphic pelitic rocks

Kubler (1968)	boundary values used in this study (Kisch, pers.comm. 1986)	Winkler (1979)
DIAGENESIS		DIAGENESIS
	0.370 °2Θ	
ANCHIZONE		VERY LOW-GRADE METAMORPHISM (zeolite facies, pumpellyite-prehnite-quartz facies)
	0.205 °2Θ	
EPIZONE		LOW-GRADE METOMRPHISM (greenschist facies)

4.2 METAMORPHISM

4.2.1 Terminology

Various subdivisions of the realm of diagenesis and incipient metamorphism exist; see Kisch (1983) for a review. Each subdivision is based on one or more metamorphic indicators, such as metamorphic minerals (Winkler, 1979), porosity and microstructure (Kossovskaya and Shutov, 1970), coalification (Teichmüller and Teichmüller, 1981) or illite crystallinity (Kubler, 1964, 1967a, 1968). Correlations between the various subdivisions are very difficult (Teichmüller et al., 1979; Kisch, 1980a,b). Therefore the terminology one uses to describe the metamorphic grade should depend on the indicators used.

In this study illite crystallinity is used as the main indicator of metamorphic grade and therefore the terminology of Kubler (1964, 1967a, 1968) will be used. Near the onset of metamorphism three zones are distinguished: diagenesis, anchizone and epizone (see Table 4-I). These zones correspond roughly with Winkler's non-metamorphic (diagenetic), very low-grade and low- grade metamorphic zones (Winkler 1979; Teichmüller et al. 1979). In some cases the metamorphic grade was determined using mineral paragenesis. In that case terms like greenschist facies will also be employed.

4.2.2 Mineralogical indicators

The main minerals of the rocks of the Orri Dome are musovite, chlorite, quartz and albite. This mineral assemblage is stable from the diagenetic field up to the middle greenschist facies (e.g. Winkler, 1979). Careful analysis of the samples, using optical microscopy, X-ray diffraction, electron microscopy and microanalysis have revealed no typical low-grade metamorphic minerals such as pumpellyite or epidote.

Detrital minerals such as biotite, K-feldspar and Ca-plagioclase are entirely absent. These minerals are unstable during diagenesis and disappear completely near the anchizone (Kisch, 1983). X-ray diffraction analyses have shown that muscovite and chlorite are the only phyllosilicates present, with minor quantities of kaolinite (Fig 4.3). The absence of clay minerals with expandable layers, such as smectite,

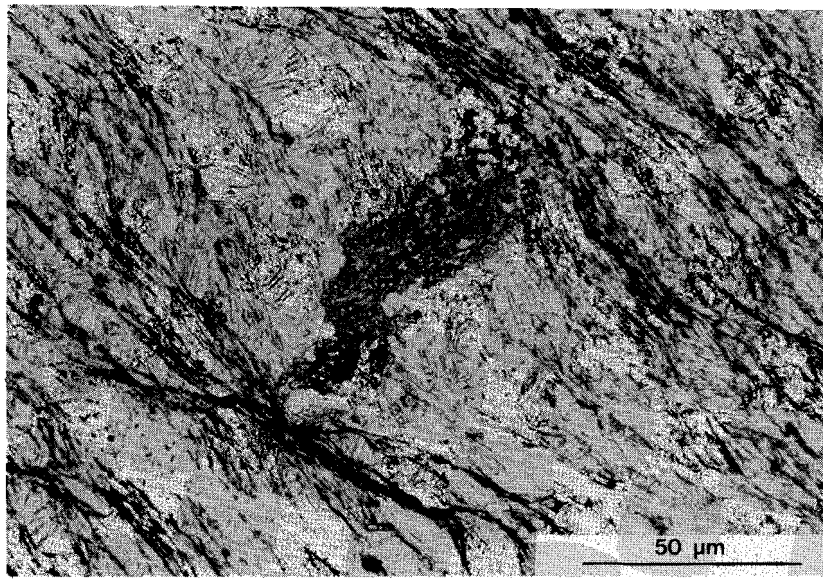

FIGURE 4.2. Optical micrograph (plan-polarized light) of a monazite porphyroblast from an outcrop near Albet (central part of the Orri Dome). Many small inclusions form an internal fabric parallel to the long dimension of the grain.

confirms that the high-grade boundary of the diagenetic field has been reached (Kisch, 1983).

Along the southern border of the Pallaresa Anticlinorium and in the Massana Anticline (Fig. 4.1) the slates of the Seo Formation show the mineral assemblage muscovite + chlorite + quartz + albite + epidote. Metamorphic chloritoid has been found in the Llavorsi Syncline and along the southern border of the Massana Anticline (Zwart, 1959). The presence of epidote and chloritoid in these rocks indicates greenschist facies metamorphism. The bulk chemistry of the Orri Dome slates does not differ significantly from the Cambro-Ordovician slates of the Pallaresa and Massana Anticlines, which contain epidote even in the samples low in Ca (see Table 4-II). Therefore it seems likely that epidote could also have been formed in the slates of the Orri Dome if the degree of metamorphism had reached the greenschist facies zone. Thus, the absence of epidote in the Seo Slates of the Orri Dome can be used as an indication that the greenschist facies zone has not been reached in the Orri Dome.

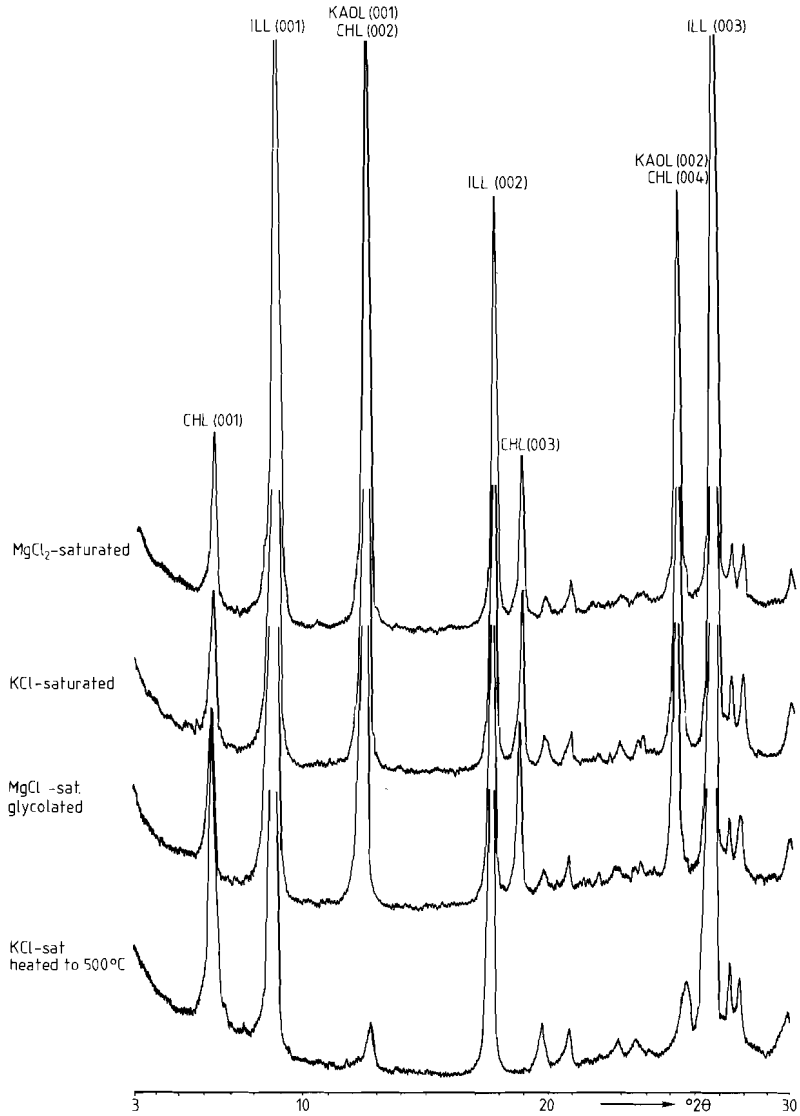

FIGURE 4.3. X-ray diffractograms of the clay- size fraction (<2 μm) of a sample from an outcrop near Albet. Kaolinite (KAOL) is destroyed at 500 °C. The chlorite (CHL) (001) peak intensity increases at 500 °C, while the higher-order peaks decrease. This is typical for Fe-rich chlorites (Brown and Bailey, 1980). The illite/muscovite (ILL) peaks are not affected.

TABLE 4-II Major element oxide data (wt%), pelitic rocks from the Seo Formation, Massana Anticline and Orri Dome

A. *MASSANA ANTICLINE*

sample	SiO_2	Al_2O_3	FeO	MgO	CaO	Na_2O	K_2O
P-HH1	53.4	19.5	4.5	0.9	6.5	0.9	0.5
P-HH2	57.7	21.2	8.1	2.2	0.2	1.2	3.9
P-HH3	63.5	18.6	7.2	2.0	0.6	1.5	3.2
P-HH4	61.4	20.0	6.9	1.9	0.2	1.9	3.4
P-HH5	58.5	16.0	6.0	1.4	5.4	0.4	3.4
P-HH6	74.4	10.2	3.2	0.8	1.8	0.8	2.0
P-HH7	54.2	21.1	8.6	2.5	1.0	1.5	3.4
P-HH10	53.6	21.6	8.4	2.3	0.2	1.6	3.6
average	59.6	18.5	6.6	1.8	2.0	1.2	2.9

B. *ORRI DOME*

sample	SiO_2	Al_2O_3	FeO	MgO	CaO	Na_2O	K_2O
P-HH11	59.9	20.2	8.0	2.2	0.1	1.3	3.5
P-HH12	59.3	19.4	7.8	1.9	0.0	0.7	3.7
P-HH13	60.0	22.4	8.6	2.7	2.8	0.9	4.4
P-HH14	62.5	17.9	7.3	2.3	0.1	1.3	3.1
P-HH15	51.7	25.1	5.2	2.1	0.0	0.8	5.0
P-HH16	47.4	27.7	8.9	2.2	0.2	0.7	5.7
P-HH17	58.2	21.2	7.0	2.2	0.0	1.1	3.8
P-HH19	60.4	19.2	8.7	0.6	0.4	0.5	5.2
P-HH20	65.0	14.9	5.7	1.3	0.2	1.9	2.8
P-HH21	58.4	17.6	4.5	1.5	0.4	0.7	3.5
P-HH22	58.2	20.8	7.1	1.7	0.8	0.5	4.6
P-HH23	59.4	20.1	7.8	2.2	0.2	1.1	4.0
P-HH24	60.2	21.2	8.0	2.0	0.2	0.7	4.2
P-HH25	59.6	21.3	12.7	2.2	2.5	1.2	3.6
P-HH26	68.0	15.8	6.0	2.1	0.2	1.6	2.6
P-HH27	64.7	17.4	6.8	2.2	0.3	1.2	3.2
P-HH28	61.4	19.7	7.2	2.3	0.2	1.3	3.4
P-HH29	61.2	18.4	6.7	1.9	0.3	1.2	3.1
average	59.8	20.0	7.4	2.0	0.5	1.0	3.8

4.2.3 Illite crystallinity

Another method to determine the metamorphic grade in (very) low-grade pelitic rocks is the measurement of illite crystallinity (Weaver, 1960; Kubler, 1964; Weber, 1972a,b).

With increasing metamorphic grade the crystallinity of illite improves due to increasing size of the crystallites and increasing ordering of the crystal layers; the high-grade end member is muscovite. The increase of illite crystallinity is reflected in the sharpness of the X-ray diffraction peaks of illite/muscovite. Thus the sharpness of the illite 10 Å-peak can be used as a measure of metamorphic grade; the first to use this parameter was Weaver (1960). The peak sharpness can be measured as the width of the peak at half height; this quantity is called the crystallinity index (Kubler 1964), henceforward abbreviated to "IC index". The IC index can be expressed in mm on the paper chart of the X-ray diffractometer (Kubler, 1964, 1967a, 1968), or in degrees of the angular separation ($\Delta 2\Theta$) (Kisch 1980a,b, 1981, 1983). A small value of the IC index indicates a narrow peak and thus a high degree of diagenesis or metamorphism.

The samples for the illite crystallinity measurements were collected from the pelitic layers in fresh roadside outcrops. One to three samples per outcrop were measured. Four samples from the Rabassa Dome, an outcrop of the Seo Formation north of the Orri Dome, have also been measured. The IC-index is strongly influenced by sample preparation and measurement techniques. In this study the preparation techniques and X-ray diffractometer settings of Kisch (1980a, 1981, 1983 p.348-350) are used (see Table 4-III).

The crystallinity of detrital micas is usually better than that of the authigenic micas. The mean IC index of samples consisting of a mixture of detrital and authigenic micas will therefore be smaller than that of the authigenic micas that indicate the true degree of diagenesis or metamorphism. As the clay-size fraction (< 2 μm) is generally free of detrital micas, this fraction is usually used for determination of the crystallinity index. Following Kisch (1980a,b, 1981, 1983), the fraction <2 μm is used in this study, while the fractions 2-6 and 6-50 μm were also measured, in order to monitor the influence of the detrital micas.

To check for the presence of clay minerals like smectite and vermiculite, and to compensate for loss of K^+- ions during weathering and

TABLE 4-III. Illite crystallinity measurement: sample preparation and instrument settings (after Kisch, 1980a,b, 1983, pers. comm. 1986)

A. SAMPLE PREPARATION

Desintegration, removal of organic matter and calcium carbonate

1. crush the sample in a mortar to pass a 0.2 mm sieve
2. transfer 5 g to a 250 ml Erlenmeyer flask containing 50 ml 6% H_2O_2 and put flask in an ultrasonic bath for 30 minutes
3. add 5 ml 1N HCl and put flask in a 70°C water bath for 30 minutes
4. wash the suspension with destilled water until the pH of the water is neutral

Separation of size fractions

5. use a 50 µm sieve to remove the size fraction >50 µm
6. transfer the suspension to a 20 cm high sedimentation cylinder, stir well; after 70 minutes pipette out the upper 15 cm: this contains the fraction <6 µm. Repeat once most of the fraction <6 µm is thus removed and the remaining suspension contains the fraction 6-50 µm
7. transfer the fraction <6 µm to a 30 cm high sedimentation cylinder, stir, and let settle for 17 hours 10 minutes; pipette out the upper 25 cm of liquid, this contains the fraction <2 µm. Repeat this step once; most of the fraction <2 µm is now removed and the remaining suspension contains the fraction 2-6 µm.
8. concentrate all size fractions using a centrifuge

Saturation with K and Mg

9. transfer 10 ml of the suspension <2 µm to a 50 ml tube and add 10 ml 0.5N KCL; transfer another 10 ml to a second tube and add 10 ml 1N $MgCl_2$
10. stir for 20 minutes, concentrate the suspension with the centrifuge; repeat step 9 and 10 twice
11. wash once with water and at least three times with alcohol (check with $AgNO_3$).
12. concentrate the suspensions with the centrifuge, pipette out the alcohol and add a few ml water

Preparation of slides

13. freeze-dry the four suspensions <2 µm K^+, <2 µm Mg^{2+} ,2-6 µm and 6-50 µm
14. dilute 0.020 g of each dry fraction in 0.500 ml water and put the suspension on a glass slide
15. let the sample settle and the water evaporate at room temperature

---

B. X-RAY DIFFRACTOMETER SETTINGS

1. Philips X-ray difractometer, CuKα radiation, 40 kV/30 mA
2. monochromator, discriminator
3. sample spinner on
4. slits: 1° - 0.2 mm - 1°
5. time constants: TC=2 at range $>1 \cdot 10^3$; TC=4 at range $4 \cdot 10^2$
6. goniometer speed 0.5 °2Θ/min
7. paper speed 20 mm/min
8. usually only the range 7-11 °2Θ is measured

---

sample preparation, the fraction < 2 μm was saturated with K^+-ions. A parallel set of samples was saturated with Mg^{2+}-ions. If smectite or vermiculite is present, the width of the 10Å-peak will decrease after K^+-saturation, while Mg^{2+}-saturation does not affect the 10Å- peak.

In order to interpret the IC indices measured in Utrecht in terms of metamorphic zonation, using the boundary values of Kisch (see Table 4-I), the X-ray diffractometer in Utrecht was calibrated against the diffractometer at the laboratory of Kisch (University of the Negev, Beer-Sheva, Israel). This was done using polished rock slabs with varying illite crystallinity. As the IC-indices measured in Utrecht and in Beer-Sheva were exactly the same, the boundary values of the anchizone cited by Kisch can also be used in this study.

A set of house standards with known diagenetic or metamorphic grade was used to check the validity of the illite crystallinity results. These standards include a diagenetic shale (Mo2) and a greenschist facies phyllite (P251) (see Table 4-IV). The IC-index of a large single crystal of muscovite from a pegmatite (M1) has also been measured, in order to measure the maximum crystallinity (narrowest peak) of muscovite. The IC- indices of the standards are in good agreement with their degree of diagenesis or metamorphism, while the crystallinity of the muscovite crystal is the same as the value quoted by Kisch (1983, p. 348-350).

The measured IC indices are given in Table 4-V and Fig. 4-1. There is no significant difference between the K^+ and Mg^{2+} saturated samples. This means that clay minerals like smectite and vermiculite are

TABLE 4-IV. Internal illite crystallinity standards

zone	sample no.	<2μm K	<2μm Mg	2-6μm [°2Θ]
1. diagenesis	Mo2	0.530	0.530	0.580
2. greenschist facies (epizone)	P251	0.190	0.190	0.190
3. muscovite single crystal M1 (1 cm^2): 0.105 °2Θ				

1: Shale from the North Sea, maximum paleotemperature ca. 130 °C.
2: Phyllite from the Massana Anticline: epidote + allanite porphyroblasts
3: Flake from a 10 cm large crystal from a pegmatite (value quoted by Kisch, 1983 p. 348-350, for "maximum" illite crystallinity: 0.11 °2Θ)

TABLE 4-V Illite crystallinity indices, Seo Formation, Orri Dome. See fig. 4.1 for the location of the section. (all values in °2Θ)

	km	sample no.	<2µm K	<2µm Mg	2-6µm	6-50µm
Section A-A'	1.100	P113	0.213	0.218	0.200	0.170
	3.450	P106	0.218	0.195	0.200	0.218
	5.550	P99	0.243	0.275	0.213	0.158
	7.950	P98	0.230	0.225	0.200	0.155
	9.500	P89	0.205	0.213	0.188	0.155
	10.550	P78	0.300	0.325	0.213	0.195
	11.650	P77	0.230	0.230	0.213	0.163
	12.500	P74	0.225	0.213	0.213	0.170
	23.000	P189	0.213	0.213	0.193	0.138
	23.750	P185	0.205	0.213	0.200	0.150
Section B-B'	3.650	P18	0.210	0.260	0.180	-
	6.950	P31	0.250	0.263	0.200	0.163
	7.900	P33	0.243	0.225	0.195	0.150
	8.400	P34	0.250	0.255	0.200	0.175
	8.900	P35	0.243	0.250	0.200	0.150
	9.550	P37	0.238	0.238	0.205	0.188
	9.650	P48	0.238	0.263	-	0.193
	10.600	P50	0.305	0.300	0.225	0.180
	10.650	P59	0.268	0.275	0.238	0.188
	10.750	P60	0.218	0.205	0.200	0.168
	11.050	P51	0.288	0.250	0.205	0.188
	11.200	P52	0.263	0.313	0.218	0.200
	11.750	P55	0.225	0.250	0.213	0.175
	11.750	P57	0.225	0.283	0.225	0.168
	11.850	P54	0.225	0.250	0.213	0.175
	11.850	P61	0.243	0.263	0.213	0.163
	23.000	P192	0.230	0.230	0.205	0.155
Section C-C'	2.500	P150	0.243	0.263	0.225	0.205
	2.500	P151	0.275	0.263	0.213	0.168
	2.500	P152	0.263	0.258	0.218	0.163
	3.050	P153	0.275	0.293	0.238	0.188
	3.050	P154	0.300	-	0.238	0.175
	3.050	P155	0.300	0.305	0.238	0.188
	5.100	P217	0.268	0.275	0.225	0.183
	5.100	P218	0.288	0.300	0.225	0.205
	6.450	P215	0.313	0.275	0.193	0.155
	6.750	P220	0.305	0.268	0.225	0.195
	6.750	P221	0.313	0.293	0.250	0.205
	6.750	P222	0.300	0.288	0.213	0.200
	7.300	P213	0.263	0.288	0.218	0.195
	7.300	P214	0.275	0.275	0.200	0.180
	7.800	P208	0.318	0.318	0.250	0.195
	8.350	P211	0.288	0.263	0.238	0.200
	11.300	P226 *)	0.238	0.305	0.230	0.188
	11.550	P236 *)	0.263	0.280	0.250	0.193
	12.150	P230 *)	0.208	0.230	0.193	0.155
	12.300	P231*)	0.225	0.230	0.200	0.145

*) Seo Formation, Rabassa Dome, Andorra

absent, and that there was no significant loss of K^+ions during weathering and sample preparation.

Weathering can reduce the crystallinity of illite, although the effect of weathering is usually within the standard deviation of the IC measurements (Schramm, 1981). The IC indices of the samples from the Pallaresa Anticlinorium and the Massana Anticline fall within the epizone field; this is in good agreement with a greenschist facies metamorphic grade, which has been determined using mineral assemblages. Apparently the IC indices of these rocks have not been affected by weathering. As the samples from the Orri Dome were collected in outcrops of similar quality, it can be assumed that weathering did not significantly affect their IC index either.

The grainsize of the detrital micas in the slates is in the range 10-100 μm. In the fractions 2-6 μm and 6-50 μm there will be an increased contribution of the detrital micas. The IC index decreases with increasing grainsize. The fraction 6- 50 μm, which consists almost entirely of detrital micas, shows IC indices of 0.15-0.20 °2Θ, well within the epizone field. This suggests that the detrital micas were derived from igneous rocks or from rocks with at least an epizonal grade of metamorphism.

The total range of IC indices of the grainsize fraction <2 μm of all slate samples is 0.23-0.30 °2Θ. The average IC index of the K+ saturated fraction <2 μm of the Orri- Dome samples is 0.26 ± 0.03 °2Θ. The low-grade boundary of the anchizone lies at 0.37 °2Θ, while the anchizone-epizone boundary lies at 0.205 °2Θ (Kisch, pers.comm. 1986; Table 4-I). Therefore it can be concluded that the Seo Formation of the Orri Dome has been metamorphosed in the high-grade part of the anchizone. Within the Orri Dome, there is no significant trend in the IC indices with geographical position.

It is very difficult to connect illite crystallinity data to a temperature scale. Based on correlations between illite crystallinity, coalification and mineral zonations, Teichmüller et al. (1979, p.268) suggest that the anchizone represents a temperature range from ca. 200 °C to ca. 350 °C (Table 4-I). This would suggest paleotemperatures between 250 °C and 350 °C for the rocks of the Orri Dome. For a geothermal gradient of 30 °C/km this would imply pressures on the order of 200-300 MPa. However, this is a maximum estimate, as the

geothermal gradient during Variscan metamorphism has probably been much higher (Zwart, 1962, 1979).

4.2.4 Conclusions on metamorphic grade

Illite crystallinity measurements indicate metamorphism in the high-grade part of the anchizone. This is confirmed by the absence of detrital minerals such as K-feldspar and Ca-plagioclase and of clay minerals such as smectite, and by the absence of epidote. A tentative estimate for the paleotemperature is 250-350 °C. The paleopressure probably did not exceed 300 MPa. The high degree of crystallinity of the detrital micas indicates that they originate from igneous or metamorphic rocks with at least epizonal grade of metamorphism.

4.3 METAMORPHIC MONAZITE

4.3.1 Metamorphic monazite: survey of literature

Monazite is common as an accessory mineral in igneous and metamorphic rocks. It is resistant to weathering and therefore it is quite common as a detrital mineral in sediments. Due to its high specific gravity (5.0-5.3 g/cm^3) it is often concentrated in deposits from high-energy environments such as stream and beach sands. Metamorphic monazite is quite common in the amphibolite facies zone and higher grades; in the greenschist facies zone monazite is rare (Overstreet, 1967). So far no secondary monazite from sub-greenschist rocks has been described. However, primary monazite can form in epithermal veins (Overstreet, 1967), and synthetic monazites have been formed at temperatures as low as 200 °C (Anthony, 1957 - quoted in Deer et al. 1962 p.341).

Monazite is a rare-earth element (REE) phosphate with a general chemical formula $REE(PO_4)$, the main REE being Ce and La. The REE may be substituted by Th^{4+}, Ca^{2+} and Y^{3+}, and some phosphorous may be substituted by Si^{4+} (Overstreet, 1967; Mohr, 1984). In all modes of occurrence, monazite shows an increase in Th-content with increasing temperature of formation, from none in hydrothermal crystals to over 10 wt% ThO_2 in igneous rocks (Overstreet, 1967).

Metamorphic monazites have been described by various authors (Overstreet, 1967; Donnot et al., 1973; Serdyuchenko and Kochetkov, 1974; Izrailev and Solov'eva, 1974; Mohr, 1983, 1984). All these monazites occur in metapelites. The monazites are often poikiloblastic (Serdyuchenko and Kochetov, 1974; Izrailev and Solov'eva, 1974) but they can also be idiomorphic (Mohr, 1984) or grow in spherical nodules (Donnot et al., 1973). They are usually too large to be of sedimentary origin. Mohr (1984) describes zoned porphyroblasts from the staurolite-kyanite zone. The Th-content of these zoned porphyroblasts decreases from core to rim, correlated with a small decrease of average atomic number of the REE.

Overstreet (1967) has proposed the following model for the metamorphic evolution of monazite: detrital monazite is unstable in the early stages of diagenesis and metamorphism; it breaks down and shares its components with other minerals such as allanite, sphene and clay minerals. At higher grades of metamorphism monazite becomes stable again and starts to form at a few centres of crystallisation. The Th-content increases with metamorphic grade. The main sources for REE and Th are clay minerals, micas and allanite, while P is mainly derived from apatite. Finally the rock may contain considerably more monazite than it had originally detrital monazite (Overstreet, 1967). The present study leads to a slight modification of this model.

4.3.2 Monazites of the Orri Dome

Monazite crystals, large enough for observation in the optical microscope, were identified in thin sections from the area around Albet (central part of the Orri Dome), and north of Seu d'Urgell (E. part of the Orri Dome). The crystals are 100- 400 μm long, elongated, strongly poikiloblastic grains (Fig. 4.2). They have a greenish-brown color, very high refractive index and moderately high birefringence; $2V_{\gamma}<20°$. The identification was confirmed with X-ray diffraction and microprobe analyses.

The cleavages in the slates are all wrapped around the monazite crystals, and strain shadows have developed (Fig. 4.2). This indicates that the monazite has been formed before the cleavages were developed. The inclusions form an internal fabric, usually parallel to the long dimension of the porphyroblast. There is no relation between the

a

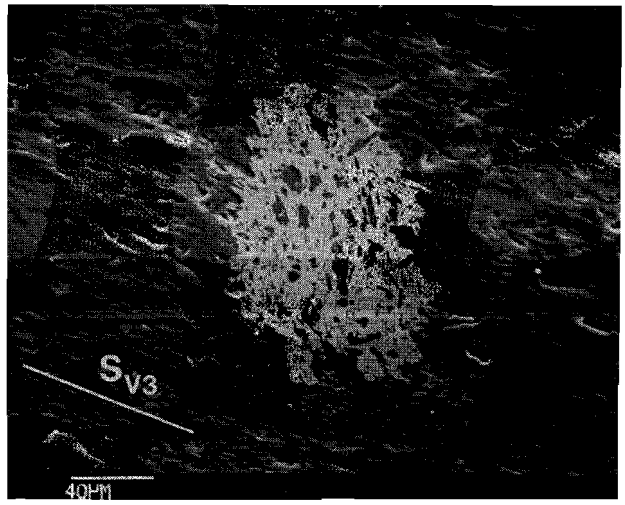

b

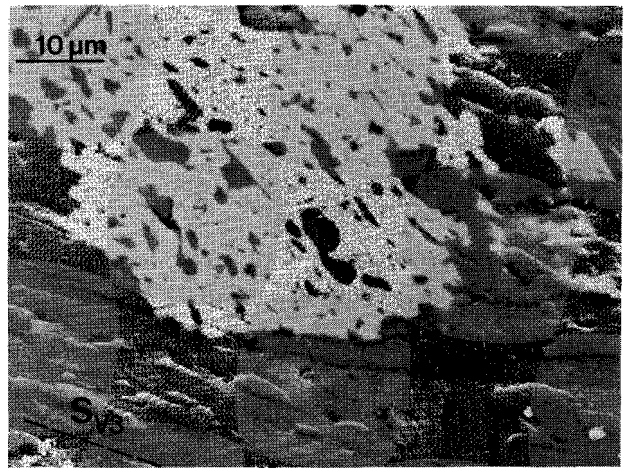

FIGURE 4.4. a. micrograph of a porphyroblast from an outcrop in the centre of the Orri Dome, showing the internal fabric. The horizontal bands are an artefact. b. Detail of a porphyroblast showing the relation between internal and external fabric. (SEM micrographs showing both SE and BSE contrast)

c

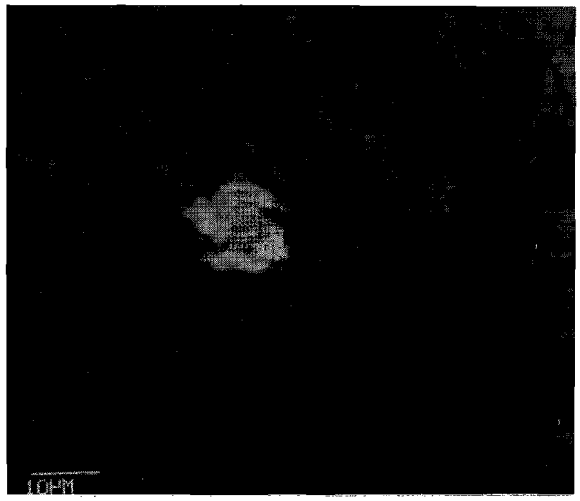

d

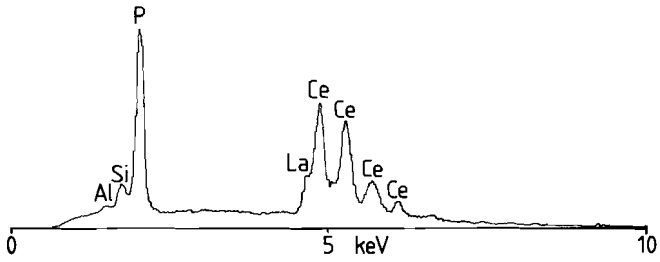

e

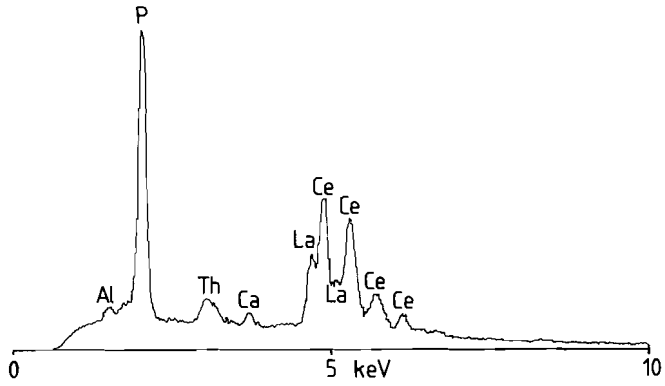

c. Small monazite porphyroblast (BSE image). d. EDS spectrum of the large porphyroblast of Fig. 4.4b; P, Ce and La are present, but no Th is detected. e. EDS spectrum of the small porphyroblast of Fig. 4.4d; Th and Ca are now clearly detected.

shape of the porphyroblasts or the internal fabric, and the crystallographic orientation of the crystal.

A set of polished thin sections from a traverse from Seu d'Urgell to Albet was studied in the scanning electron microscope (SEM). In back-scattered electron (BSE) images the contrast is due to the mean atomic number of the material (Hall and Lloyd, 1981). Due to its very high mean atomic number, monazite is extremely bright in BSE-images; thus it is easy to find even very small (<10 μm) isolated monazite grains.

Monazite crystals were found in every sample, most were too small to be identified in the optical microscope. The large (400 μm) poikiloblastic grains (Fig 4.4) are most abundant in the area around Albet and Castellbo. They are the same type as the monazites identified in the optical microscope. The size of the porphyroblasts varies strongly in each sample, with small grains (10 μm) present in all samples.

The inclusions in monazite are quartz, chlorite, muscovite, and albite, minerals that also form the matrix. The inclusions are not randomly oriented but form an internal fabric (Fig. 4.4a,b), usually parallel to the long axis of the monazite crystal. At the rim of the crystal the matrix grains are partially enclosed in the monazite (Fig 4.4a,b). In the strain shadows around the monazites a pre-cleavage fabric is visible (Fig. 4.4a) which is parallel to the sedimentary layering (see section 5.5.1). There is a clear continuity between this pre- cleavage fabric and the internal fabric of the monazites. Both in the matrix and inside the monazites the phyllosilicates are aggregates of mica and chlorite. The phyllosilicates outside the monazites are deformed during slaty cleavage development; however, the phyllosilicate inclusions in monazite are strainfree.

EDS-microanalyses show that the main rare-earth elements are Ce and La; Pr, Nd and Sm could also be identified. Most of the larger poikiloblastic grains show no Th or Ca. Sometimes Si is detected, but this might well be caused by the silicate inclusions. Detailed element mapping of Th has revealed a zonation in some of the medium-sized (10-30 μm) porphyroblasts (Fig. 4.5). These porphyroblasts show a core which is relatively rich in Th; sometimes Ca is detected (Fig. 4.4e). The poikiloblastic rim is virtually free of Th.

The poikiloblastic monazite is clearly of metamorphic origin: the grains are much too large to be of detrital origin, they have ragged outlines, and detrital grains from the matrix are also present as

inclusions, or straddle the monazite-matrix boundary. Similar poikiloblastic monazite porphyroblasts from metamorphic pelites have been described by Serdyuchenko and Kochetkov (1974) and Izrailev and Solov'eva (1974). The fact that the cleavages are wrapped around the porphyroblasts and strain shadows have developed indicates that the monazite has grown prior to cleavage development. This is supported by the presence of undeformed phyllosilicate aggregates inside the monazite, while the same aggregates in the matrix have been deformed during cleavage development (see chapter 5).

All phyllosilicates in the slate are aggregates of chlorite and mica. Chlorite-mica aggregates are formed during diagenesis and incipient metamorphism (Craig et al. 1982; Van der Pluijm & Kaars Seijpesteijn, 1984; Gregg, 1986; Dimberline, 1986; see section 2.1.2). As complete chlorite-mica aggregates are enclosed in the monazites, the formation of the monazite porphyroblasts can be timed after the diagenesis and incipient metamorphism of the rock. The fact that the chlorite-mica inclusions are undeformed confirms the pre-kinematic growth of the monazite.

The smaller monazite porphyroblasts show a core which contains a few percent of Th. This core is smaller than the average grain size of the matrix and shows no inclusions. According to Overstreet (1967) monazite containing a few percent of Th can only form at high temperatures (corresponding to amphibolite facies zone and higher grades). This suggests that these Th-containing cores were not formed in situ but were deposited as detrital grains originating from some high-grade hinterland. Such a provenance has also been suggested by the high crystallinity of the detrital micas (see section 4.2.4). The size of the cores would be in agreement with a detrital origin.

The monazite overgrowths on the detrital cores contain little or no Th. The overgrowths are poikiloblastic and are similar to the larger porphyroblasts described above. Following similar lines as mentioned above, these Th-free overgrowths can be interpreted to be of metamorphic origin, postdating diagenesis and incipient metamorphism, and predating the cleavage development. The absence of Th is in agreement with formation under (very) low-grade metamorphic conditions (Overstreet, 1967).

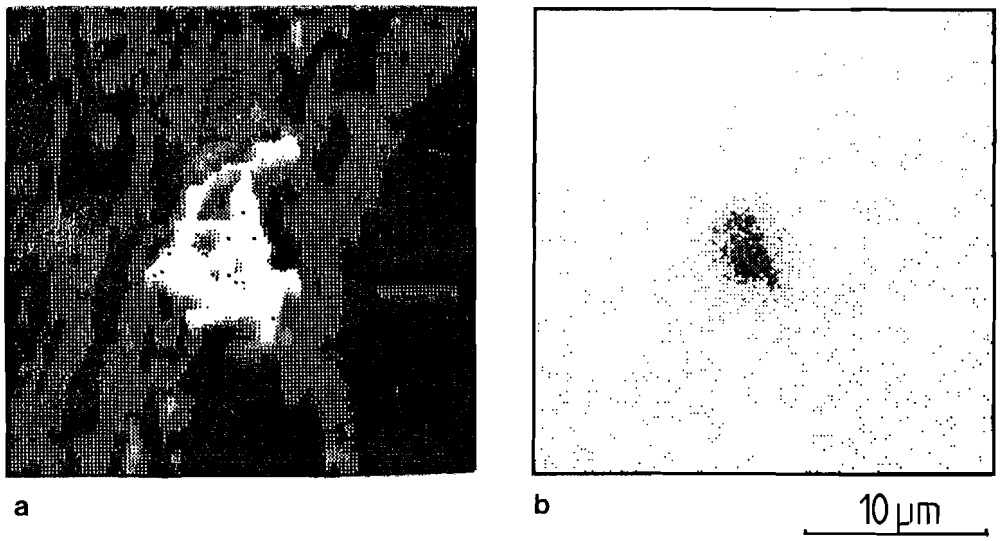

FIGURE 4.5 a. digitized SEM image (BSE) of a small monazite porphyroblast (white). b. Element map of Th of the same grain. Th is concentrated in the core; no Th is detected in the poikiloblastic rim.

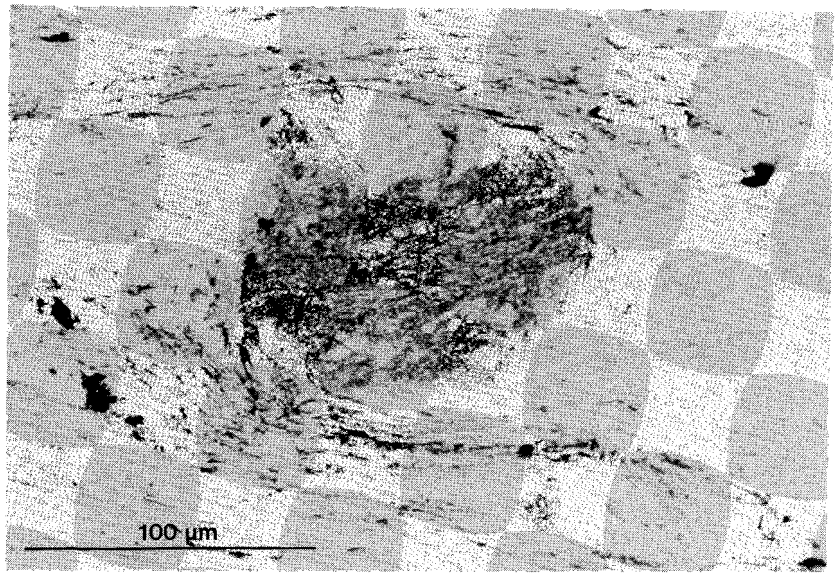

FIGURE 4.6 Optical micrograph of an epidote porphyroblast from the Massana Anticline (plane polarised light)

4.3.3 Allanite porphyroblasts in the Massana Anticline

The Seo Formation of the Massana Anticline (Andorra; see Fig. 4.1) is lithologically similar to that of the Orri Dome. Bulk chemical analyses of rocks of both areas shows no significant differences (see Table 4-II). However, the metamorphic grade is different. The main minerals of the rocks of the Massana Anticline are muscovite, chlorite, quartz, albite and epidote. The presence of epidote and chloritoid, and the absence of biotite indicate lower greenschist facies metamorphism. Another difference is the absence of the REE-mineral monazite in the Massana Anticline, and the presence of REE-rich allanite porphyroblasts instead. Allanite (orthite is sometimes used as a synonym) is a member of the epidote group. Compared to epidote, Al^{3+} in allanite is partly substituted by Fe^{2+}, compensated by replacement of Ca^{2+} by La^{3+}, Ce^{3+} and Th^{4+}. Allanite occurs as an accessory mineral in a wide variety of rocks. (Deer et al. 1986).

The allanites of the Massana Anticline grew over the slaty cleavage microstructure. The minerals of the matrix are recogniseable as inclusions and ghost structures in the allanites (Fig. 4.7). The epidote porphyroblasts clearly predate the slaty cleavage (Fig. 4.6).

EDS analyses of the allanites (Fig 4.8) show that La and Ce are the major REE; the allanite porphyroblasts themselves contain little or no Th. They are overgrown by a narrow rim of REE-free epidote. Sometimes there are very small patches of Th-rich allanite, which are usually concentrated in the epidote rim or at the allanite-epidote boundary.

Based on the data presented above, a time sequence for the growth of the allanites can be proposed: after development of the main-phase slaty cleavage allanite started to grow, rich in Ce and La, but low in Th. Very small Th-rich allanite grains grew mainly in a later stage. In a final stage a rim of pure epidote was formed. Because there are both pre-cleavage epidote porphyroblasts and post-cleavage epidote overgrowth, it is likely that the allanites grew under lower greenschist conditions.

4.3.4 REE distributions

The concentrations of REE in the rocks of the Orri Dome have been measured in the samples studied with SEM. Also, a set of

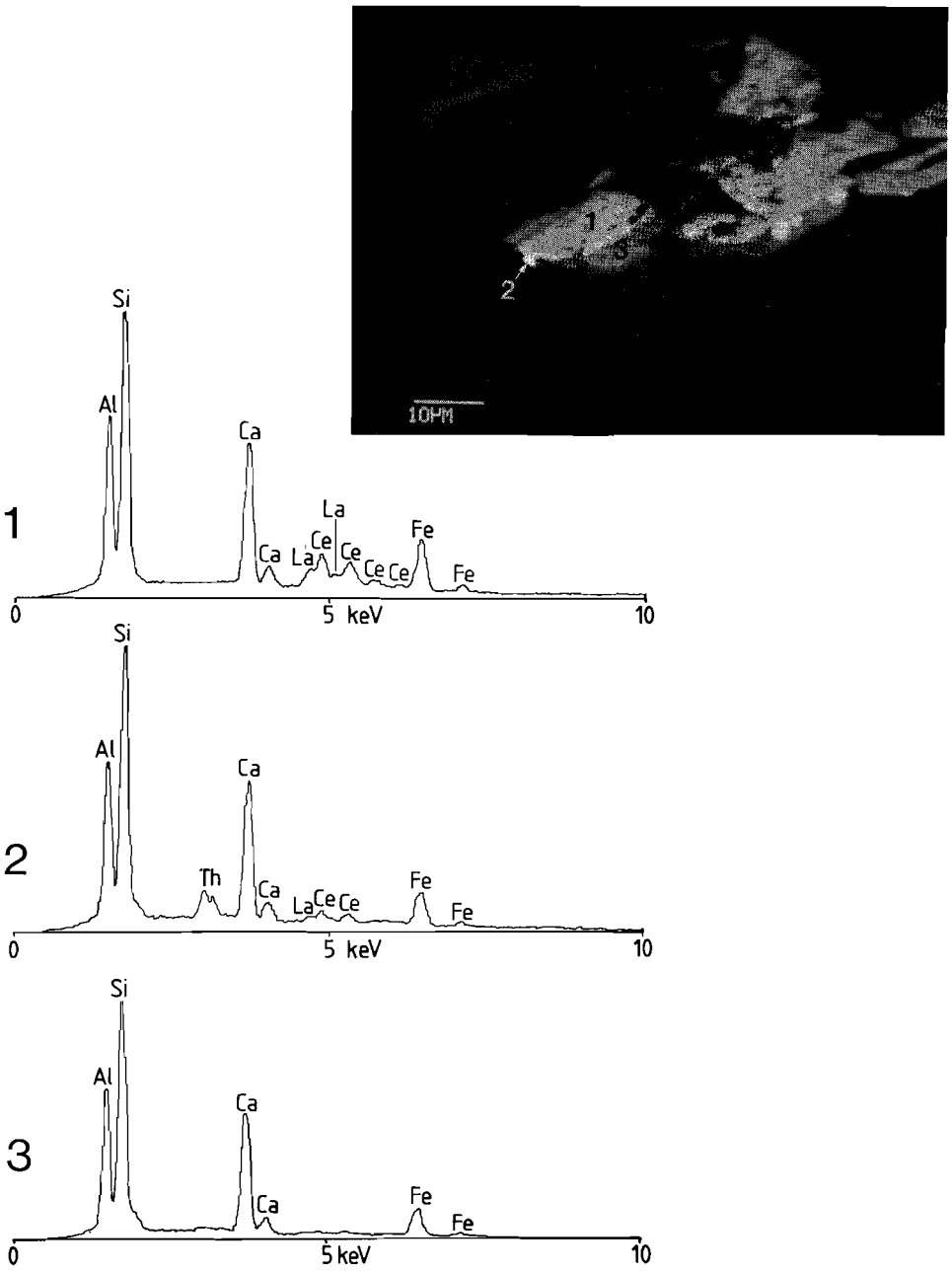

FIGURE 4.7 Post-kinematic allanite porphyroblast from the Massana Anticilne, showing inclusions and ghost structures (SEM micrograph, BSE image). black: quartz, albite, muscovite; drak gray: chlorite; EDS-spectra: spot 1: Allanite free of Th; spot 2: Th-containing allanite; spot 3: epidote without Th or REE.

samples from the Massana Anticline has been analysed. The results are given in Table 4-VI. In general the REE concentrations show no significant relationships with geographical position, lithology, or monazite porphyroblast size. There is no significant difference between the rocks from the Orri Dome and the rocks from the Massana Anticline.

Chondrite normalised REE patterns are given in Fig. 4.8. When these patterns are compared with international shale standards, it is clear that the curves coincide for the heavier REE such Tb, Yb and Lu. However, the Pyrenean rocks show increased concentrations of La, Ce, Sm and Eu. Due to this enrichment of the lighter REE the chondrite-normalised REE-patterns of the Pyrenean rocks lack the dip in the curve at Eu which is typical for most REE-patterns of shales.

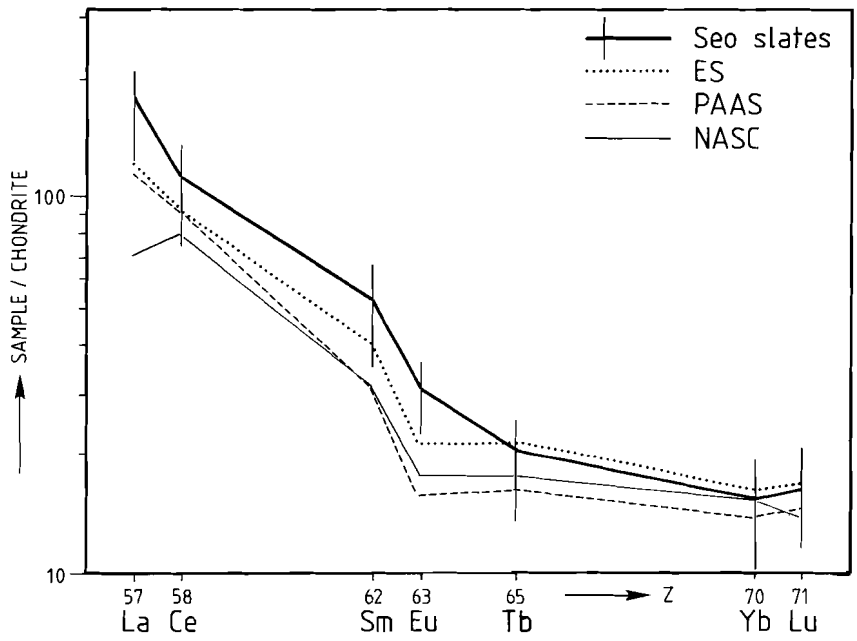

FIGURE 4.8. Chondrite-normalised REE-patterns. Chondrite values from Haskin and Haskin (1966). The mean values and total range of the Seo Slates from the Orri Dome and Massana Anticline are plotted together with international shale standards: ES: European Shales (Haskin and Haskin, 1966); PAAS: Post-Archaean Australian Shales (Nance and Taylor, 1976); NASC: North-American Shale Composite (Haskin and Haskin, 1966).

TABLE 4-VI. REE concentrations (ppm) in Cambro-Ordovician rocks from the Central Pyrenees, Spain and Andorra. See Fig. 4.1 for locations of the sections.

sample	km	La	Ce	Sm	Eu	Tb	Yb	Lu
Orri Dome, section B-B':								
HH-P27	4.150	59.980	98.760	10.300	2.109	1.206	3.490	0.736
HH-P26	5.250	58.590	97.240	10.070	2.228	1.170	3.780	0.935
HH-P25	6.150	57.800	90.450	9.440	1.920	0.941	2.380	0.601
HH-P24	7.000	55.130	90.400	8.800	1.852	1.036	3.180	0.367
HH-P23	7.100	66.290	109.300	10.590	2.582	1.040	3.450	0.710
HH-P22	8.050	70.390	120.000	12.000	2.471	0.800	3.950	0.680
HH-P21	8.700	53.540	104.990	8.850	2.020	0.865	3.180	0.394
HH-P20	9.400	56.710	106.990	9.570	2.250	0.930	3.240	0.503
HH-P19	9.550	52.390	91.930	8.250	1.859	1.040	3.150	0.424
HH-P18	9.550	36.810	60.920	6.370	1.390	0.799	2.110	0.324
HH-P17	10.100	70.110	107.100	10.800	2.130	0.802	2.530	0.811
HH-P16	10.100	89.380	135.390	13.500	2.671	1.304	4.180	0.601
HH-P15	10.100	58.750	101.700	8.720	2.398	1.080	3.370	0.529
HH-P14	10.650	49.570	89.280	8.120	1.918	0.910	2.740	0.253
HH-P13	11.500	61.110	90.870	9.350	2.190	1.099	2.383	0.655
Orri Dome, section C-C':								
HH-P12	7.300	59.000	88.760	8.735	1.969	0.916	2.820	0.557
Massana Anticline, section D-D':								
HH-P 1	0.150	52.770	87.850	7.580	1.919	0.730	1.830	0.219
HH-P 2	0.250	57.350	101.000	8.750	2.108	0.710	3.080	0.538
HH-P 3	0.870	61.270	103.890	0.000	2.119	0.700	2.380	0.725
HH-P10	1.160	69.730	112.490	10.690	2.129	1.243	2.950	0.865
HH-P 4	1.930	51.460	86.300	7.610	1.729	0.924	2.440	0.595
HH-P 5	2.430	40.920	64.870	6.300	1.593	0.639	1.980	0.393
HH-P 7	2.440	60.350	104.990	9.272	2.049	0.970	3.210	0.690
HH-P 6	2.460	48.460	80.030	6.982	1.677	0.575	1.634	0.137
HH-P 8	2.660	41.960	68.690	6.630	1.469	0.833	2.261	0.260
HH-P 9	2.820	17.540	24.420	3.390	0.804	0.420	2.450	0.487

Assuming that the rocks of the Seo formation had an average shale composition at the time of deposition, the high concentrations of light REE indicate an influx of these elements after deposition. The enrichment in REE took place in the Orri Dome as well as in the Massana Anticline. The highest REE concentrations are found in sample HH-P.16 from the Orri Dome, which contains a pre-cleavage quartz vein. This suggests that the influx of light REE is associated with a pre-cleavage hydrothermal event. The pre-cleavage growth of monazites, minerals rich in light REE, can be correlated with this hydrothermal event, and this

also supports a pre-cleavage timing of the event.

No monazites have been encountered in the Massana Anticline. However, it is likely that the rocks of the Massana Anticline did contain monazites in an earlier stage of their metamorphic history, because they show exactly the same chemistry and REE-distributions as the rocks of the Orri Dome.

4.3.5 Metamorphic evolution of the REE-minerals monazite and allanite

Based on the assumption that the slates of both areas represent two stages in a prograde metamorphic evolution of the rocks of the Seo Formation, the Orri Dome representing the anchizone stage and the Massana Anticline representing the lower greenschist facies stage, a model can be made for the low-grade metamorphic evolution of the REE-minerals.

At the time of deposition, the rocks of the Seo Formation contained small (<10 μm) clastic monazite grains. These grains were relatively rich in Th and originated from a high-grade hinterland. After diagenesis and incipient metamorphism, but prior to the Variscan mainphase deformation, an influx of lighter REE led to the growth of large (up to 400 μm) poikiloblastc monazites, which nucleated on the small detrital grains. The metamorphic grade during this event was anchizone at most. Later the monazite breaks down completely, and, after the mainphase deformation under lower greenschist facies metamorphic conditions, metamorphic REE-rich allanite is formed. The allanite is generally low in Th, but eventually some small Th-allanites are formed.

The metamorphic evolution of monazite described above is somewhat different from the model proposed by Overstreet (1967). Instead of a breakdown of detrital monazite during the first stages of metamorphism, the rocks of the Orri Dome show extensive growth of monazite. However, during prograde metamorphism in the lower greenschist facies, the monazites are replaced by allanites, as is predicted by the model of Overstreet (1967). The very low Th-content of the metamorphic monazites from the anchizone is also in agreement with the model of Overstreet (1967).

4.4 CONCLUSIONS

The rocks of the Seo formation of the Orri Dome have been metamorphosed in the anchizone. The same rocks in the Pallaresa Anticlinorium and the Massana Anticline have been metamorphosed in the lower greenschist facies zone.

A hydrothermal event, which took place after diagenesis and incipient metamorphism, but prior to the development of the mainphase cleavage, led to an enrichment in the lighter REE (La, Ce, Sm, Eu) in both the Orri Dome and the Massana Anticline. The metamorphic grade during this event was anchizone at most. During this very low-grade hydrothermal event Th-free monazite porphyroblasts were formed, nucleating on small Th-containing detrital monazites. During prograde metamorphism in the lower greenschist facies the monazites are replaced by allanites.

It is not clear whether the hydrothermal event took place prior to the Variscan orogeny or during an early Variscan stage.

The detrital components of the rocks of the Seo Formation were derived from a hinterland of high-grade metamorphic or igneous rocks.

Chapter 5
SLATY CLEAVAGE DEVELOPMENT

5.1 INTRODUCTION

The mainphase cleavage in the Orri Dome has been described in the field as a slaty cleavage in the pelitic layers and a spaced (disjunctive) cleavage in the siltstone layers (e.g. Speksnijder, 1986). In the optical microscope the slaty cleavage appears to be a disjunctive cleavage.

Within a single thin section the cleavage intensity can vary from a weak cleavage in strain shadows to an intense, almost continuous cleavage at the edges of rigid objects. Undeformed grains are present as inclusions in pre-kinematic monazite porphyroblasts. Therefore the rocks from the Orri Dome can be used to investigate the development of slaty cleavage as a function of strain alone, as all other parameters can be assumed to be constant within such a small volume of rock.

Some information on the role of metamorphic grade on cleavage development can be obtained by comparing the disjunctive slaty cleavage from the anchizonal Orri Dome with the continuous cleavage *s.s.* in exactly the same rocks from the lower greenschist facies in the Pallaresa Anticlinorium.

The aim of this chapter is to describe the morphology of the slaty cleavage in the pelitic rocks of the Seo Formation, and to discuss its development. The study concentrates on the slates in the central part of the Orri Dome, where the mainphase cleavage is the only tectonic foliation.

5.2 FIELD DESCRIPTION OF THE CLEAVAGES

5.2.1 Mainphase cleavage

The first deformation structures on the scale of an outcrop are the mainphase structures. Small-scale folds are relatively rare, but the mainphase cleavage (S_{V3}) is always present. In the north-central area of

the Orri Dome, around Seix, the mainphase cleavage is the only deformational structure. The rocks in this area are mainly slates and silty slates; pure quartzites are rare. The mainphase cleavage in the pelitic parts is homogeneous and continuous on the scale of the hand specimen. In the silty layers a spaced cleavage occurs, with a weak continuous cleavage *s.l.* in the microlithons. Cleavage refraction towards a high angle to bedding occurs when the cleavage crosses a silty layer (Fig. 5.1).

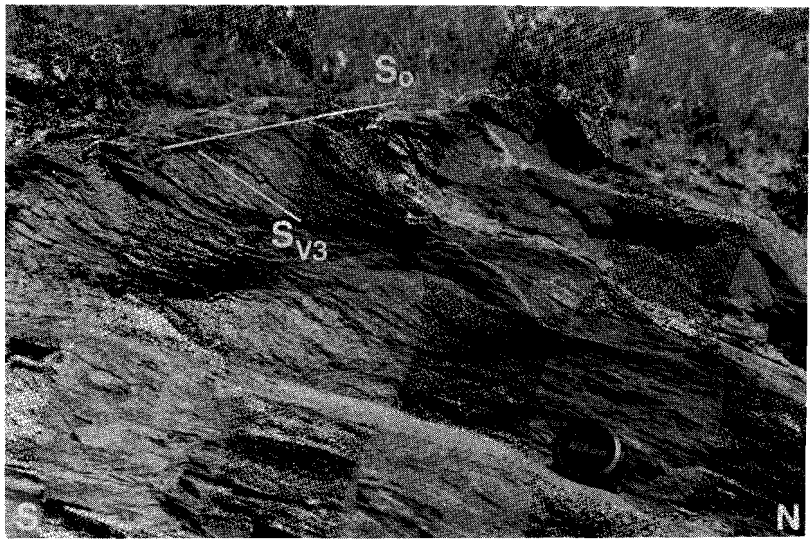

FIGURE 5.1. Mainphase cleavage (S_{V3}) in the central part of the Orri Dome. Bedding is subhorizontal. Cleavage refraction occurs in the silty layers.

In regions where the Seo Formation contains more silt, e.g. in the south and the east of the Orri Dome, the mainphase cleavage is often less obvious. In the silty layers it is a discrete disjunctive cleavage, and the cleavage is often absent in pure quartzite layers. In regions with alternating thin pelitic layers and quartzite layers, the rock seems to be uncleaved at first sight; however, microscopical investigation shows an almost continuous cleavage in the pelitic layers.

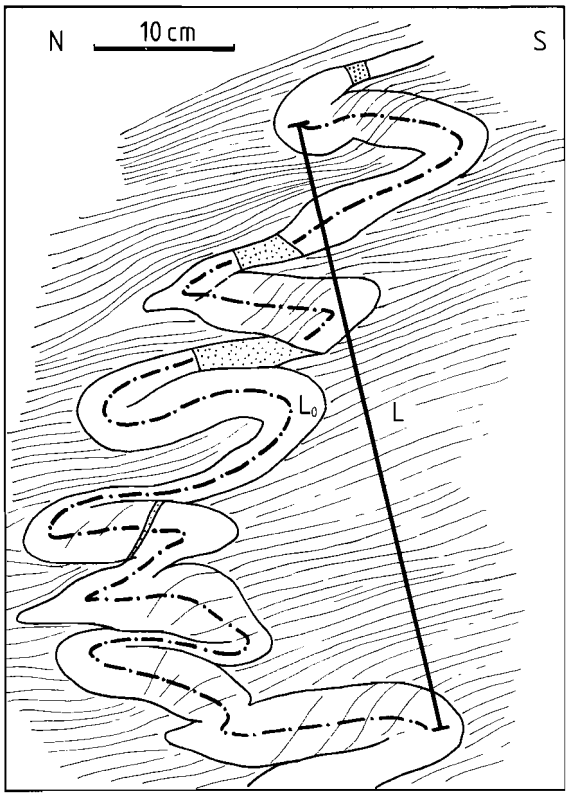

FIGURE 5.2. Folded quartzite layer in the Seo Formation. Facing is towards te South. Normal limbs are cleaved, overturned limbs are stretched and boudinaged. Quartz in boudin necks is stippled. The length along the folded layer (L_0) is160 cm, the present length normal to the cleavage (L) is 45 cm. (Tracing from a photograph)

5.2.2 Post-mainphase cleavages

In the pelitic layers the post-mainphase cleavages (mainly S_{V4}) are easily recognised as crenulations of the mainphase slaty cleavage (S_{V3}). In the area SE of La Seu d'Urgell several overprinting crenulation cleavages can be found. In the silty layers the post-mainphase cleavages are developed as a disjunctive cleavage, often at a high angle to bedding due to refraction. In that case the mainphase and the post-mainphase cleavages can only be distinguished if they have clearly different orientations.

In the sandy parts of the Seo Formation the post-mainphase cleavage is often developed as a disjunctive cleavage in quartzites and slates alike. The cleavage domains are bands rich in phyllosilicates, while the microlithons consist of either undeformed or folded bedding fragments.

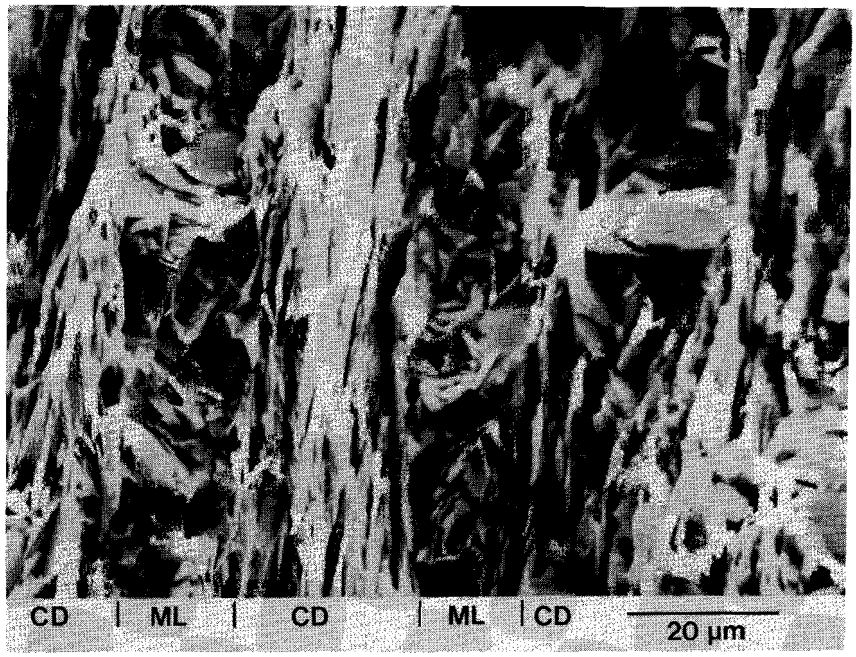

FIGURE 5.3. SEM micrographs (SE-image) of the slaty cleavage microstructure. a. Typical slaty cleavage microstructure in the pelitic layers of the Seo Formation in the Orri Dome. CD=cleavage domain; ML=microlithon.

b

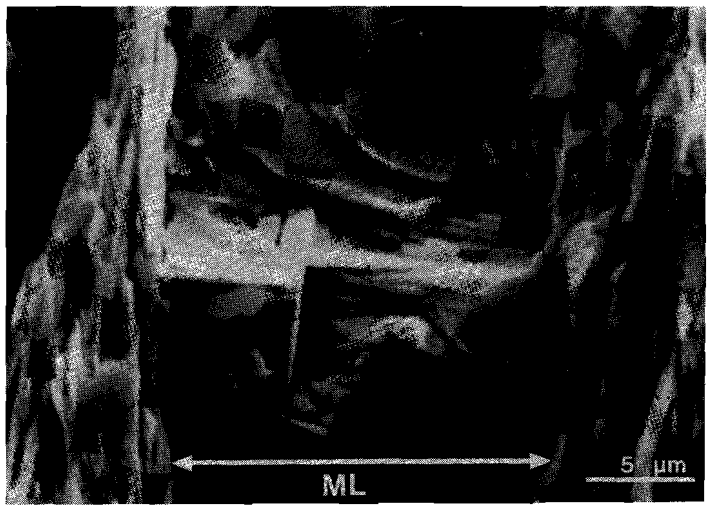

c

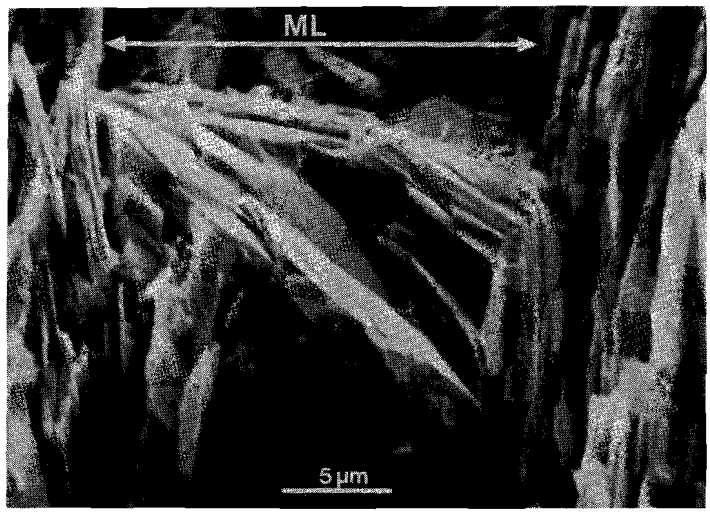

FIGURE 5.3 (continued). b. Detail of (a) showing a small mica parallel to cleavage in the middle of the microlithon. Some phyllosilicate flakes are bent into the cleavage domain. c. Phyllosilicate in a microlithon. The grain is partly bent into a cleavage orientation.

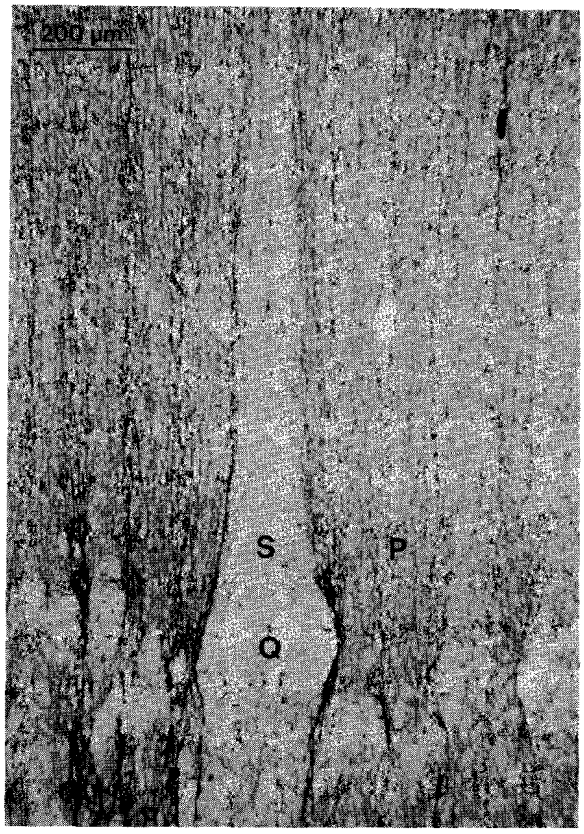

FIGURE 5.4. Inhomogeneous cleavage across a silty layer. In the pelitic layer (P) the cleavage is homogeneous, but near the quartz-rich layer (Q) cleavage bundles are formed. Strain shadows (S) are formed next to competent layer fragments. (optical micrograph, plane-polarized light)

5.2.3 Strain estimates

The amount of strain associated with slaty cleavage formation is very difficult to estimate, because good strain markers are absent. The only way to estimate the amount of shortening in the field is by analysing folded uncleaved quartzite layers in a slate matrix; if the cleavage is at a high angle to bedding this gives a reasonable estimate of the amount of shortening perpendicular to the cleavage. An example is given in Fig. 5.2; assuming the quartzite layer is deformed purely by buckling, this would give an estimated shortening perpendicular to the cleavage of 70%. However, the normal fold limbs have been shortened and show some cleavage, while the overturned limbs have been stretched and are boudinaged; therefore the value L_0 does not represent the true original length of the layer. Nevertheless, as shortening and extension in the limbs might cancel each other out, the true shortening perpendicular to the cleavage will probably be on the order of 60-70%, and it is obvious that there has been extension parallel to the cleavage. Other observations have yielded similar values.

5.3 SLATY CLEAVAGE MICROSTRUCTURE

5.3.1 Techniques

The microstructures of the slates have been studied with optical microscopy, scanning electron microscopy (SEM) and transmission electron microscopy (TEM).

In order to resolve the microstructure of the rock in the optical microscope, the thickness of the thin sections should be less than the average grainsize. As the average grainsize of the slates is on the order of 10-20 μm, the thin sections were polished down to a thickness of about 10 μm. The thin sections are cut perpendicular to the cleavage/bedding intersection.

Two types of samples were used in the SEM. In order to study the cleavage morphology, small pieces of rock (ca. 1 cm^3) were cut with a diamond blade, and cleaned in alcohol in an ultrasonic bath. Then the samples were fixed to SEM sample stubs and coated with gold. This gives good secondary electron (SE) contrast and resolution, but back-scattered electron imaging is not possible. Polished thin sections, coated with carbon, were used when detailed mineralogical or microchemical information was needed.

Most of the SEM work and energy-dispersive X-ray microanalysis (EDS) was performed on a Cambridge Stereoscan S-150 SEM fitted with a semiconductor detector for back-scattered electrons (BSE), and a Link Systems energy dispersive X-ray analytical system. Some work was done on a Jeol JXA-8600 Superprobe, with Tracor-Northern X-ray analysis and image processing facilities.

Most of the TEM study of the cleavage microstructure was done using the high-voltage TEM (HVTEM) of the "Stichting Geavanceerde Metaalkunde", installed in Apeldoorn, The Netherlands. An accelerating voltage of 0.9 MV was used. This gives good penetration of thicker parts of the specimen compared to the normal accelerating voltages of 100-200 kV, and therefore larger areas can be studied. Also, the HVTEM images give information on subgrains and crystal defects through electron diffraction contrast. In this way the gap between optical microscopy and the detailed TEM observations (chapter 6) can be bridged.

5.3.2 General microstructure

The average cleavage in the pelitic layers of the Seo Formation is an anastomosing discrete zonal disjunctive cleavage, with an average spacing of 20 μm (Fig. 5.3a). The cleavage domains are a few microns wide; they consist of muscovite and chlorite oriented with their basal planes parallel to the cleavage. They show relatively high concentrations of opaque minerals. The microlithons contain chlorite, muscovite, quartz and albite. The phyllosilicates in the microlithons have their basal planes at an angle to the cleavage.

The morphology of the cleavage varies strongly due to changes in lithology and the presence of rigid objects. Most samples show a fine lamination of silty layers. Within a slate layer the cleavage is quite

homogeneous, but on the transition to a silty lamina the cleavage planes converge to form bundles with a small spacing and a high cleavage intensity (Fig. 5.4). In between these bundles the cleavage has a large spacing and a low intensity. In the silty lamina the cleavage is only developed at the cleavage bundle; in between the bundles the cleavage is weak or absent. This morphology is similar to the "bundled slaty cleavage" of Southwick (1987). Similar variations in cleavage morphology can be observed around rigid objects (see 5.3.5).

5.3.3 Cleavage domains

The cleavage domains are formed by muscovite and chlorite oriented parallel to the cleavage; quartz and albite are absent. Optical micrographs (Fig 5.5) show an enrichment of opaque minerals in the cleavage domains. When studied in the SEM with BSE, which gives atomic-number contrast, the cleavage domains show many small grains of pyrite, haematite, ilmenite and other metal oxides. However, the concentration of these minerals does not seem high enough to explain the continuous dark seams along the cleavage domains. Part of the opaque material is probably formed by organic matter, which gives very low contrast in BSE-images, and cannot be analysed with EDS.

The phyllosilicates in the cleavage domains are strongly elongated and have aspect ratios up to 25:1 (Fig. 5.6, 5.7). Both their long axis and their basal planes are parallel to the cleavage. Muscovite is more abundant than chlorite. In the optical microscope and the SEM many phylloslicates seem to be pure muscovite or pure chlorite. However, detailed TEM-observations have revealed that some interlayers of chlorite or muscovite on a scale of 0.1-1 μm are always present.

5.3.4 Microlithons

The microlithons are mainly formed by phyllosilicates, quartz and albite. The phyllosilicates are always interstratifications of chlorite and muscovite, chlorite being the most abundant. The grains are often barrel-shaped and are elongated parallel to the cleavage; however, the basal planes are inclined to the cleavage. Some aggregates have both their long axis and the basal planes parallel to the cleavage (Fig. 5.7).

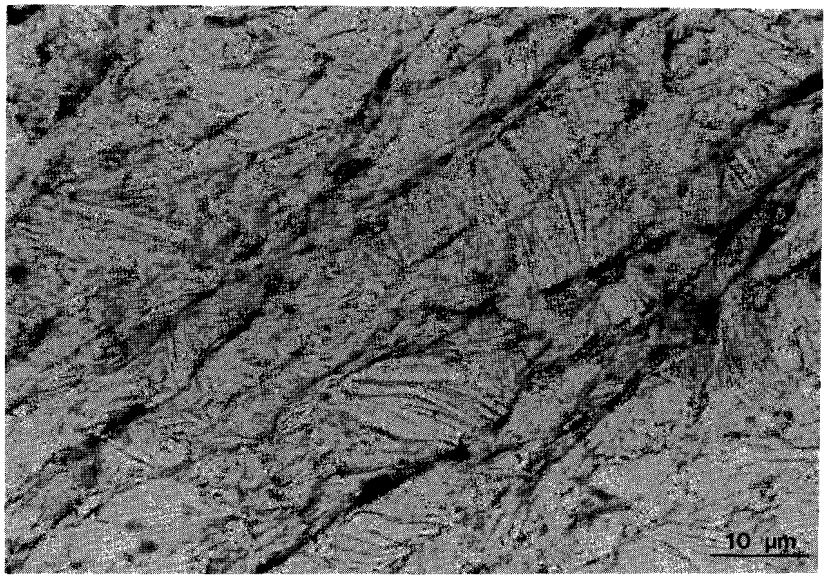

FIGURE 5.5. Optical micrograph (plane-polarized light) of the slaty cleavage fabric, showing enrichment of opaque minerals in the cleavage domains.

FIGURE 5.6. Long narrow muscovite (A) extending from a cleavage domain (B) into a microlithon (C) (optical micrograph, crossed nicols)

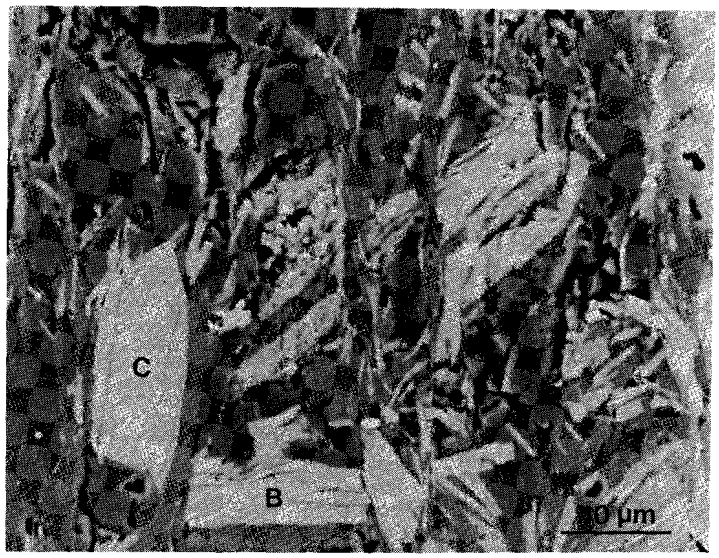

FIGURE 5.7. SEM-micrograph (BSE-contrast) of the slaty cleavage microstructure. Phyllosilicates in the cleavage domains are strongly elongated (A). Chlorite-mica aggregates in the microlithons can be oriented perpendicular to cleavage (B) or parallel to cleavage (C). (white = chlorite; light gray = muscovite; dark gray = quartz)

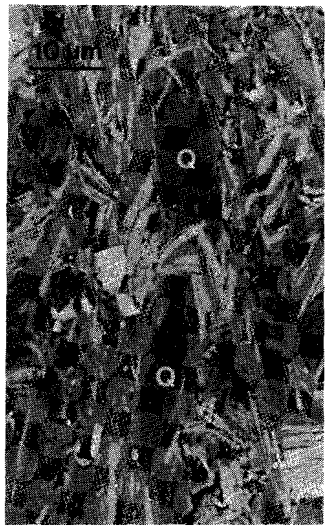

FIGURE 5.8 (left). Elongated quartz grains (Q) and deformed chlorite-mica aggregate in a microlithon from the cleavage bundle of Fig. 5.12b. (SEM-BSE micrograph; white = chlorite; light gray = muscovite; dark gray = quartz)

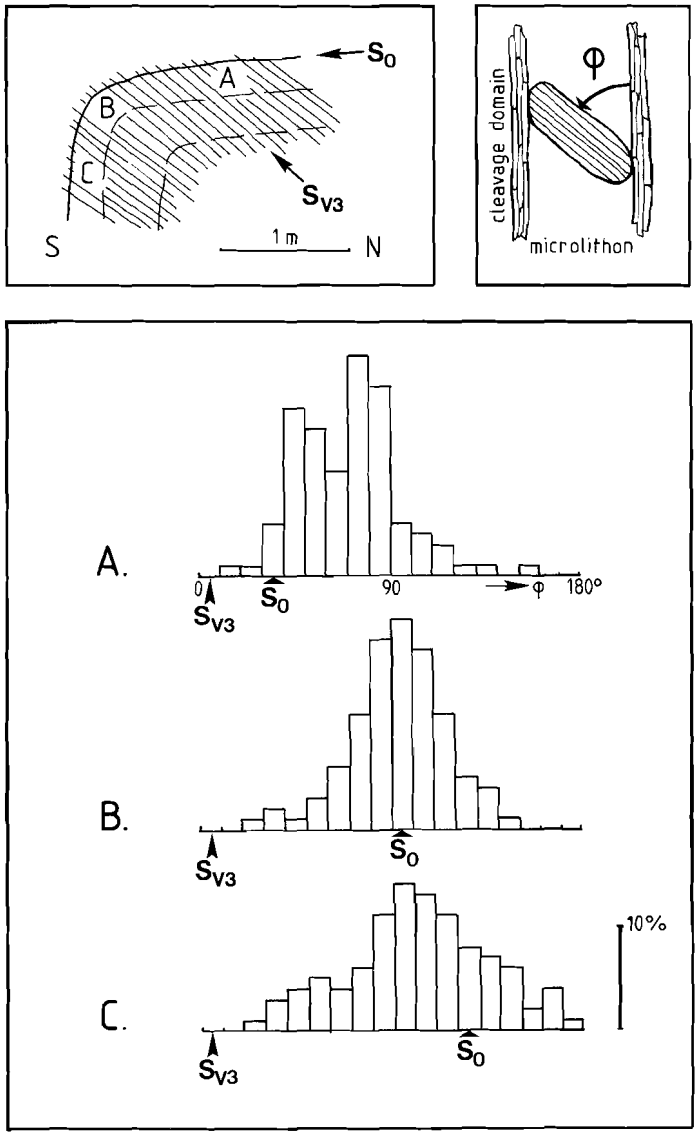

FIGURE 5.9. Orientation distribution of the basal planes of phyllosilicates in the microlithons from three samples around a fold. The cleavage orientation (S_{V3}) is taken constant in the histograms, the bedding orientation is indicated with S_0. ϕ is the angle between the basal planes and the cleavage. N = 100 in each sample.

The phyllosilicates show complex internal deformation structures. Occasionally small isolated micas parallel to the cleavage occur inside grains in the microlithons (Fig. 5.3b). These intragranular substructures will be discussed in more detail in section 5.3.6.

Quartz and albite grains are often equidimensional, although in areas with a strong cleavage they are elongated parallel to the cleavage (Fig. 5.8). There is no undulose extinction, and no crystallographic preferred orientation of quartz or albite has been observed.

As has been mentioned above, the phyllosilicates in the microlithons are generally oriented with their basal planes inclined to the cleavage. Usually the angle between the basal planes and the cleavage is quite high, often 90°. Figure 5.9 shows histograms of phyllosilicate orientations in the microlithons from three different positions around a fold. The interpretation of this orientation distribution will be discussed in section 5.5.2.

The transition from microlithon to cleavage domain is usually sharp: phyllosilicates in the microlithons abut against the cleavage domain boundaries. However, occasionally phyllosilicates are bent from an orientation at a high angle to cleavage in the microlithon to parallelism with the cleavage in the cleavage domain (Fig. 5.3b,c).

5.3.5 Variation of cleavage around rigid objects

Strain shadows are developed around monazite porphyroblasts (Fig. 4.2, 5.10), competent layer fragments (Fig. 5.4) and isolated bodies of silt (Fig. 5.11). On transition from the centre of the strain shadow to the edge of the rigid object, the slaty cleavage changes from a rough spaced cleavage to a zonal, almost continuous fabric. This variation in cleavage morphology is the same as the variation observed across cleavage bundles.

Inside the strain shadows the main fabric is a weak preferred orientation of phyllosilicates, which is not parallel to the cleavage (Fig. 5.10). If the strain shadow is developed adjacent to a silty sedimentary layer, this fabric is parallel to bedding; in strain shadows around monazite porphyroblasts the fabric is parallel to the internal fabric of the porphyroblast. In the centre of the strain shadows a rough cleavage is developed. The short, discontinuous cleavage domains are a few microns wide and a few tens of microns long, and are formed by phyllosilicates

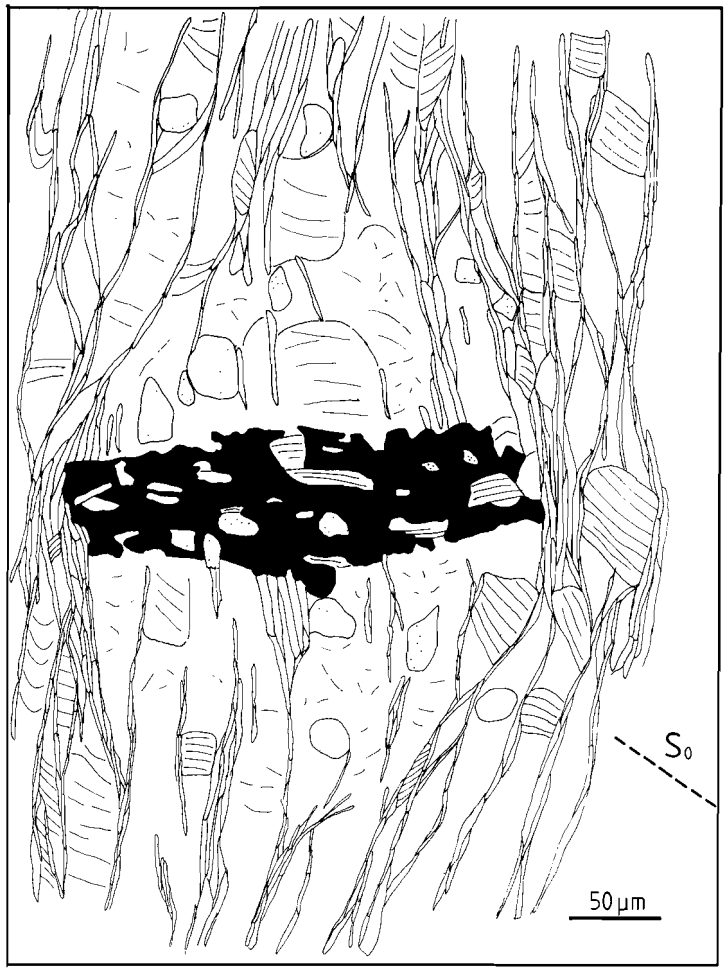

FIGURE 5.10. Variation in cleavage morphology across a strain shadow around a pre-kinematic monazite porphyroblast (black). The slaty cleavage is vertical. (tracing from a SEM-SE micrograph)

(mainly muscovite) oriented parallel to the cleavage. The microlithons are formed mainly by phyllosilicates, quartz and albite. The phyllosilicates in the microlithons are often folded and kinked, but these microfolds are too chaotic to speak of a crenulation cleavage. The spacing of the rough cleavage is quite regular, and it is of the same order of magnitude as the average grain size.

In small areas at the edges of the rigid objects the cleavage is stronger than the average cleavage fabric of the sample. The cleavage domains are wide and uninterrupted; microlithons are almost absent.

There is a gradual transition between these two cleavage types. The transitional fabric is a clearly spaced discrete disjunctive cleavage, and it is clear that the fabric in the microlithons is the same as the main fabric in the strain shadow.

The concentration of the tectosilicates quartz and albite inside strain shadows is higher than in the matrix. This is shown in Fig. 5.11 and 5.12, where the proportion of tectosilicates is measured around an isolated silt body. This has been done by quantitative analysis of the BSE-images, where each gray tone is representative for a mineral phase; in this technique quartz and albite can not be distinguished from each other. Inside the strain shadow the tectosilicates form ca. 50% of the rock; the grains are equidimensional and most phyllosilicates are oriented parallel to bedding. In the area adjacent to the strain shadow the amount of quartz+albite is reduced to ca. 15%. The grains are now elongated parallel to the cleavage, and the phyllosilicates show a strong preferred orientation parallel to the cleavage. The optical micrograph (Fig. 5.11) shows that there is an enrichment of opaque minerals in the areas of intense cleavage.

5.3.6 Substructures within chlorite-mica aggregates

All phyllosilicates in the slates of the Seo Formation are intergrowths of muscovite and chlorite. The thickness of the chlorite and muscovite layers can vary from several microns down to a few nanometers. In the literature intergrowths of chlorite and mica, wich are larger than the average grainsize, are called chlorite stacks or chlorite-mica aggregates (see section 2.2.5) and have been treated as a special population of grains (e.g. Craig et al., 1982; Van der Pluijm and Kaars Sijpesteijn, 1984; Gregg, 1986; Dimberline, 1986). In the present

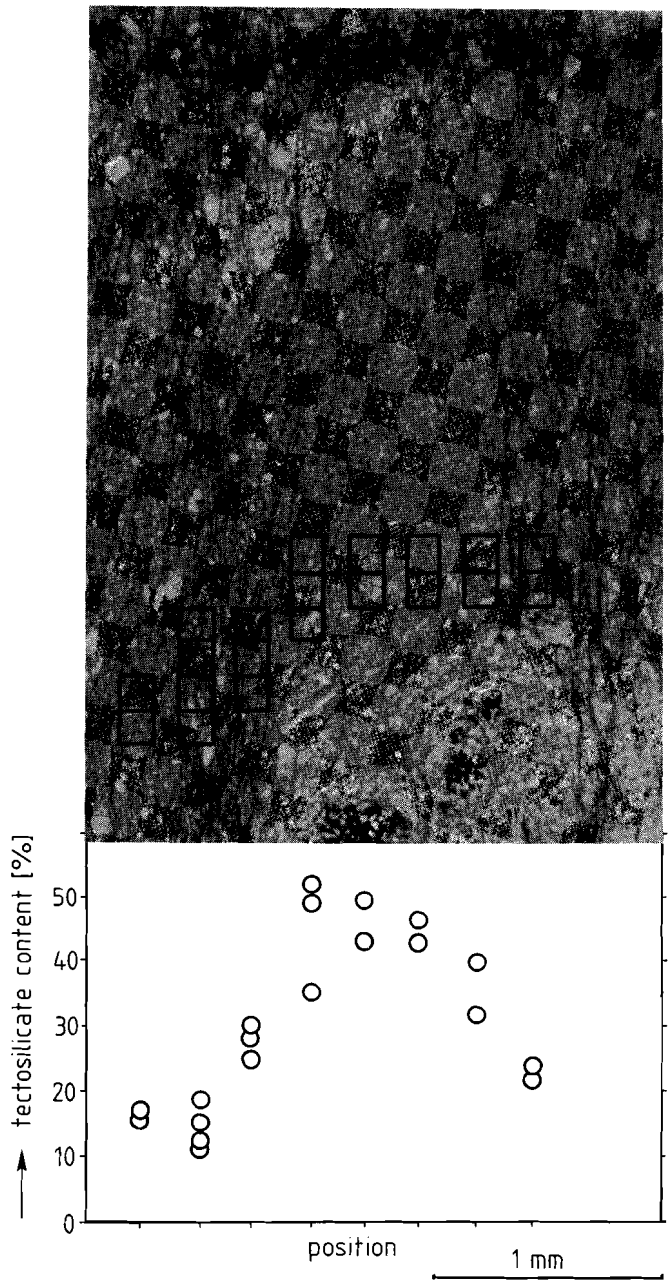

FIGURE 5.11. Variation in tectosilicate content across a strain shadow around an isolated silt body. The optical micrograph shows the strain shadow and the analysed areas. The graph shows the tectosilicate (quartz + albite) content plotted against the position in the strain shadow. The measurement technique is explained in Fig. 5.12.

study every phyllosilicate grain is in fact a chlorite-mica aggregate, and they cannot be regarded as a special grain size population.

Almost all chlorite-mica aggregates, both deformed and undeformed, show internal low-angle boundaries (e.g. Figs. 5.13-5.16). These boundaries are usually parallel to the basal planes on one side, while the basal planes of the crystal on the other side run against the boundary at a small angle. Because the morphology of these boundaries is very similar to the stratigraphic unconformity, these boundaries will henceforward be termed *internal unconformities*.

Chlorite-mica aggregates within weakly deformed siltstone layers in between the cleavage bundles show very little signs of deformation. They are straight elongated grains (aspect ratios up to 1:8) oriented parallel to bedding (Fig. 5.13). They consist of only a few relatively thick laminae of chlorite and mica, with a few very low-angle internal unconformities. These aggregates are very similar, in morphology and orientation, to aggregates in tectonically undeformed diagenetic silty shales from the North Sea (Fig. 5.14).

Chlorite-mica inclusions in pre-kinematic monazite porphyroblasts within the pelitic layers (Fig. 5.15) have essentially the same morphology as the aggregates in the silt layers. They are elongated parallel to the basal planes and show some low-angle internal unconformities, but are otherwise undeformed.

In the pelitic layers the aggregates show complex internal structures (Fig. 5.16). Most chlorite-mica aggregates have a grainsize of the same order of magnitude as the cleavage spacing, that is, they fill the entire width of the microlithon. These grains are usually slightly elongated parallel to the cleavage (aspect ratios between 1:1 and 1:2), but their basal planes are inclined to the cleavage (see section 5.3.4). The structures inside these grains include folds, kinks, displacements of grain sections and internal unconformities. Larger grains are often transected by the cleavage. Sometimes a complete cleavage domain has developed across the aggregate (Fig. 5.17), but in other cases the aggregates show a zone of intense deformation as a continuation of the external cleavage domain (Fig. 5.16d,e).

Many grains are folded or kinked (Fig. 5.16c, 5.18); the axial planes of the microfolds are parallel to the cleavage. Bent grains also occur; often the bulk of the grain has its basal planes at a high angle to

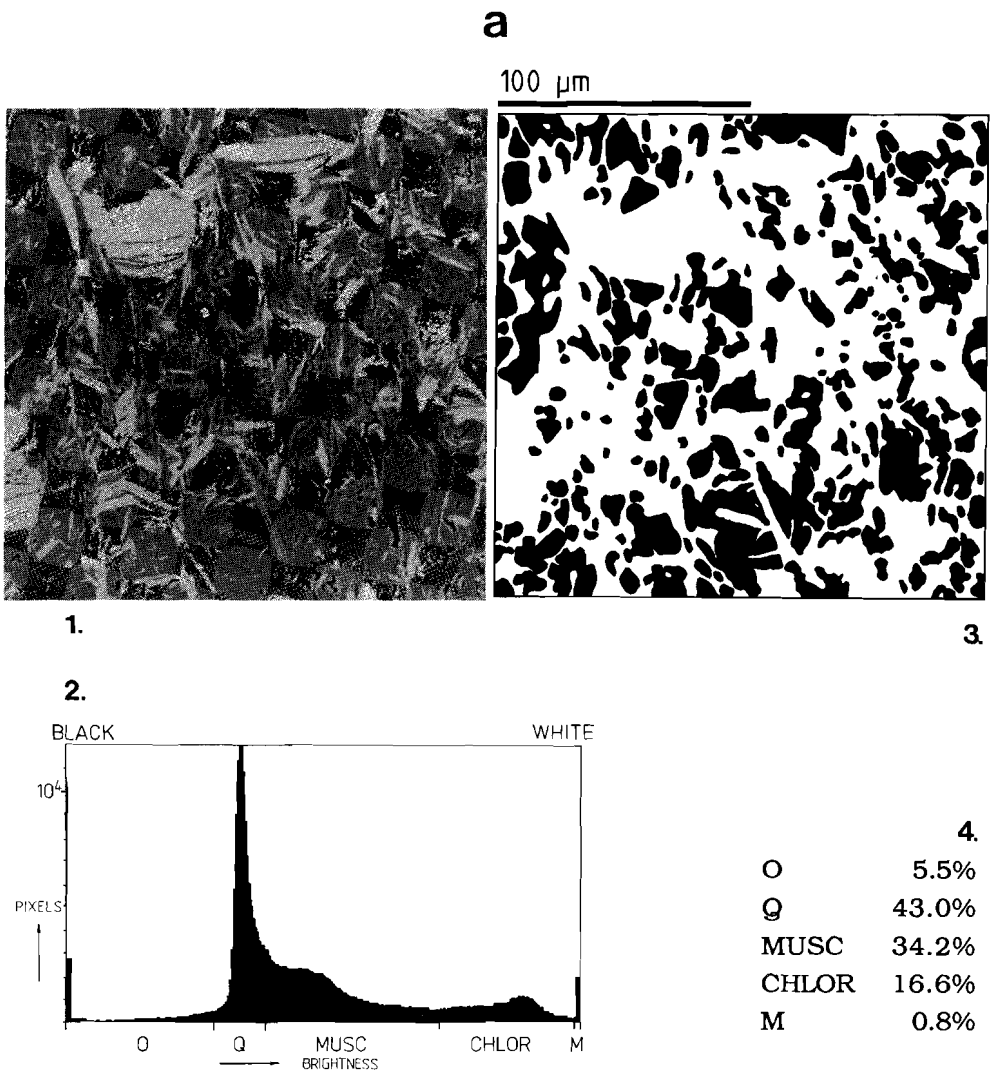

FIGURE 5.12. Measurement of tectosilicate content using BSE-images of polished thin sections. a. Area inside the strain shadow. b. Area of intense cleavage in the cleavage bundle next to the shadow. First a BSE-image is recorded (1) and stored in the memory of the image processing computer. In BSE-images minerals with different avarage atomic number show different contrast. Then a histogram of gray values is produced (gray spectrum), and windows are set for the various mineral phases (2): O = Organic matter (and holes in the thin section), Q = Quartz and albite, MUSC = Muscovite, CHLOR = Chlorite, M = Metal oxides and monazite. An image of the distribution of one mineral phase, e.g.

b

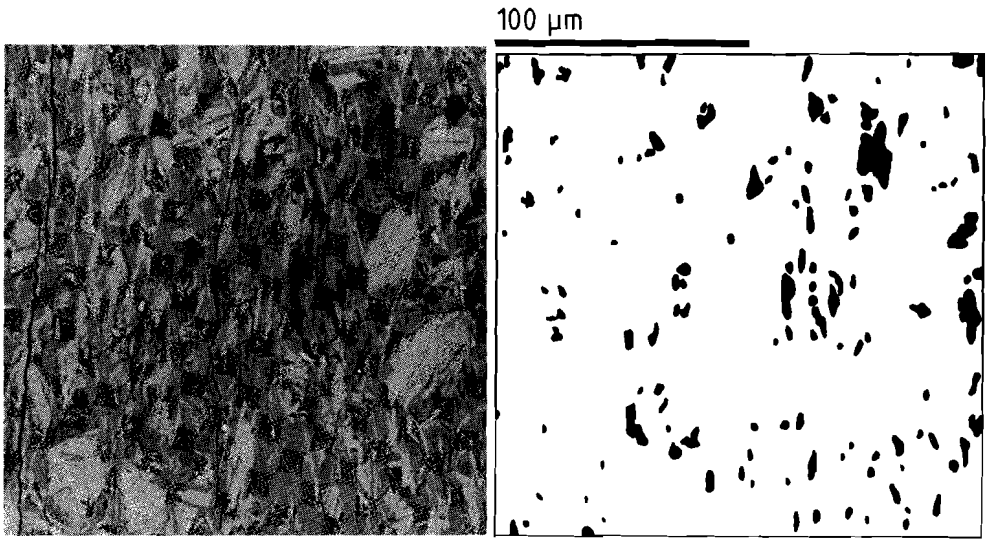

1.

3.

2.

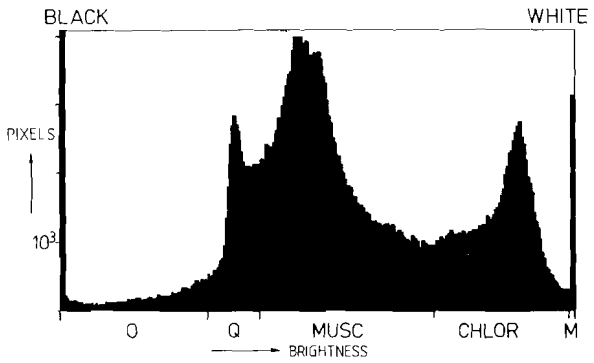

4.

O	4.7%
Q	11.3%
MUSC	54.6%
CHLOR	28.1%
M	1.3%

the tectosilicates (3), can now be formed by selecting the pixels from one window. Also, the number of pixels in each window can be calculated into the percentage of each gray tone window (=mineral phase) in the image (4). Because the back-scattered electrons come from a layer of a few microns thick, these values are the volume percentages of each mineral in a slice of rock of a few microns thickness. If this slice is representative of the whole rock in the third dimension, these values can be interpreted as volume percentages of each mineral in the rock.

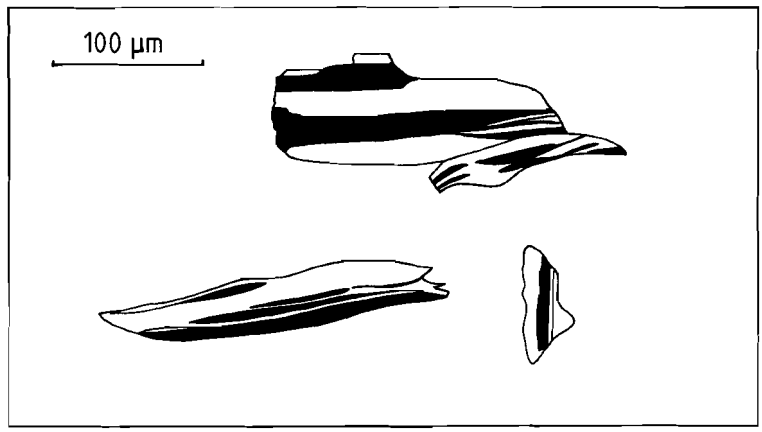

FIGURE 5.13. Chlorite-mica aggregates in a weakly deformed silt layer. (tracing from a photograph)

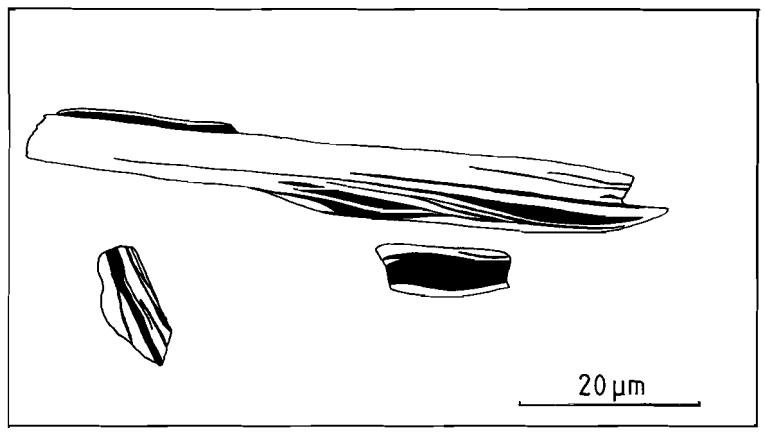

FIGURE 5.14. Chlorite-mica aggregate from a tectonically undeformed diagenetic sediment from a drillcore from the North Sea. (tracing from a photograph)

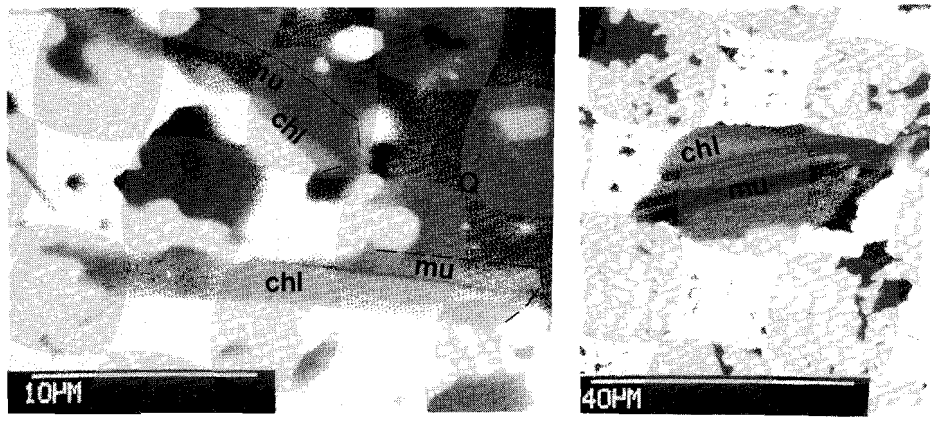

FIGURE 5.15. Chlorite-mica aggregate inclusions in pre-kinematic monazite porphyroblasts. Monazite is white. MU=muscovite; CHL=chlorite (SEM-BSE micrographs)

the cleavage, and part of the grain is rotated into parallellism with the cleavage (Fig 5.3c, 5.16d). A striking feature is the difference between chlorite and the mica lamellae in such deformed grains: chlorite is bent into almost continuous curves, showing severe undulose extinction, while muscovite is often sharply kinked, with serrated kinkband boundaries, and is hardly undulose (Fig. 5.18).

Small mica grains parallel to the cleavage are sometimes observed inside aggregates in microlithons. These micas are a few microns long, and are either completely incorporated in the host aggregate or straddle the boundary between the aggregate and the matrix (Fig. 5.3b, Fig. 5.19).

The boundary between the aggregates in the microlithons and the cleavage domains is usually quite sharp: the chlorite and mica lamellae simply abut against the cleavage domain boundary. In some cases phyllosilicate lamellae can be traced from the aggregate in the microlithon into the cleavage domain.

5.3.7 HVTEM observations

High-voltage TEM observations have essentially confirmed the observations in the optical microscope. Deformed aggregates show a difference in substructure between chlorite and muscovite: the chlorites

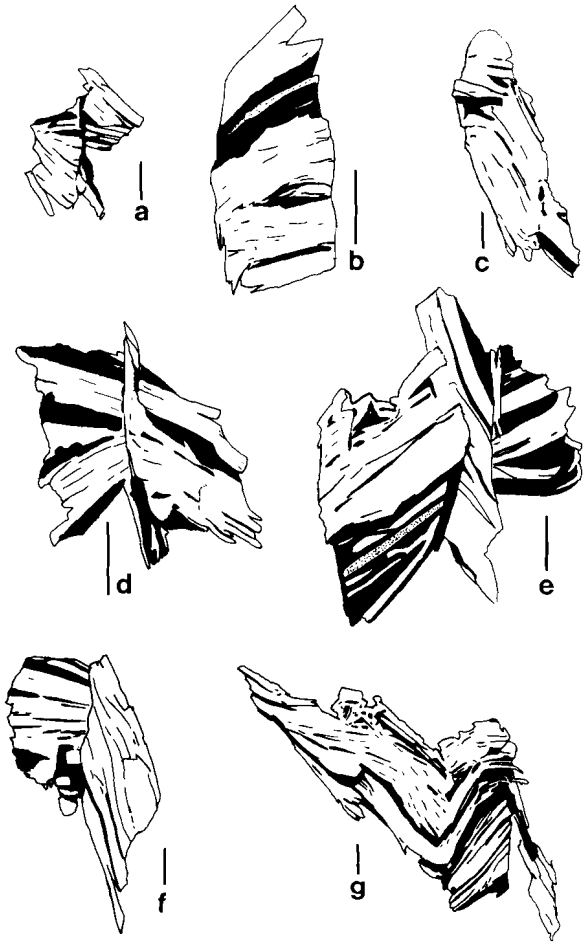

FIGURE 5.16. Complexely deformed chlorite-mica aggregates. The scale bar is 10 µm and is parallel to the cleavage. (tracings from SEM-BSE-images: black=muscovite, white=chlorite)

are bent and show many subgrains and dislocations, while the muscovite crystals are only slightly bent and show few crystal defects (see section 6.4 for more details).

The transition between microlithon and cleavage domain is often a very sharp high-angle contact. The boundaries are usually not straight, but steps of 0.1 μm to a few microns occur (Fig. 5.20).

Isolated mica grains in a cleavage orientation, inside aggregates which are inclined to the cleavage, are always associated with evidence of strain in the host crystal, e.g. high dislocation densities or microkinks (see chapter 6).

5.3.8 Microchemical analyses

A number of aggregates have been analysed quantitatively with EDS. The size of the analysed spot is on the order of 4 μm^2, which means that very narrow laminae cannot be measured.

The analyses of the micas vary from true muscovite to a mica with a more phengitic composition. However, the phengitic composition can also be explained by intercalations of chlorite lamellae on a very small scale within true muscovite, as has been observed frequently with TEM. There is no systematic variation of mica composition from microlithon to cleavage domain.

Most chlorite analyses fall in the ripidolite field (classification of Hey, 1954). Intercalations of mica in chlorite is also very common. However, the contamination of chlorite analyses by intercalations of mica laminae is easily detected by the presence of potassium, and pure chlorite analyses can thus be selected. The average composition of all the analysed chlorites is: $Mg_{3.0}Fe_{5.5}Al_{3.3}[(Si_{5.2}Al_{2.8})O_{20}/(OH)_4](OH)_{12}$. The chlorites in the microlithons show a slightly higher Mg-content than the chlorites in the cleavage domains (see fig. 5.21).

5.4 SLATY CLEAVAGE IN THE PALLARESA ANTICLINORIUM

In the Pallaresa Anticlinorium, north of the Orri Dome, the rocks of the Seo Formation can be described as phyllites, rather than slates. Apart from the appearance of small epidote porphyroblasts, and the absence of monazites, the mineralogy is not different from the Seo

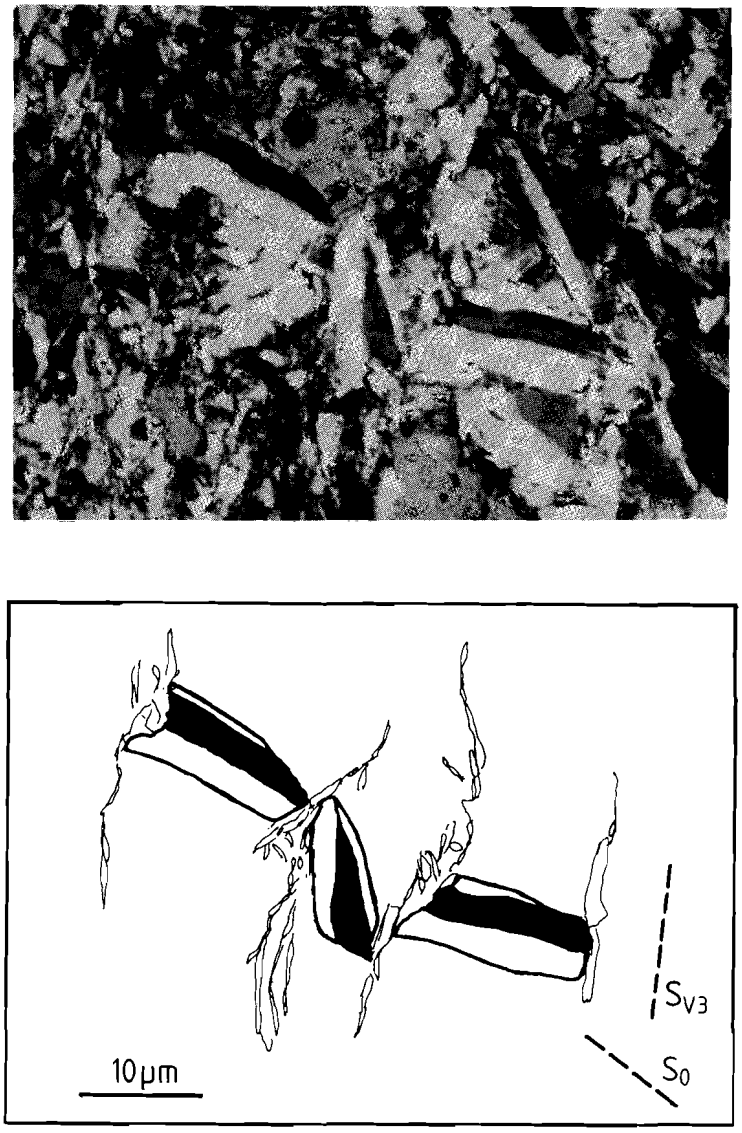

FIGURE 5.17. Chlorite-mica aggregate transected by the cleavage. The two outer sections are still parallel to bedding, the middle section is being rotated towards a cleavage orientation. (optical micrograph, crossed nicols)

Formation in the Orri Dome. The rocks in the southern part of the Pallaresa Anticlinorium have a lower greenschist facies metamorphic grade (see chapter 4).

The cleavage in the Pallaresa Anticlinorium is a continuous cleavage *s.s.*. All phyllosilicates are parallel to the cleavage. Isolated quartz and albite grains are elongated parallel to the cleavage (Fig. 5.22), but quartz in silt layers shows a foam texture. The average grain size is on the order of 100 μm, and there is little variation in grain size. The grains parallel to the cleavage do not show any undulose extinction.

In the pelites only occasional remnants of microlithons are observed (fig. 5.22). The grains in these microlithons are inclined to the cleavage and show undulose extinction. The boundaries of the microlithons show irregular curves and bulges.

5.5 DISCUSSION

5.5.1 Pre-cleavage fabric

The presence of a fabric in strain shadows and inside pre-kinematic porphyroblasts indicates that there has been a fabric prior to the development of the mainphase cleavage. Inside weakly deformed siltlayers and next to rigid bedding fragments the pre-cleavage fabric is parallel to bedding. As there is no indication of any intense deformation prior to the mainphase, it is concluded that this bedding parallel fabric is the result of sedimentation and compaction processes (O'Brien, 1970; Heling, 1970; Zwart, 1979; see section 2.2.3).

The internal fabric in the monazite porphyroblasts is often parallel to the long axis of the crystal, but both the internal fabric and the crystal shape are unrelated to the crystallographic axes (see section 4.3.2). Apparently the shape of the porphyroblasts is controlled by the pre-cleavage fabric. This could be explained by the higher diffusion rates parallel to the fabric, which allows a more rapid growth of the monazite in a direction parallel to the fabric.

The presence of chlorite-mica aggregates inside the monazite porphyroblasts indicates a pre-cleavage origin of the aggregates. The aggregates inside the monazites and in the weakly deformed silt layers have high aspect ratios parallel to the basal planes, and show some

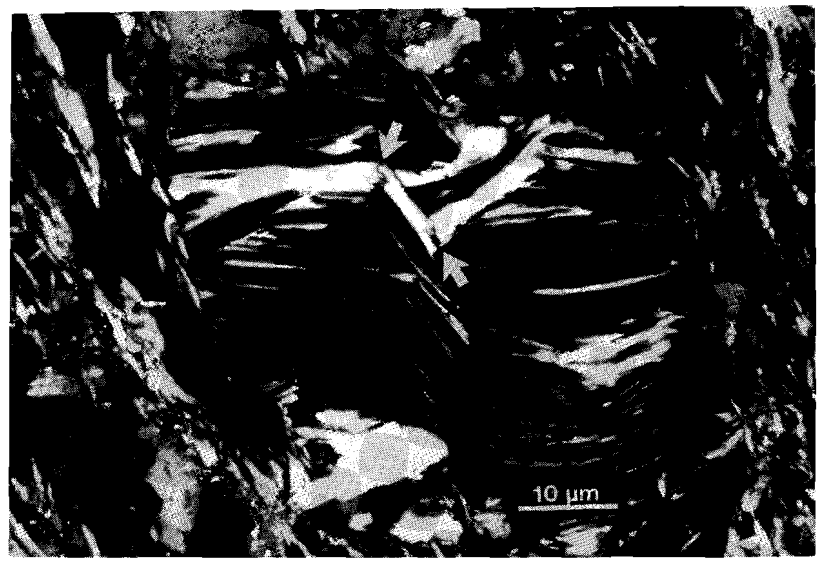

a

b

FIGURE 5.18 a, b. Kinked mica layers in deformed chlorite-mica aggregates. The kink-band boundaries are serrated (arrows). Chlorite is not kinked but is gently folded and shows undulose extinction (optical micrographs, crossed nicols)

low-angle internal unconformities. Very similar chlorite-mica aggregates have been observed in tectonically undeformed diagenetic sediments by the present author (e.g. North Sea sediments; Fig. 5.14), and by a number of other authors (e.g Beutner, 1978). This is consistent with the hypothesis that chlorite-mica aggregates are formed prior to tectonic deformation (Beutner, 1978; Zwart, 1979; Craig et al., 1982; Woodland, 1982, 1985; Van der Pluym and Kaars Sijpesteijn, 1984; Gregg, 1986; Dimberline, 1986; see section 2.2.5). Whether these grains are deposited as complete aggregates (Beutner, 1978), or the aggregates have developed during diagenesis and incipient metamorphism (Craig et al., 1982), is not clear.

Summarizing, it can be stated that there was a pre-cleavage bedding-parallel sedimentation/compaction fabric formed by chlorite-mica aggregates elongated parallel to the basal planes, with aspect ratios of about 8:1. The only internal structures were a few low-angle internal unconformities.

5.5.2 The fabric in the microlithons

In strain shadows a rough cleavage is present, but the dominant fabric is the pre-cleavage bedding fabric. Along the transition from strain shadow to matrix the cleavage domains become continuous along their trace, and the pre-cleavage fabric is now enclosed between the cleavage domains and forms the microlithons. However, as the slaty cleavage becomes more intense, the fabric in the microlithons is more and more modified.

Orientation data of the phyllosilicates in the microlithons are presented in Fig. 5.9. The histogram of the horizontal limb shows two peaks, one nearly perpendicular to the cleavage and the other close to the bedding orientation. The steep limb shows an asymmetric orientation distribution which is askew towards the bedding orientation. The fold hinge shows one strong symmetric peak. These histograms can be interpreted in terms of two superimposed peaks, i.e. two superimposed preferred orientations: one perpendicular to the cleavage and a weaker one close to the orientation of the sedimentary layering. In the fold hinge these two orientations coincide and a single preferred orientation is observed. This orientation close to bedding is probably a remnant of the pre-cleavage bedding orientation, and it may be formed by grains that

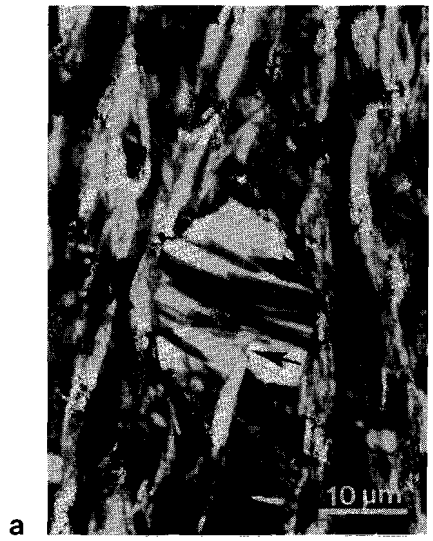

FIGURE 5.19. a. Mica grain parallel to the cleavage (arrow), growing into a chlorite-mica aggregate. b. Small mica grains (arrows) growing into a chlorite-mica aggregate; the aggregate shows evidence of splitting. (optical micrographs, crossed nicols)

have not, or only slightly, been rotated. The stronger preferred orientation perpendicular to the cleavage is formed by grains that have a stable orientation with respect to the cleavage.

5.5.3 Cleavage formation in the Orri Dome

Rotation of grains, bending, folding and kinking all lead to a re-orientation of grains in whole or in part (Fig. 5.23). Evidence for each of these processes is abundant. Rotation of a complete grain section without any internal deformation (rigid-body rotation) is illustrated in Fig. 5.17. The other processes have been illustrated in Fig. 5.16 and 5.18.

Rotation of grains, in whole or in part, can explain the preferred orientations in the microlithons described above: many grains have been rotated into a cleavage orientation and form the cleavage domains (and are therefore not included in the histograms of Fig. 5.9), some grains have not been rotated and have an orientation close to bedding; only grains perpendicular to the cleavage have a stable orientation and are not rotated.

The decrease in tectosilicate content with increasing cleavage intensity (Fig. 5.11) suggests that the tectosilicates are selectively removed during cleavage development. The quartz grains in strain shadows are equidimensional, while the grains in a region with intense cleavage in the same layer are flattened parallel to the cleavage. The dimensions of the deformed grains parallel to the cleavage are the same as the undeformed dimensions (Fig. 5.12), indicating that material is removed from the stressed faces parallel to cleavage, but the material is not redeposited on the unstressed faces perpendicular the the cleavage (Fig. 5.24). This means that the material is removed from the local rock system, and therefore the volume is reduced. In the example of Fig. 5.11 the volume loss due to the removal of quartz (and albite) is on the order of 35%. The absence of quartz and albite and the relative concentration of opaque material in cleavage domains confirms that the tectosilicates are preferentially removed from the slate. Quartz veins are abundant in the Seo Formation, and it is very likely that these veins contain the quartz that has been removed from the slate. The path length of the mass transfer is therefore never more than a few decimeters.

Truncation of phyllosilicate grains (e.g. Fig. 5.16e) suggests that some pressure solution of phyllosilicates does occur. However, the

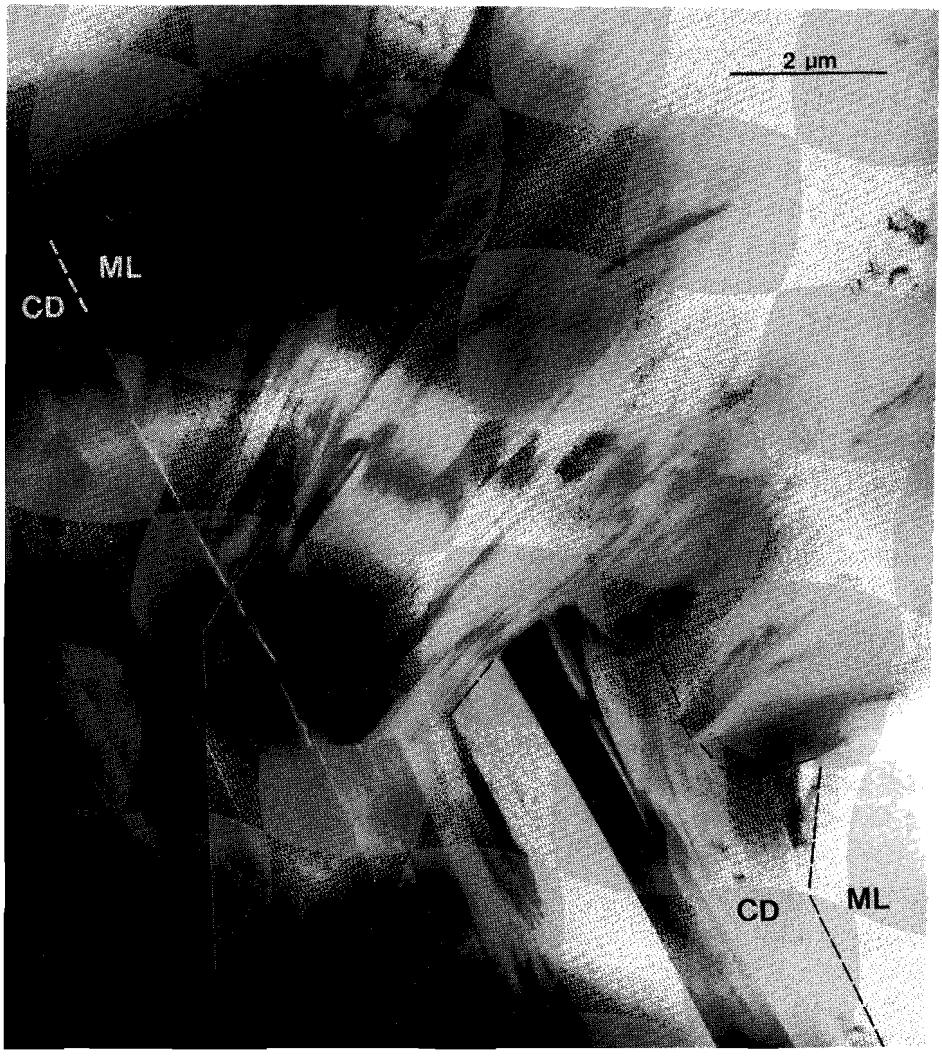

FIGURE 5.20. Stepped boundary between cleavage domain (CD) and microlithon (ML). (BF HVTEM micrograph)

observation that quartz (and albite) are selectively removed (see above), and the abundant intracrystalline deformation structures in the phyllosilicates indicate that pressure solution is not the dominant deformation mechanism for the phyllosilicates. This is illustrated in Fig. 5.8, where the quartz is deformed by pressure solution, while the chlorite-mica aggregate is internally deformed. Fig. 5.8 also illustrates how, due to removal of the quartz by pressure solution, the phyllosilicate grain is partly rotated into a cleavage orientation.

The extensive deformation structures inside the phyllosilicates indicate that intracrystalline deformation was important during cleavage development. When grains are bent, kinked or folded, the crystal lattice is deformed. Most chlorites show severe undulose extinction, indicating that subgrains have been formed. Muscovite also shows folds and kinks, but the grains show no undulose extinction. Kinkband boundaries have been adjusted into sharp, serrated high-angle boundaries (Fig. 5.18). These observations suggest that the deformation of chlorite involves formation of new low- and high-angle grain boundaries and rotation of subgrains, while intracrystalline strain in muscovite leads to grain boundary migration. This subject will be treated in more detail in chapter 6.

The occurrence of small isolated muscovite grains in a cleavage orientation in the middle of differently oriented grains in the microlithons (Fig. 5.19), and very long narrow muscovites extending from cleavage domains into microlithons (Fig. 5.6) are hard to explain by rotation processes. It seems likely that these grains have grown at the expense of the host grain, a process referred to in general as recrystallisation (see section 2.2.4). These muscovite grains grow preferentially in areas of intense deformation such as kinks. This suggests that the stored strain energy in the host grain is one of the driving forces, and controls the site of growth. Another factor might be the enhanced diffusion rates due to the high dislocation densities, which leads to rapid mass transfer and therefore rapid growth in these areas.

New chlorite grains growing in a cleavage orientation have been observed (e.g. Fig. 5.16 d,e), but less frequently than muscovites. Several authors have described crystallisation of chlorite in extension sites in deformed chlorite-mica aggregates (e.g. Van der Pluijm and Kaars Sijpesteijn, 1984). It seems likely that this has also occurred in the slates of the Orri Dome, as deformed aggregates usually contain far more

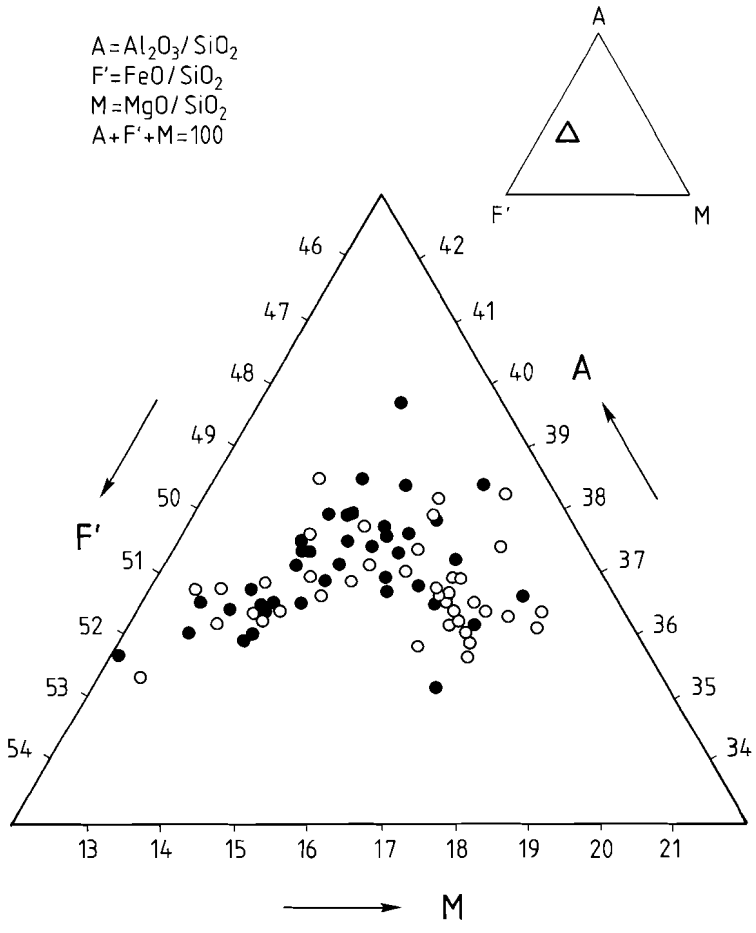

FIGURE 5.21. Triangular plot of chlorite compositions, measured with X-ray energy-dispersive analysis. Open circles: grains in microlithons. Filled circles: grains in cleavage domains

chlorite than the undeformed grains. The larger aggregates show evidence for splitting and folding of the muscovite lamellae, and filling of the extension sites with chlorite (Fig. 5.19b; cf. Van der Pluijm and Kaars Sijpesteijn, 1984).

Some of the chlorites in the microlithons show a slightly higher Mg-content than the chlorites in the cleavage domains. In general, the Mg-content of chlorite increases with metamorphic grade (Dunoyer de Segonzac, 1970; Frey, 1978). This may indicate that some of the chlorites in the microlithons, i.e. in the deformed chlorite-mica aggregates, have crystallised under higher metamorphic conditions than the chlorites in the cleavage domains. This is in agreement with the assumption that crystallisation of chlorite occurs in extension sites in the microlithons rather than in cleavage domains. However, it is in contradiction with the observations of Knipe (1979, 1981), who found that recrystallisation, both of chlorite and mica, occurred mainly in the cleavage domains. Although part of the chlorite in the aggregates may have crystallised during cleavage development, no strain-free chlorites have been observed by TEM. If new chlorite has been present, it must have been deformed during progressive deformation.

There is a marked difference in behaviour between chlorite and muscovite. One difference lies in the intracrystalline deformation mechanisms: formation and rotation of subgrains in chlorite, grain boundary migration in muscovite; this will be discussed in detail in chapter 6. The other difference is the preferential crystallisation of muscovite in a cleavage orientation, which is rare for chlorite. This might be explained by the difference in elastic anisotropy between the two minerals: muscovite has a much stronger elastic anisotropy than chlorite (Alexandrov and Ryzhova, 1961). Due to its high elastic anisotropy muscovite is thermodynamically most stable with the basal planes perpendicular to σ_1 (Kamb, 1959). New muscovite will therefore grow preferentially with the basal planes in a plane perpendicular to σ_1; this plane will usually coincide with the cleavage plane. This effect will be less for the more isotropic chlorite.

There is no evidence for shear along cleavage planes. Grains that have been transected by the cleavage show no displacement of the opposite grain sections (Fig. 5.16d, 5.17). The irregular stepped boundaries between cleavage domains and microlithons (Fig. 5.20) also exclude any shearing along these planes.

FIGURE 5.22. Continuous cleavage s.s. in phyllite from the southern rim of the Pallaresa anticlinorium, near Llavorsí. An isolated remnant of a microlithon is visible in the centre. (optical micrograph, crossed nicols)

From the above discussion it will be clear that various processes have operated simultaneously during development of the slaty cleavage. Pressure solution, mainly of quartz and albite, led to a shortening of the rock in a direction normal to the cleavage, accompanied by volume loss. Due to the local removal of material the adjacent fabric collapsed, and grains were plastered against the cleavage domains.

Rotation, bending, folding and kinking due to shortening also occurred in quartz-free layers. These re-orientation processes involve

intracrystalline deformation and grain boundary sliding. The re-orientation of existing grains finally leads to a preferred orientation parallel to the cleavage. Only grains perpendicular to the cleavage have a more stable orientation and will not be rotated easily. This leads to the bimodal orientation distribution observed in many slates: one preferred orientation parallel to the cleavage and another normal to the cleavage; if there are still remnants of a bedding fabric a trimodal fabric is possible (Fig. 5.9). Crystallisation of muscovite contributes to the preferred orientation parallel to the cleavage. Crystallisation of chlorite occurs both in the cleavage domains and in the microlithons.

The total strain inside the strain shadows is less than outside the shadows, but it is likely that it has been achieved in the same amount of time. Therefore, strain rates must also have been lower in the strain shadows. The variation in cleavage morphology from the strain shadow to the matrix is caused by variation in strain and strain rate; these two parameters cannot be separated.

In the strain shadows the dominant fabric is the bedding fabric. The grains forming this fabric are folded and kinked, and some are bent into a cleavage orientation. However, many micas which form the short discontinuous cleavage domains (rough cleavage) are isolated and cannot be explained by rotation; they have been formed by (re)crystallisation.

The regular spacing of the rough cleavage is of the same order of magnitude as the average grain size, which suggests that the cleavage domains nucleate at the edges of grains. Phyllosilicate grains in weakly deformed areas often show a strong internal deformation at the edges facing the cleavage. The stored strain energy and the high diffusion rates at these sites may enhance crystallisation.

With increasing strain and strain rate internal deformation and pressure solution become more evident. The cleavage domains increase in width and in length, by growth of cleavage grains and because existing grains are rotated into a cleavage orientation and become part of the cleavage domain. In first instance the original bedding fabric is preserved in the microlithons. Subsequently the cleavage domains become interconnecting, and an anastomosing cleavage is formed. The bedding fabric inside the microlithons is gradually destroyed by folding, bending and kinking (involving intracrystalline deformation) of the old grains, removal of material by pressure solution, and crystallisation of

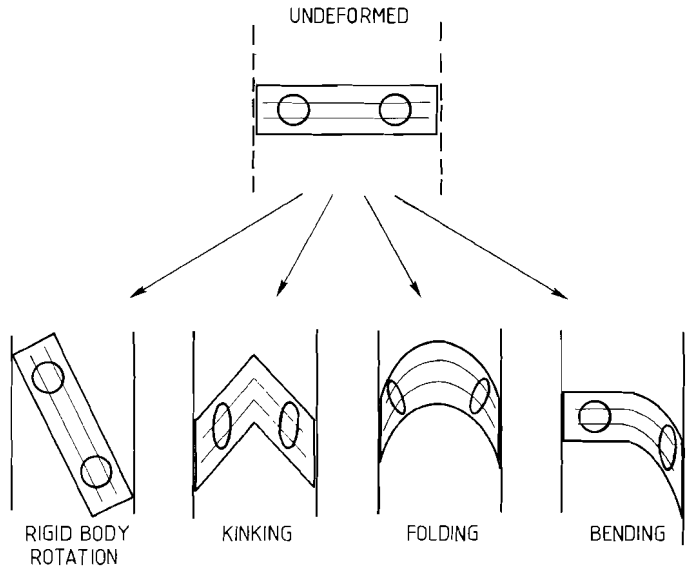

FIGURE 5.23. Mechanical re-orientation processes: rigid-body ,rotation kinking, folding and bending; strain ellipses have been sketched to indicate where intracrystalline deformation occurs.

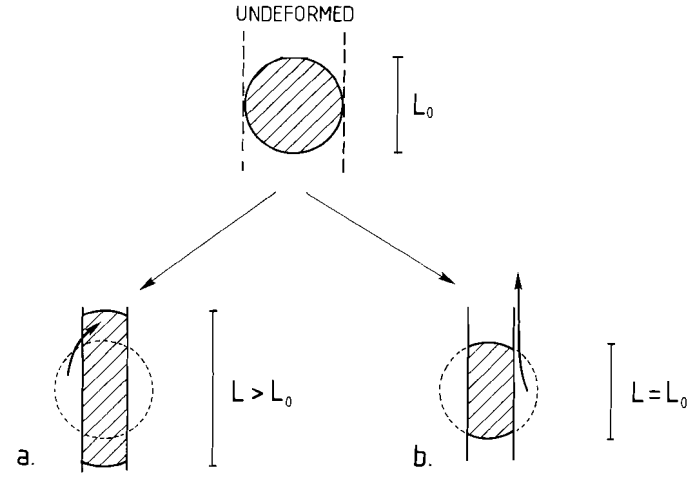

FIGURE 5.24. Deformation of a quartz grain by pressure solution. a. The removed material is redeposited on the unstressed faces of the grain; the grain grows in a direction parallel to the cleavage. b. The material is removed from the local rock system; the grain maintains its original length parallel to the cleavage.

muscovite (in a cleavage orientation - therefore nuclei for new cleavage domains) and of chlorite (in extension sites - usually normal to the cleavage). Eventually an anastomosing zonal disjunctive cleavage is formed, with isolated microlithons where the majority of the phyllosilicates is normal to the cleavage.

5.5.4 The Pallaresa Anticlinorium

No signs of rotation, kinking, folding or pressure solution are preserved in the phyllites of the Pallaresa Anticlinorium. The average grainsize is larger than that of the same sediments in the Orri Dome, and quartz grains are equant and strain free. This suggests that recrystallisation and grain growth occurred during cleavage development. The remnants of the microlithons contain undulose phyllosilicates, and have very irregular boundaries, suggesting that the strain-free cleavage grains are growing at the expense of the deformed grains in the microlithons.

The increase in grain size and the growth of strain-free grains at the expense of internally deformed grains indicates that recrystallisation is the main process responsible for the continuous fabric s.s. in the Pallaresa Anticlinorium. The rocks in the Pallaresa Anticlinorium have undergone higher temperatures (lower greenschist metamorphism; T > 350 °C) than the Orri Dome slates (anchizone, 250°C<T<350°C). The strain state in the Pallaresa Anticlinorium is not known. Asuming that in an early stage the cleavage microstructure in the Pallaresa Anticlinorium has been similar to that in the Orri Dome, and that the paleotemperature is the only difference between the two areas, the fabric in the Pallaresa Anticlinorium can be regarded as the result of annealing of a spaced fabric which is still preserved in the Orri Dome (see e.g. Nicolas and Poirier, 1976).

5.6 CONCLUSIONS

The slaty cleavage in the anchizonal Seo Formation of the Orri Dome is an anastomosing zonal disjunctive cleavage with an average spacing of 20 μm. The same rocks from the lower greenschist facies in the Pallaresa anticlinorium show a continuous cleavage *s.s.* with an

average grain size of 100 μm. In the Orri Dome the evolution of slaty cleavage with increasing strain and strain rate can be studied in strain shadows around rigid objects.

Slaty cleavage in the Orri Dome is the product of several processes. The cleavage domains nucleate at the edges of grains, by rotation of grains (in part or in whole) in a cleavage orientation or by crystallisation. With increasing strain (and strain rate) the cleavage domains grow in length and in width by grain growth and rotation of grains in a cleavage orientation. In the microlithons the pre-cleavage fabric is destroyed by removal of material (mainly quartz) by pressure solution, (re)crystallisation, rotation, bending, folding and kinking.

Pressure solution leads to a shortening of the rock in a direction normal to the cleavage, and to a volume reduction up to 35%. As a secondary effect grains are rotated and thus pressure solution contributes indirectly to the re-orientation of grains.

Rotation of grains, and recrystallisation in an orientation parallel to the cleavage (mainly muscovite) lead to a new preferred orientation. Other processes which contribute are bending, folding and kinking; all these processes involve intracrystalline deformation. Intracrystalline deformation in its turn can contribute to (re)crystallisation processes through dislocation enhanced diffusion, and by providing a driving force in the form of stored strain energy.

In the lower greenschist facies phyllites of the Pallaresa Anticlinorium the main cleavage forming process is grain growth.

Chapter 6
INTRACRYSTALLINE DEFORMATION

6.1 INTRODUCTION

Observations in thin sections have revealed evidence for intracrystalline deformation of phyllosilicates during slaty cleavage development (see section 5). There is also a marked difference in the behaviour of chlorite and muscovite. Chlorite is usually undulose on a very small scale, suggesting deformation by polygonization. Muscovite is hardly undulose, but shows kinks with serrated boundaries and newly grown grains, which indicates that migration of grain boundaries occurs, and that polygonization is of minor importance.

Intracrystalline deformation during cleavage development has gained little attention in the literature. Furthermore, very little is known about the intracrystalline deformation processes in chlorite. This chapter describes a detailed TEM study of the intracrystalline deformation of phyllosilicates in the slates of the Seo Formation of the Orri Dome, with special emphasis on chlorite.

6.1.1 Crystal structures

The intracrystalline deformation of phyllosilicates is dominated by the highly anisotropic crystal structure; therefore a brief description of the crystal structure will be given below. For a more detailed description and for further references the reader is referred to the literature (e.g. Bailey 1975, 1984).

The basic structure of all phyllosilicates is a sheet of $(Si,Al)O_4$-tetrahedra linked together in a pseudo-hexagonal pattern (the tetrahedral sheet or T-sheet), in which the **a**- and **b**-axes lie (Fig. 6.1a). In the group of 2:1-phyllosilicates, to which chlorite, mica and talc belongs, two of these tetrahedral sheets are sandwiched together to form a sheet of octahedral sites in between (the octahedral sheet or O-sheet). The octahedral sites can be occupied by various metal ions. This packet of tetrahedral-octahedral-tetrahedral sheets is often called the "talc" layer or T-O-T layer, although the term "2:1 layer" is preferable (Bailey 1980a). The 2:1-layers are stacked in the direction of the **c**-axis with or without interlayers.

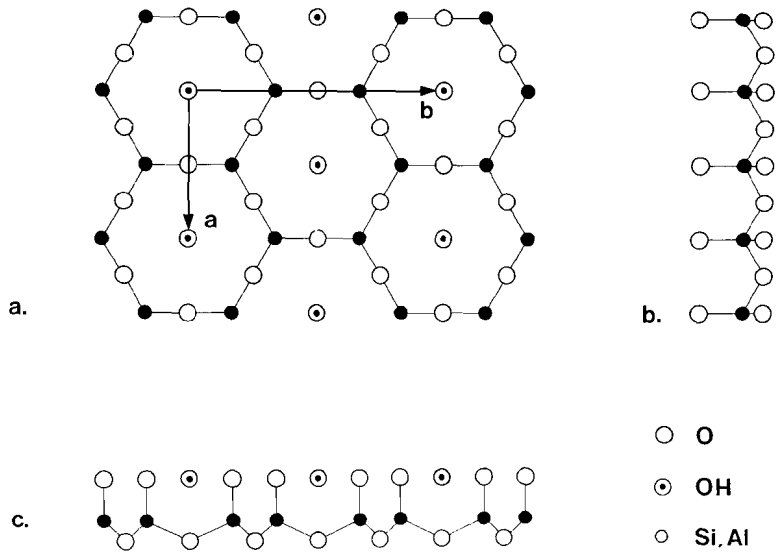

FIGURE 6.1. The tetrahedral sheet of the crystal structure of the phyllosilicates. a. Plan view of the tetrahedral sheet; the crystal axes **a** *and* **b** *are indicated; the oxygens directly above the (Si,Al) positions have been omitted for clarity. b. Projection of the tetrahedral sheet parallel to [010]. c. Projection of the tetrahedral sheet parallel to [100]. In this projection the tetrahedra are concentrated in columns of two tetrahedra wide, the* tetrahedral columns.

Because of the pseudo-hexagonal symmetry of each sheet, every direction in the (001) plane has more or less equivalent directions at 60° intervals. For example, the pseudo-equivalent directions for [100] are [110] and [1$\bar{1}$0], and the pseudo-equivalent directions for [010] are [310] and [3$\bar{1}$0]. These pseudo-equivalent directions cannot be distinguished in practical TEM, and therefore the directions [100], [110] and [1$\bar{1}$0] will henceforward be indicated with <100>, and [010], [310] and [3$\bar{1}$0] with <010>. When the tetrahedral sheet is projected along the <100> directions, the tetrahedra are grouped to form "columns" with a width of two tetrahedra (Fig. 6.1c). These "columns" will henceforward be called *tetrahedral columns*. Projections parallel to <010> directions do not show such tetrahedral columns (Fig. 6.1b).

In talc the 2:1-layers are electrostatically neutral, and they are stacked in the direction of the c-axis without any layer in between (Fig. 6.2d). The chlorite structure consists of alternating 2:1-layers and brucite-like Mg,Fe,Al-hydroxide interlayers. In the case of micas the electrical charge of the 2:1 layer is compensated by an interlayer of cations (Fig 6.2e).

A single chlorite unit is formed by one 2:1-layer and one brucite interlayer; the total thickness is about 14 Å (Fig. 6.2a). Brown and Bailey (1962) determined that four different structural units, consisting of four different relative arrangements of 2:1- and interlayers, are theoretically possible. These structural units can be stacked in various ways, leading to a large number of regular one-layer polytypes (see Brown and Bailey, 1962, Bailey, 1980b, and Spinnler et al., 1984). However, many chlorites have irregular stacking sequences. In diffraction patterns they show sharp k=3n reflections and streaking of the $k\neq$3n reflections, indicating that the layers are related to one another by shifts of magnitude b/3 parallel to the sheets; this is termed semi-random stacking (Brown and Bailey 1962; Bailey 1975, 1980b; Brindley, 1980). The shifts can occur both at the level of the interlayer and within the 2:1 layer (Spinnler et al. 1984; this study). Most ordered chlorites in nature have a monoclinic symmetry (polytype 2b-II, β=97°, see Brown and Bailey, 1962), but the symmetry of the semi-random stacking sequences will usually be triclinic (Bailey, 1980b).

The 1:1 phyllosilicates are characterised by a single tetrahedral sheet attached to a single octahedral sheet (Fig. 6.2c). The basal spacing of the 1:1 phyllosilicates is ca. 7 Å (Bailey, 1980b).

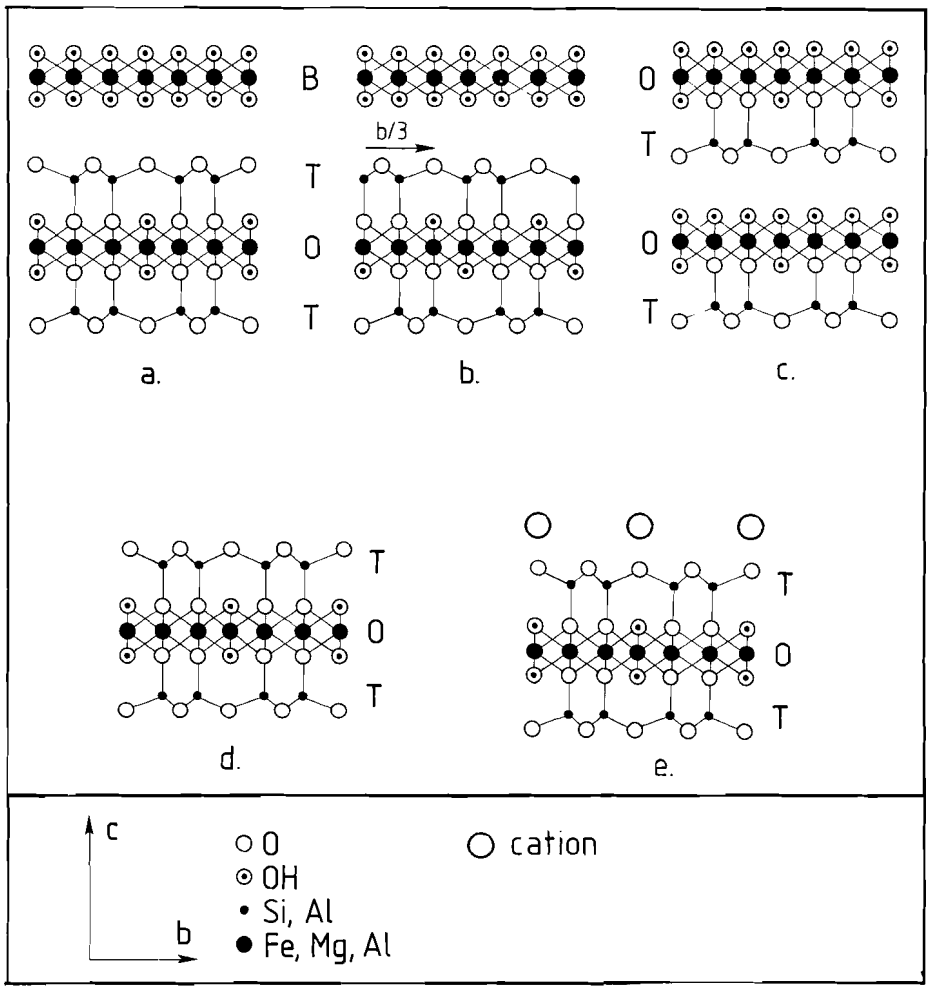

FIGURE 6.2. Schematic representation of the crystal structure of chlorite and related phyllosilicates, projected parallel to [100]. a. Chlorite; total thickness of one unit layer is 14 Å. b. Chlorite with a shift of b/3 in the octahedral sheet of the 2:1 layer. c. 1:1 phyllosilicate, e.g. septechlorite; two layers of 7 Å are drawn. d. Talc structure; unit layer thickness is 9 Å. e. mica (10 Å).

6.1.2 Deformation of phyllosilicates

Studies of phyllosilicate deformation have concentrated mainly on micas. Many experimental studies have shown that the slip plane is (001) and that the dominant slip directions are [100], ±[110] and ±[1$\bar{1}$0] (Mügge 1898, Griggs et al. 1960, Borg and Handin 1966, Hörz and Ahrens 1969, Hörz 1970, Schneider 1972, Etheridge et al. 1973). Early studies on dislocations in mica have reported dislocations parallel to the (001) plane with Burgers vectors $\boldsymbol{b}$=[100], $\boldsymbol{b}$=1/2[110] and $\boldsymbol{b}$=1/2[1$\bar{1}$0], without any visible dissociation (Silk and Barnes 1961, Amelinckx and Delavignette 1962, Demny 1963a); these dislocations occur in the cation interlayer, where dissociation into partials is unlikely (Olives 1985a). These dislocations are not mobile in the electron microscope, not even when the foil is heated (Silk and Barnes 1961).

Bell and Wilson (1977, 1981, 1986) have reported stacking faults and dislocations in muscovite and biotite. The stacking faults were the result of both crystal growth processes and deformation. The observed stacking fault vectors were ±1/3[010], ±1/6[310] and ±1/6[3$\bar{1}$0]. These stacking faults were supposed to occur in the octahedral sheet of the 2:1-layer without significant increase in energy, rather than in the cation interlayer, where the increase in energy would be considerable (Bell and Wilson 1977, Olives 1985a). The dislocations were all contained in the (001) plane; some of the dislocations were clearly dissociated into partials with stacking faults inbetween. In regions where the mica lattice was gently curved slip occurred parallel to (001) by the generation and movement of (partial) dislocations, and subgrains were developed, bounded by dislocation walls subparallel and subnormal to (001). With increasing rotation the strain was no longer accommodated by dislocation creep but dilation along the (001) cleavage plane occurred. This deformation mechanism is thought to be typical for crystalline materials with only one active slip plane (Nicolas and Poirier, 1976; Bell and Wilson, 1981; Bell et al., 1986).

Amelinckx and Delavignette (1962) studied deformed talc crystals with TEM. They observed dislocations with Burgers vectors $\boldsymbol{b}_{total}$=[100], $\boldsymbol{b}_{total}$=1/2[110] and $\boldsymbol{b}_{total}$=1/2[1$\bar{1}$0], dissociated into wide dislocation ribbons of four partial dislocations; the Burgers vectors of the partials are $\boldsymbol{b}_p$=±1/6[010], $\boldsymbol{b}_p$=±1/12[310] and $\boldsymbol{b}_p$=±1/12[3$\bar{1}$0]. These dislocations, and the associated stacking faults, occur inbetween the

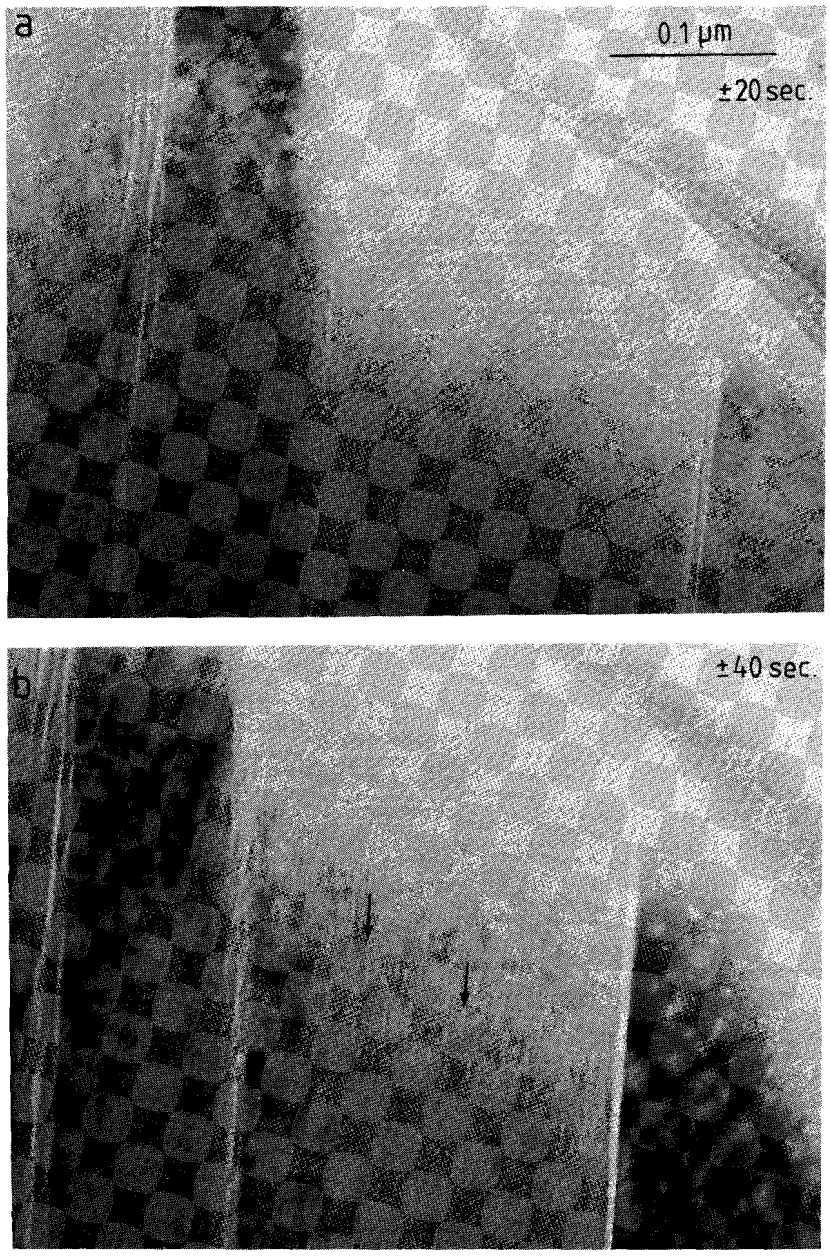

FIGURE 6.3. Beam damage in muscovite. The (001) lattice fringe images are taken at intervals: a. after ca. 20 seconds exposure to the beam, b. after 40 seconds. A mottled structure appears, and some layer separations occur (arrows).

2:1-layers, where stacking fault energy is very low due to the weak bonds between the layers.

It is clear that the deformation of phyllosilicates is dominated by the (001) slip plane, while slip directions are parallel to [100], [010] and other directions which are equivalent due to the pseudo-hexagonal symmetry in the (001) plane. The slip can take place either at the level of the octahedral sheet of the 2:1-layer or inbetween the 2:1-layers.

6.1.3 Techniques

For the TEM study selected areas from thin sections were fixed to copper support grids and thinned down to perforation by ion beam milling. The samples were then coated with carbon and studied in a JEOL 200C electron microscope, fitted with a side-entry goniometer stage, operating at 200 kV.

Often the dislocations were so closely spaced that they could not be resolved by conventional bright field (BF) or dark field (DF) methods. The techniques that have been used in this case are weak beam imaging (WB) and lattice fringe imaging. During lattice fringe imaging, axial illumination was used, i.e. the transmitted beam lies on the optic axis and the diffracted beams are symmetrically disposed about it, so that the position of the resulting lattice fringes is independent of crystal thickness (Edington 1975).

The high-resolution electron microscopy (HRTEM) study was performed at the University of Antwerp (RUCA), Belgium, on a JEOL 200CX fitted with a high-resolution top-entry pole piece, in cooperation with Dr. D. Schryvers (Bons and Schryvers, 1988a,b). Computer simulations of the HRTEM-images have been done using the multislice approach (Goodman and Moodie, 1974). These calculations have been repeated using the real-space method (Van Dyck and Coene, 1984; Coene and Van Dyck, 1984a,b), yielding similar images.

6.1.4 Practical aspects of the TEM observation of mica and chlorite

Most phyllosilicates are rapidly damaged by the electron beam (Demny 1963b, Bell and Wilson 1981, Ahn et al. 1986). Due to beam damage the crystal structure is destroyed and eventually the material becomes amorphous. Beam damage can result from various processes:

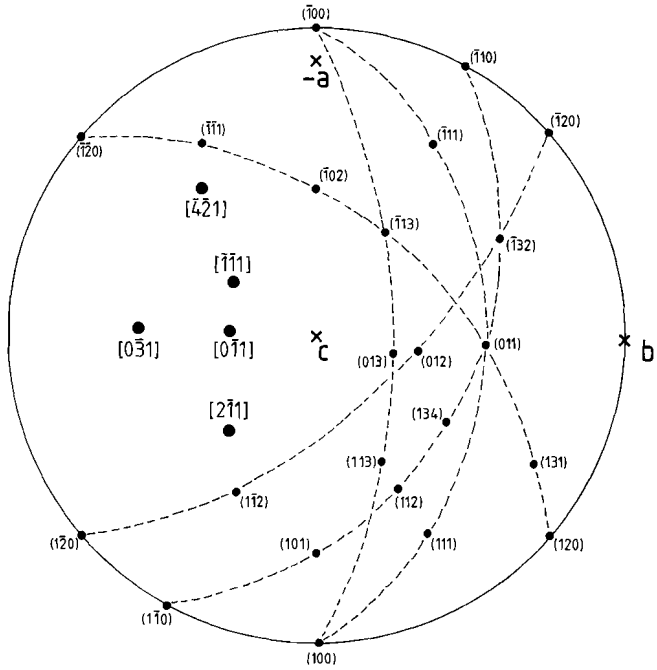

FIGURE 6.4. Upper-hemisphere stereographic projection of the zone axes used in this study to obtain good two-beam diffraction conditions, indexed assuming monoclinic symmetry with β=97°.

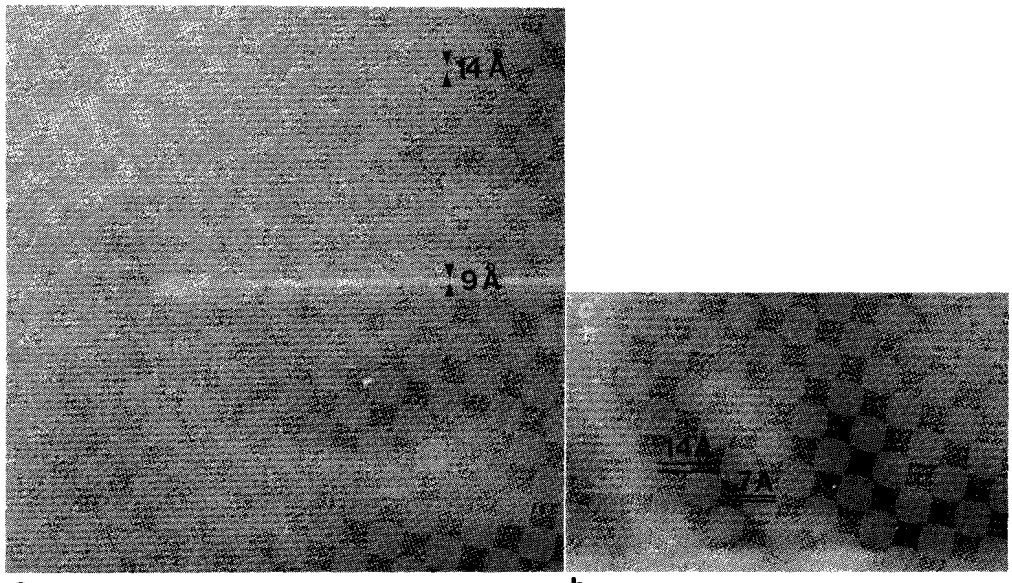

FIGURE 6.5. Deviating lattice fringe spacings in chlorite. a. 9Å-fringe between 14Å-chlorite (001)-fringes b. 7Å fringes in 14Å chlorite-(001)-fringes.

1. *Specimen heating.* When the sample is irradiated by the electron beam, the energy transfer from the beam to the specimen will lead to heating of the specimen. In general the temperature rise in the TEM sample will be on the order of 100°C (Stenn and Bahr, 1970). X-ray diffraction studies of samples heated to 500°C have shown no changes in chlorite and muscovite (see Section 2.3, Fig. 4.3). The first phase change to be expected is the destruction of chlorite above 600°C (Brown and Brindley, 1980). Indeed, no phase changes have been observed in the TEM, and cooling of the sample to -196°C does not affect the radiation damage rate of muscovite. Therefore it can be concluded that specimen heating is probably not very important for the samples in this study.

2. *Ionisation.* The electron beam is strongly ionizing. The amount of energy transferred from the electron beam to the specimen decreases with increasing accelerating voltage, and it has been demonstrated that higher voltages result in less damage to the crystal structure (see e.g. Stenn & Bahr, 1970). This has also been observed in the present study: at 900 kV the radiation damage rate in muscovite is lower than at 200 kV.

3. *The effect of vacuum.* The accelerating voltage is not the only factor affecting the radiation damage rate: destruction of muscovite is found to be slower in a Philips EM-420 operating at 100-120 kV than in a JEOL 200C at 200 kV. This is probably caused by the difference in column vacuum: the vacuum in the column of the JEOL 200C is relatively low and contains fragments of cracked vacuum oil molecules, which is evident from the rapid formation of contamination cones when the beam is concentrated on a single spot. These fragments are also accelerated and will damage the specimen by both ionisation and by displacement of atoms. This effect is less in the Philips EM420.

The muscovites in the slate samples are destroyed within seconds to a minute (see Fig. 6.3). The chlorites however are much more stable and can be studied for several minutes. Beam damage in micas has often been attributed to the removal of hydroxyl from the crystal; if so, then chlorite, containing twice as much hydroxyl then micas, should damage more rapidly. As this is clearly not the case, other processes are responsible for the rapid damage of mica. One process is electron beam enhanced diffusion of cations such as Na^+ and K^+ (Ahn et al., 1986; Van der Pluijm et al., 1988), which leads to local electrostatic charges and to local separation of the crystal layers. This effect is strongest in the Na-mica paragonite (Ahn et al., 1986).

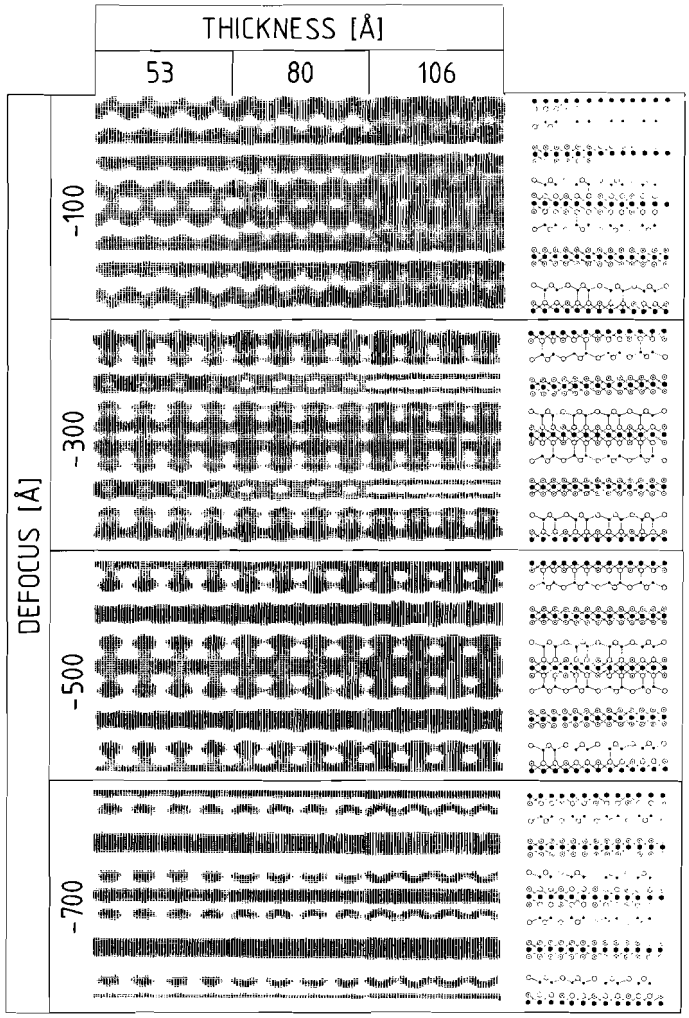

FIGURE 6.6. Calculated HRTEM images of monoclinic ripidolite chlorite projected along [100] for varying defocus value and specimen thickness. The images have been calculated using the multislice method. The atom positions and Debeye-Waller factors are derived from Bailey (1975) and Shirozu and Bailey (1965). The instrumental parameters are: accelerating voltage 200 kV, spherical abberration C_S=1.2 mm, beam divergence 10^{-3} rad, focus spread 50 Å.

In the muscovites of the slate samples some layer separations have been observed, but only to a minor extent. The main visible effect of beam damage is the appearance of patches with a different contrast, which grow in number and area (see Fig. 6.3), resulting in a mottled image instead of a clear crystal. HRTEM images of these patches show that they are associated with a reduction of the crystal thickness, without affecting the lattice spacings. The diffraction patterns show a decrease of the intensity of the diffraction spots, and a gradual appearance of diffraction rings typical for amorphous material. These effects indicate a reduction of the amount of crystalline material and an increase of the amount of amorphous material.

The chlorites show no layer separations at all, and the beam damage effects are limited to the gradual appearance of a mottled image, associated with rings in the diffraction pattern. Therefore it can be concluded that radiation damage in mica and chlorite results in amorphization of the crystal, while some cation diffusion takes place in the micas.

All chlorites studied show sharp k=3n reflections and streaked $k\neq$3n reflections, which indicates that they have a semi-random stacking sequence (Brown and Bailey 1962, Bailey 1975). Many electron micrographs of chlorite show a diffuse contrast of overlapping fringes in the background (see e.g. Fig. 6.13). This is the case in almost all micrographs where the (001) plane is inclined to the electron beam, but it is never observed in cases where (001) is perpendicular or parallel to the beam. It is most likely that the fringe contrast is caused by the stacking disorder: the irregular offsets of chlorite layers are essentially the same as stacking faults and give rise to fringe contrast if the (001) plane is inclined to the beam. Because of the close spacing between the offsets the fringes overlap and give the complex background contrast observed. This background contrast seriously hampers the interpretation of the lattice defects.

Although the radiation damage rate in chlorite is less than in micas, there still is little time for tilt experiments, which makes it difficult to do a complete Burgers vector analysis of the dislocations. Another problem is the difficulty of obtaining two-beam conditions. This effect is typical for strongly layered materials with weak bonds between the layers. During electron diffraction each layer acts as a single crystal with almost zero thickness. Every diffraction spot is thus extended into a

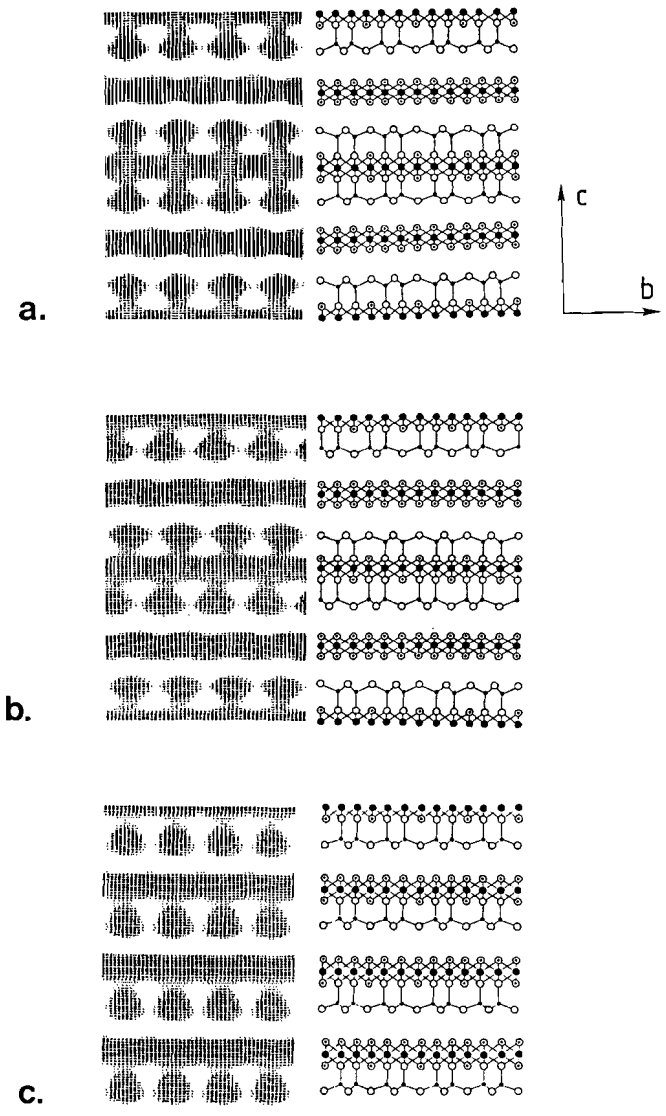

FIGURE 6.7. Calculated HRTEM images of monoclinic ripidolite and deviating structures. Specimen thickness 53 Å, defocus value -500 Å, other parameters as in Fig. 6.6 a. Ordered ripidolite chlorite. b. Ripidolite with shifts of ***b****/3 parallel to the sheets. c. 1:1 phyllosilicate with the same composition as ripidolite*

"spike" in reciprocal space, and will intersect the Ewald sphere even at very large deviations from the Bragg angle. If (001) is at a large angle to the electron beam the spots of a strong reflection zone remain visible even after tilting over several tens of degrees. The diffraction pattern itself becomes distorted and cannot be properly indexed; therefore these orientations cannot be used for quantitative analysis of dislocations. The best two-beam conditions are obtained when (001) is well inclined to the beam; a number of orientations used in the present study is given in Fig. 6.4.

6.2 HRTEM OF STACKING IRREGULARITIES IN CHLORITE

6.2.1 Introduction

Conventional electron microscopical investigations of the chlorites from the slate samples, using the JEOL JEM-200C transmission electron microscope at the University of Utrecht, has shown that these chlorites show various crystal imperfections. All the chlorite crystals, both deformed and undeformed, show extensive stacking disorder and a high density of planar defects parallel to the chlorite layers (Bons, 1988; see section 6.3). The stacking disorder is visible in electron diffraction patterns as a streaking of rows of reflections with $k \neq 3n$. Many of the planar defects, especially those in the undeformed grains, are characterised by a variation in fringe spacing: instead of the 14 Å spacing of the chlorite (001) planes, spacings of ca. 7 Å and 9 Å are observed (Fig. 6.5). The origin of these stacking irregularities is apparently unrelated to the deformation, as they occur in deformed and undeformed crystals alike. It is more likely that they originated during crystal growth; the 7 Å fringes can also be related to weathering, as they occur preferentially near grain boundaries.

Deviating lattice fringe spacings can be caused by actual variations in lattice plane spacing, but also by stacking faults (e.g. Amelinckx and Van Landuyt, 1976, Fig. 7) or by variations in specimen thickness and orientation or electron-optical conditions (Jahren, 1988). In general the nature of planar defects can be analysed with conventional TEM using diffraction contrast (e.g. Edington, 1975). In order to do this the planar defects should be inclined to the electron beam. However, in

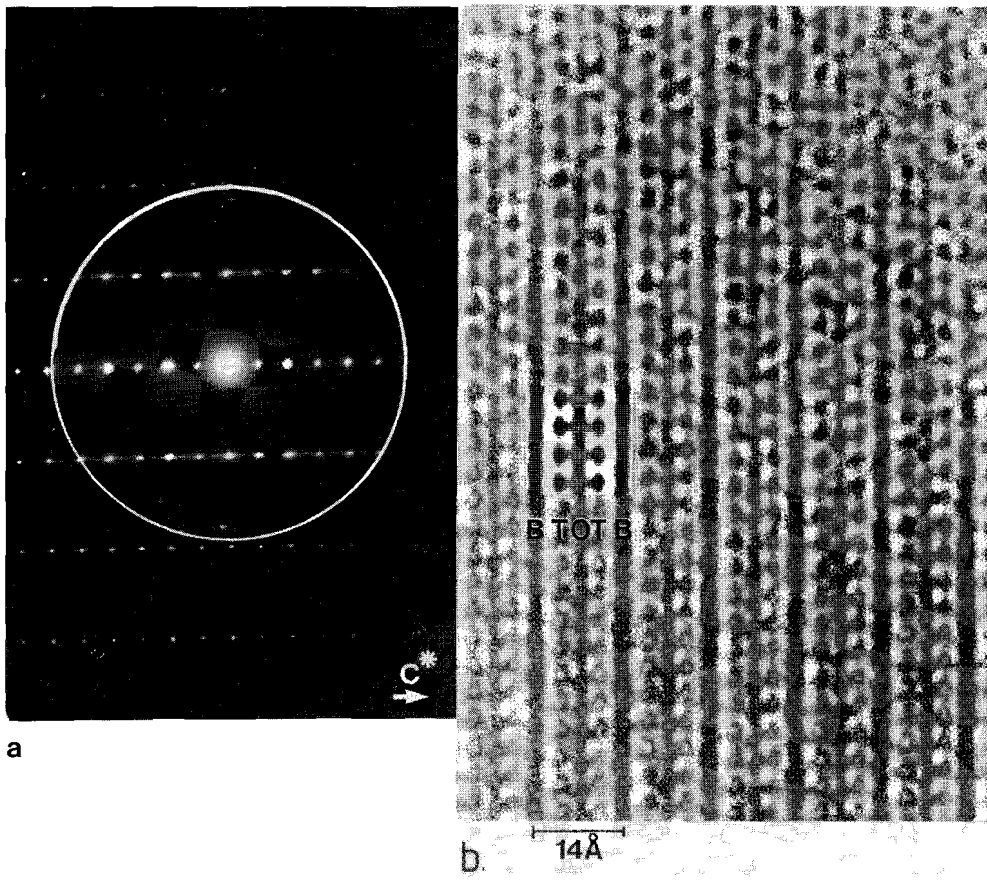

FIGURE 6.8. Relatively well-ordered ripidolite chlorite, viewed along [100] or an equivalent direction. a. Diffraction pattern showing sharp spots and only minor streaking of rows with k≠3n. The white circle indicates the objective aperture used to produce the HRTEM images. b. (following page) HRTEM image taken at a defocus of ca. -500 Å. The inset is a calculated image. Specimen thickness increases from top to bottom. There is good agreement between experimental and calculated image, allowing an interpretation of the experimental image in terms of tetrahedral (T) and octahedral (O) sheets, and brucite (B) interlayer.

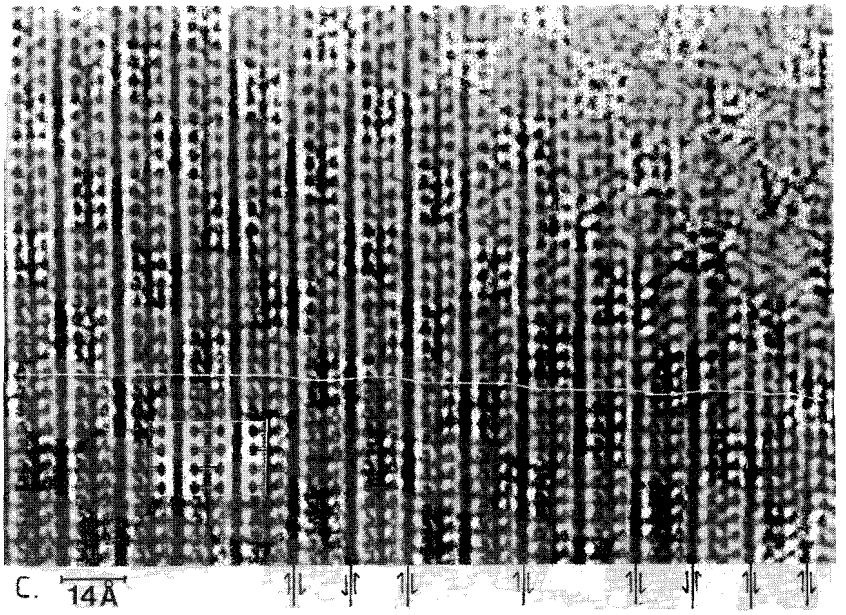

Figure 6.8 (continued). c. The same image as (b) at a lower magnification. Opposite tetrahedral columns are connected with white arrows. No shifts occur across the 2:1 layers, and only occasionally a shift occurs across a brucite interlayer.

the present case defects inclined to the beam often overlap due to the high defect density. In combination with the background fringe contrast described in section 6.1.4, this leads to a complex fringe contrast which hampers the determination of the nature of the defects. When the planar defects are imaged edge-on, i.e. without overlapping, conventional TEM images do not yield useful information. Lattice images obtained with HRTEM do give structural information if the planar defects are viewed edge-on, provided the crystal is viewed along a major zone axis, e.g. along the [100] direction to study defects parallel to (001). Thus, HRTEM is useful in distinguishing shifts between individual layers (Spinnler et al., 1984) or intercalations with a different crystal structure (Olives, 1985b).

For a good understanding of the lattice defects which are due to deformation, it is necessary to understand the nature of the crystal defects which are already present prior to deformation. The aim of this

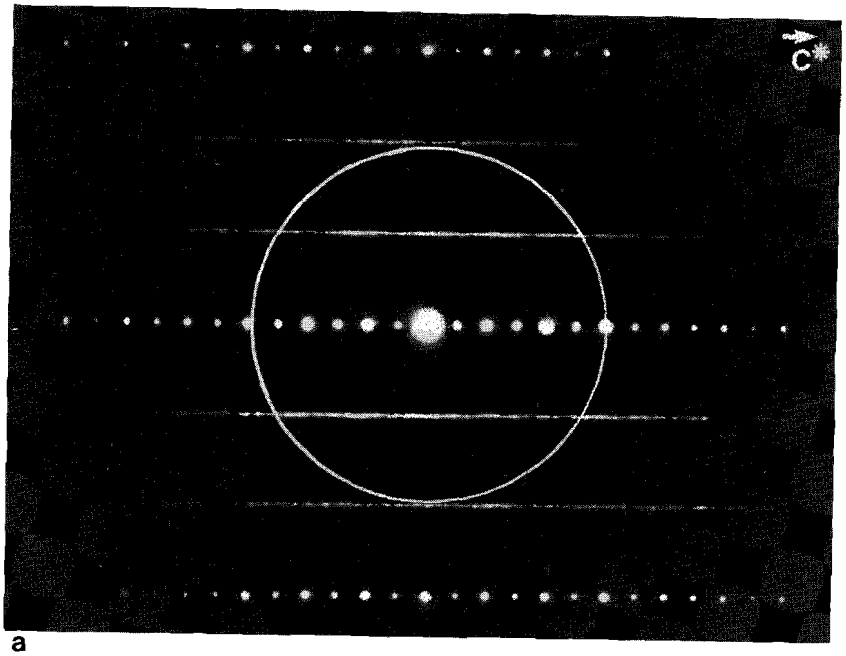

a

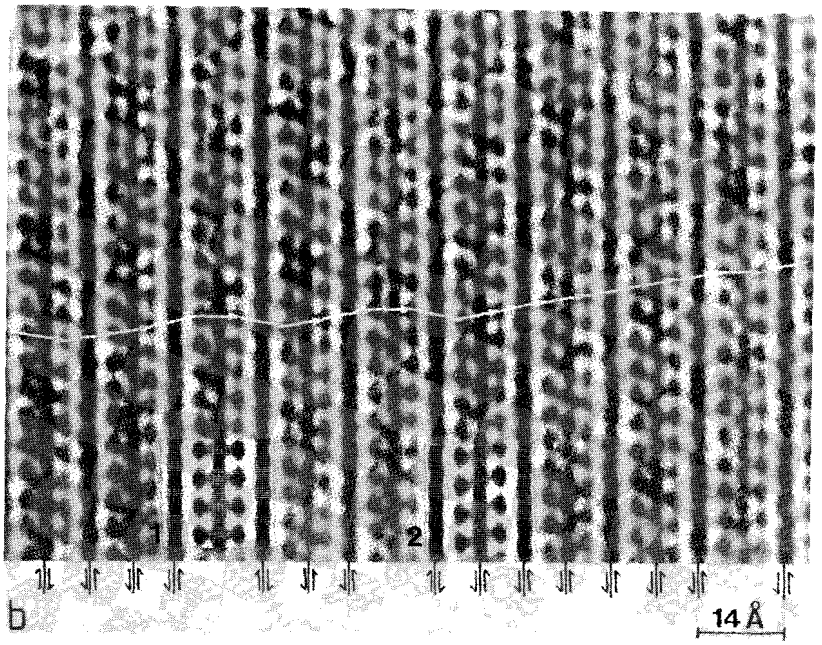

b

FIGURE 6.9. (left) Ripidolite chlorite with a semi-random stacking sequence, imaged under the same conditions as Fig. 6.8. a. Diffraction pattern showing complete streaking of rows with k≠3n. The white circle indicates the objective aperture used to produce the HRTEM images. b. Experimental HRTEM image. As in Fig. 6.8 the white arrows connect opposite tetrahedral columns; shifts occur both at the brucite interlayer and across the 2:1 layer. The insets are calculated images: (1) undisturbed ripidolite crystal, (2) ripidolite with a shift of ***b****/3 across the 2:1 layer.*

section is to analyse the nature of the stacking disorder and of the planar defects which are associated with deviating fringe spacings.

6.2.2 Computer simulations of HRTEM images

The interpretation of HRTEM images is not always straightforward. In the ideal case the image contrast of a very thin specimen at optimum (Scherzer) defocus represents the projected potential of the crystal, and a direct interpretation in terms of the crystal structure is possible. However, in the majority of cases HRTEM images should be interpreted by comparison with compu ter-simulated images, calculated using an assumed crystal structure as input and taking into account the experimental conditions of the microscope. In general some parameters will be known (e.g. spherical abberration, beam divergence, defocus value), but other parameters, such as the exact crystal structure and sample thickness will be unknown. In practice a set of images is calculated for a range of realistic defocus values and specimen thicknesses, and this set is compared with the corresponding experimental images (e.g. Self et al., 1985).

Figure 6.6 shows a set of calculated images for chlorite, viewed along the [100] direction for varying defocus and specimen thickness, assuming a ripidolite composition (see section 5.3.8) and monoclinic symmetry. It is clear that the image does not vary strongly with specimen thickness over the range considered here. Also, the images taken near -500 Å defocus are easily interpreted in terms of the crystal structure. The octahedral sheets (both the one in the 2:1 layer and the octahedral brucite sheet) are represented by continuous dark bands; the tetrahedra, which are grouped in columns in this projection (see Fig. 6.1c) are visible as dark "blobs" at both sides of the octahedral sheet of

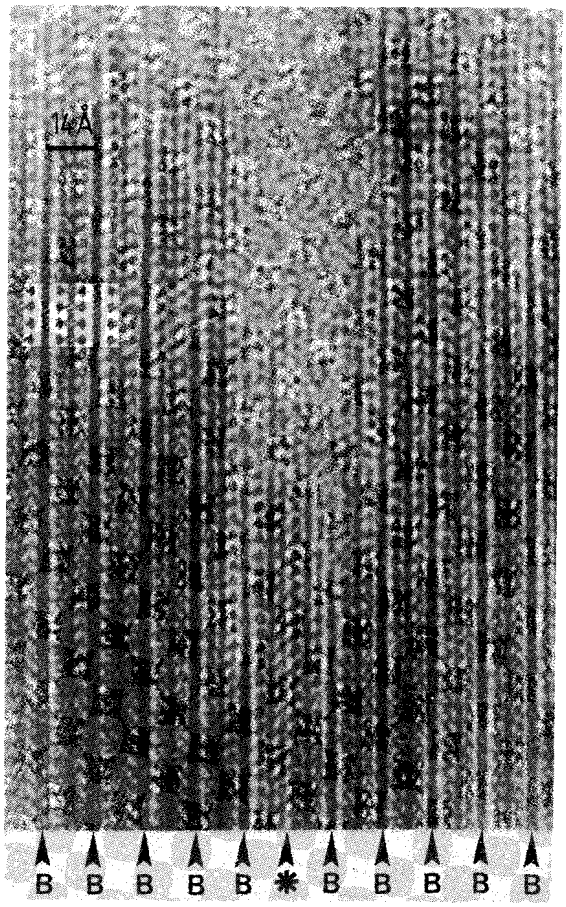

FIGURE 6.10. HRTEM image of an area where a 9 Å lattice fringe is intercalated between 14 Å chlorite (001) fringes. The inset shows a calculated image for ripidolite. At the bottom the brucite interlayers are marked with B. At the asterisk one brucite interlayer is missing.

the 2:1 layer. In the ordered structure presented here, the tetrahedral columns are exactly opposite each other, both across the 2:1 layer and across the brucite interlayer. Figure 6.7 shows some images calculated for varying crystal structures at a defocus of -500 Å. It is clear that images taken along the <100> directions are easy to interpret, as the octahedral sheets are visible as dark bands, and the tertrahedral columns form dark "blobs" attached to the octahedral sheet. Such a simple relationship between crystal structure and image is often referred to as an *imaging code*, by which many defects in the perfect structure can be readily interpreted (Van Dyck et al., 1982). Shifts between adjacent layers can then be detected as shifts between the dark blobs representing the tetrahedral columns. Deviating structures, such as the 1:1 phyllosilicate structure, are recognisable as a deviating distribution of octahedral and tetrahedral sheets (Fig. 6.7 c).

6.2.3 Experimental images: results and discussion

Four distinctive cases have been investigated with HRTEM: (1) relatively well-ordered chlorite, (2) chlorite with a semi-random stacking, (3) chlorite showing isolated 9 Å fringes, and (4) 7 Å fringes. All images are taken along a <100> direction. The defocus value is on the order of -500 Å; this has been checked by analysing the amorphous areas on the HRTEM images (Spence, 1981). The results of the four cases will be discussed below.

(1) *relatively well-ordered chlorite.* The diffraction pattern shown in Fig. 6.8a shows well-defined spots, and only minor streaking of rows with $k \neq 3n$. This indicates that the crystal has a relatively well-ordered stacking sequence. Figure 6.8b shows a HRTEM image of the same crystal; the calculated image for the appropriate imaging conditions is also given. There is good agreement between the experimental image and the calculated image. Also, the variation of the image with specimen thickness agrees well with the calulated images in Fig. 6.6. This allows an interpretation of the image in terms of the crystal structure: the 2:1 layer and the brucite interlayer are easily recognizable, as are the tetrahedral columns.

Figure 6.8c shows the same image at a lower magnification. In a perfectly ordered crystal the tetrahedral columns should all be aligned. This is not the case here: the tetrahedral columns across the 2:1 layer are

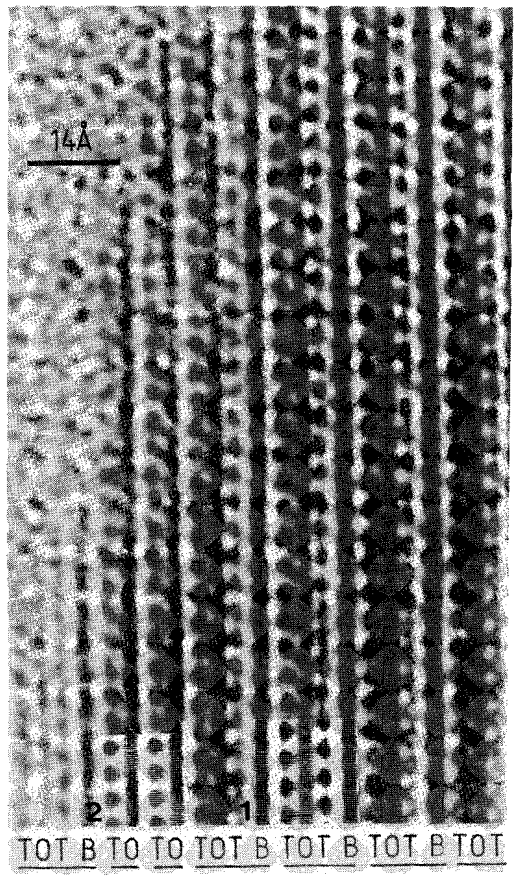

FIGURE 6.11. HRTEM image of an area with 7 Å lattice fringes. The inset shows calculated images for ripidolite (1) and a 1:1 phyllosilicate with a ripidolite composition (2). T=tetrahedral sheet, O=octahedral sheet, B=bructte interlayer. The 7 Å fringes are caused by intercalations with a 1:1 phyllosilicate structure.

always opposite each other, but occasional shifts across the brucite interlayer do occur.

(2) *semi-random stacking.* Figure 6.9a shows a diffraction pattern with sharp k=3n reflections and streaking of $k\neq3n$ reflections, indicating a semi-random stacking sequence. The HRTEM image of this area reveals that the tetrahedral columns are not opposite each other any more, but shifts parallel to the basal planes occur both at the brucite interlayer and at the 2:1 layer. There is a good correspondence bewteen the experimental image and calculated images for a chlorite structure with shifts of **b**/3 along the octahedral sheet of the 2:1 layer. There is no regular repeat sequence of these shifts, so the structure cannot be described as a polytype or a superstructure, but it is truly semi-random.

Spinnler et al. (1984) have used HRTEM to study the stacking disorder in a clinochlore chlorite crystal. X-ray observations had shown that the crystal was predominantly of the monoclinic 2b-II polytype. The semi-random stacking sequence of their crystal is reflected in electron diffraction patterns by streaking of rows with $k\neq3n$. However, the streaking is not complete and weak maxima occur along the streaks, showing that most of the crystal is monoclinic (Spinnler et al., 1984). Thus, Spinnler et al. (1984) were able to describe the stacking disorder in terms of shifts relative to the ordered 2b-II polytype, and therefore as intercalations of different polytypes.

In the case of the disordered ripidolite chlorite crystals of the present study the streaking of the rows with $k\neq3n$ in electron diffraction patterns is complete in most cases (e.g. Fig. 6.9a), and it is not possible to determine the space group of the crystals. Therefore even the diffraction pattern of the relatively well-ordered crystal of Fig. 6.8a cannot be interpreted unambiguously: the 90° angle between 00*l* and *hk*0 can either indicate the [100] zone of a monoclinic crystal, or one of the <100> directions of an ortho-hexagonal crystal. An interpretation of the HRTEM images in terms of one-layer polytypes is therefore not possible. Nevertheless, the HRTEM images clearly show that the semi-random stacking is caused by shifts in the (001) planes which can occur either at the brucite interlayer or in the 2:1 layer.

(3) *9 Å fringes.* A HRTEM image of an area where a single 9Å fringe is intercalated between 14 Å fringes is given in Fig. 6.10. The crystal structure of chlorite is easily recognised at the left- and right-hand sides of the micrograph. At the position of the 9 Å fringe the

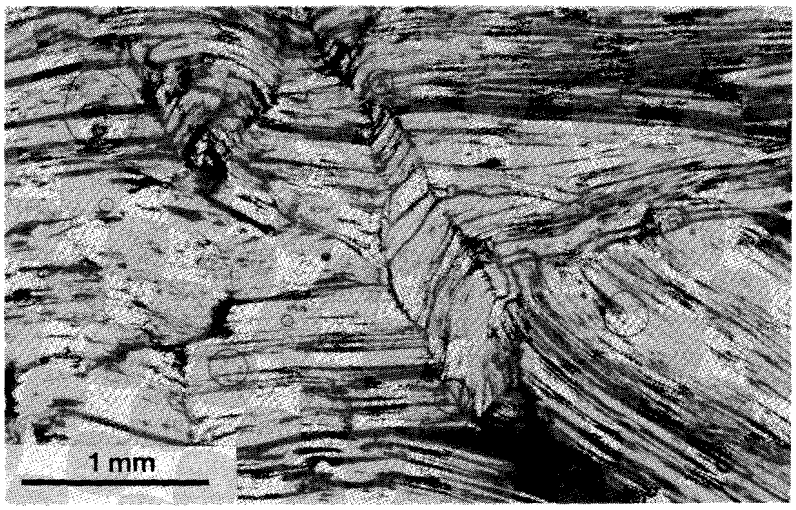

FIGURE 6.12. Kinked chlorite crystals from the Traversella region, Italian Alps (plane polarized light).

brucite interlayer is missing. Thus, locally the chlorite structure is disturbed, and one can speak of a single layer with a talc structure.

(4) *7 Å fringes.* Figure 6.11 shows a HRTEM image of an area with 7 Å fringes. Again, the chlorite structure can be recognised in the undisturbed part of the crystal. The image structure at the position of the 7 Å fringes is characterised by two dark bands, each with a series of "blobs" at one side, suggesting a structure formed by a single tetrahedral sheet attached to a single octahedral sheet, i.e. a 1:1 phyllosilicate. To check whether this interpretation is valid, the experimental image is compared with a calculated image for a 1:1 phyllosilicate. There is good agreement between experimental and calculated image, and therefore these 7 Å fringes are interpreted as intercalations of a 1:1 phyllosilicate.

The last two examples show that in the chlorites studied here the deviating lattice fringe spacings observed in a conventional transmission electron microscope are actually caused by intercalations with a different crystal structure, resulting in local deviations of the lattice spacing.

The observations mentioned above clearly demonstrate that HRTEM is a very powerful tool in the study of crystal imperfections, especially in cases where conventional TEM cannot resolve the nature of those imperfections.

6.2.4 Conclusions

Several types of stacking irregularities in ripidolite crystals from slates of the Seo Formation of the Orri Dome have been studied with HRTEM. The semi-random stacking is caused by shifts parallel to the basal planes, which occur at the level of the brucite interlayer as well as in the 2:1 layer. There is no regular repeat sequence of these shifts in the direction of the c-axis.

Deviations of the normal lattice fringe spacing of 14Å are caused by actual deviations of the crystal lattice spacing. 9 Å fringes are associated with a missing brucite interlayer, i.e. an intercalation of a single layer with a talc structure. 7 Å fringes can be explained by intercalations of a 1:1 phyllosilicate.

6.3 DEFORMATION OF CHLORITE

6.3.1 Samples

The chlorites in the slates of the Orri Dome are very complexely deformed. Therefore the deformation substructures in chlorite have first been studied in a much simpler case: relatively large kinked chlorite crystals from the Italian Alps.

The kinked chlorites were collected in the Sesia-Lanzo Zone in the Western Alps, near Traversella (Italy). The chlorites were deformed during greenschist facies metamorphism, which took place in the Eocene after the Eoalpine high pressure-low temperature metamorphism (Dal Piaz et al. 1972). The crystals are platelets up to a centimetre wide and several millimetres thick. The width of the kink bands is on the order of 200 μm (Fig. 6.12). EDS-analyses indicate a penninite composition (classification of Hey 1954):
$Mg_{9.2}Fe_{1.0}Al_{1.7}[(Si_{6.4}Al_{1.6})O_{20}/(OH)_4](OH)_{12}$.

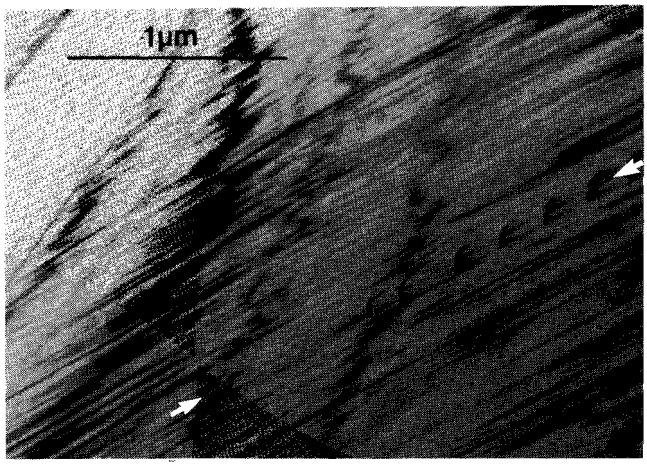

a

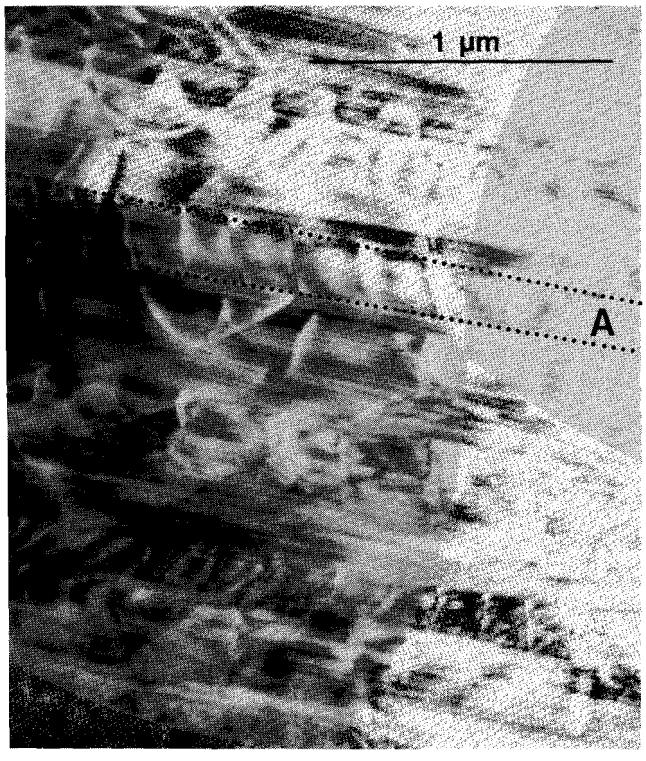

b

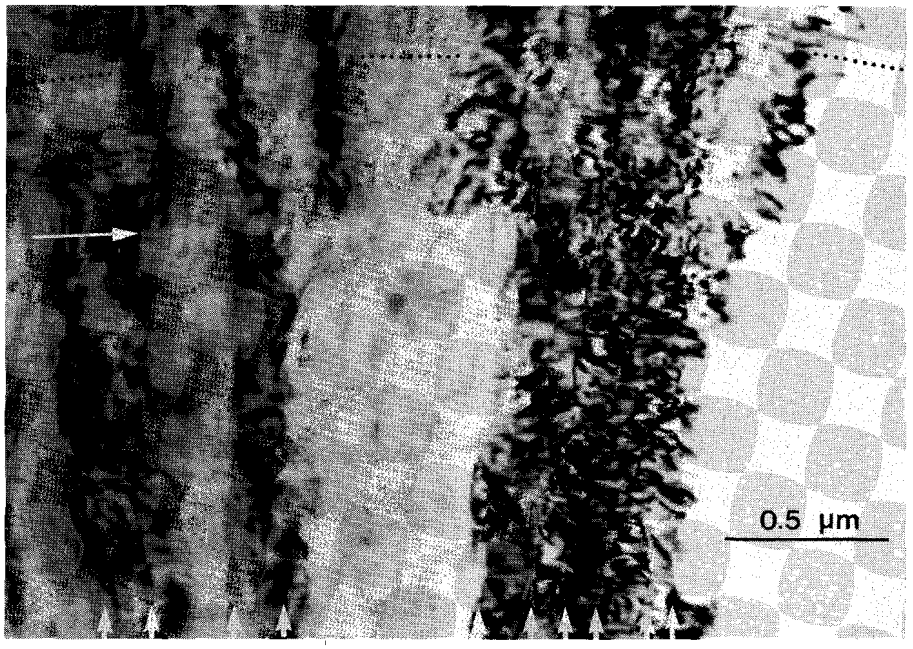

FIGURE 6.13. Dislocations in the kinked chlorite crystal of Fig. 6.12. a. BF transmission electron micrograph of an area outside the kinkband; dislocation density is low. A single dislocation band is visble between the arrows. The background fringe contrast, caused by the stacking disorder of the crystal, is parallel to the (001)-trace. b. DF micrograph of an area inside the kink band, showing a much higher dislocation density. Dislocations are arranged in dislocation bands; one dislocation band is indicated by A. Dotted lines indicate the intersections between the dislocation band A and the upper and lower surfaces of the thin foil. No subgrain walls have developed. c.. BF micrograph of the kink hinge area; the (001)trace is indicated by black dotted lines. Dislocation density is very high; dislocation walls subnormal to (001) (short arrows) and subparallel to (001) (long arrow) are visible.

6.3.2 Deformation substructures in chlorite

In the kinked chlorite crystals three deformational domains can be distinguished: (1) the areas outside the kinkbands, (2) the areas inside the kinkbands and (3) the kink hinges. The rotation axes of the kinkbands lie in the (001) plane. Electron diffraction patterns of the

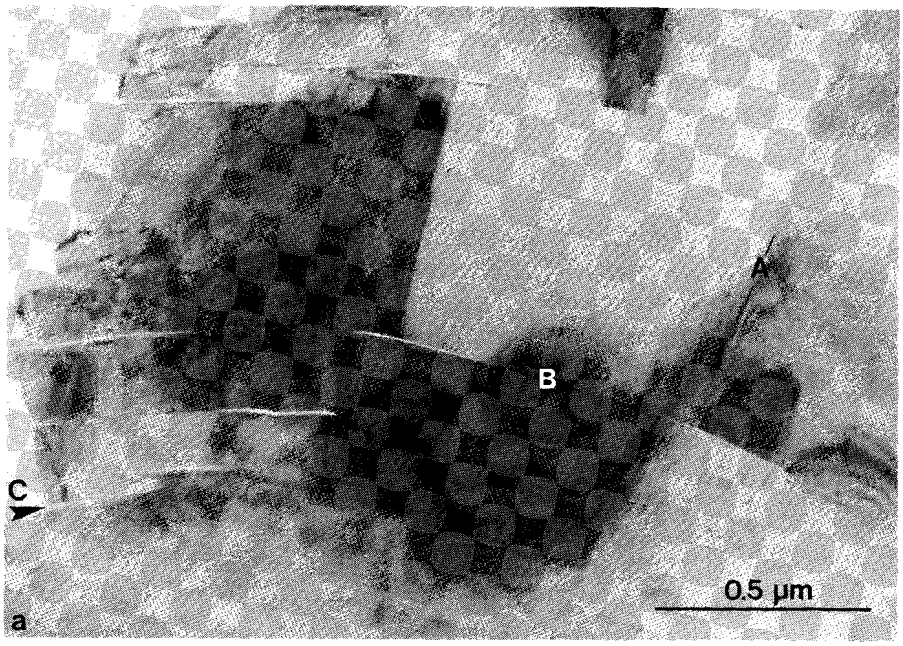

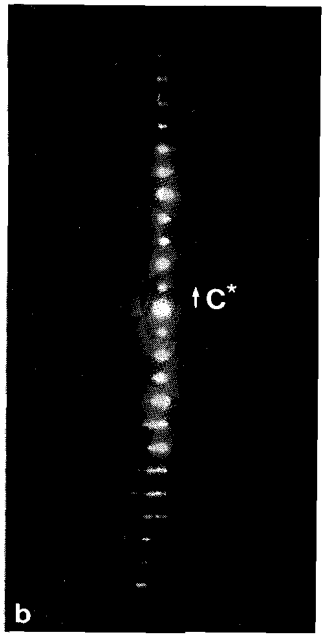

FIGURE 6.14. Subgrains in deformed chlorite from one of the slate samples. a. BF micrograph of subgrains with boundaries subnormal (A) and subparallel (B) to (001); the dilation parallel to the (001) cleavage planes is caused by electron beam irradiation. The arrow at C indicates a boundary along which the misfit decreases from 30° at the grain boundary to 0° inside the crystal. b. Selected area diffraction pattern of (00l) reflections showing discrete rotations of the crystal.

kinkband of Fig. 6.12 and Fig. 6.13 show that the rotation axis is parallel to [100].

In the areas outside the kinkbands the crystal lattice is straight (Fig. 6.13a). Dislocation density is low to moderate ($<3 \cdot 10^8$ cm^{-2}). The dislocations are usually arranged in dislocation bands; apart from this the dislocations are homogeneously distributed throughout the crystal and no subgrains have developed. The areas inside the kinkbands show much higher dislocation densities ($>2 \cdot 10^9$ cm^{-2}), but the dislocations are still homogeneously distributed and subgrains are absent (Fig. 6.13b).

Detailed study of the kink hinges (Fig. 6.13c) reveals that the rotation takes place over a wider area, instead of in one discrete kink as has been assumed in crystallographic models of kink bands in micas (Starkey 1968, Baronnet and Olives 1983). Bell et al. (1986) observed the same feature in kinked mica cristals. In chlorite the kink hinge zone is a few microns wide and it is divided into subgrains. Within each subgrain the crystal is only very slightly bent. At the subgrain boundaries there is a rotation of about 2°. The subgrain boundaries show two preferred orientations: (1) subparallel to (001) and (2) subnormal to (001). In these areas the dislocation density is so high that the individual dislocations cannot be distinguished. Apart from dilation during electron beam irradiation (Fig. 6.14a), no dilation along (001) planes has been observed.

The deformed chlorites from the slate samples show similar structures. In areas where the crystal is not bent dislocation densities are low, and dislocations are evenly distributed through the crystal. If the crystal is bent, subgrains are developed, with subgrain boundaries subnormal and subparallel to (001), and dislocation density is very high. The discrete rotations between subgrains are also clearly visible in electron diffraction patterns (Fig. 6.14b).

Individual dislocations

When dislocations are imaged using HRTEM two types of dislocations can be distinguished: (1) dislocations associated with terminating (001) lattice fringes, and (2) dislocations that do not affect the (001) lattice fringes. Because their Burgers vectors can be written in a general form as [00w] and [uv0] (see below), these two groups will be referred to as [00w] and [uv0] dislocations, respectively.

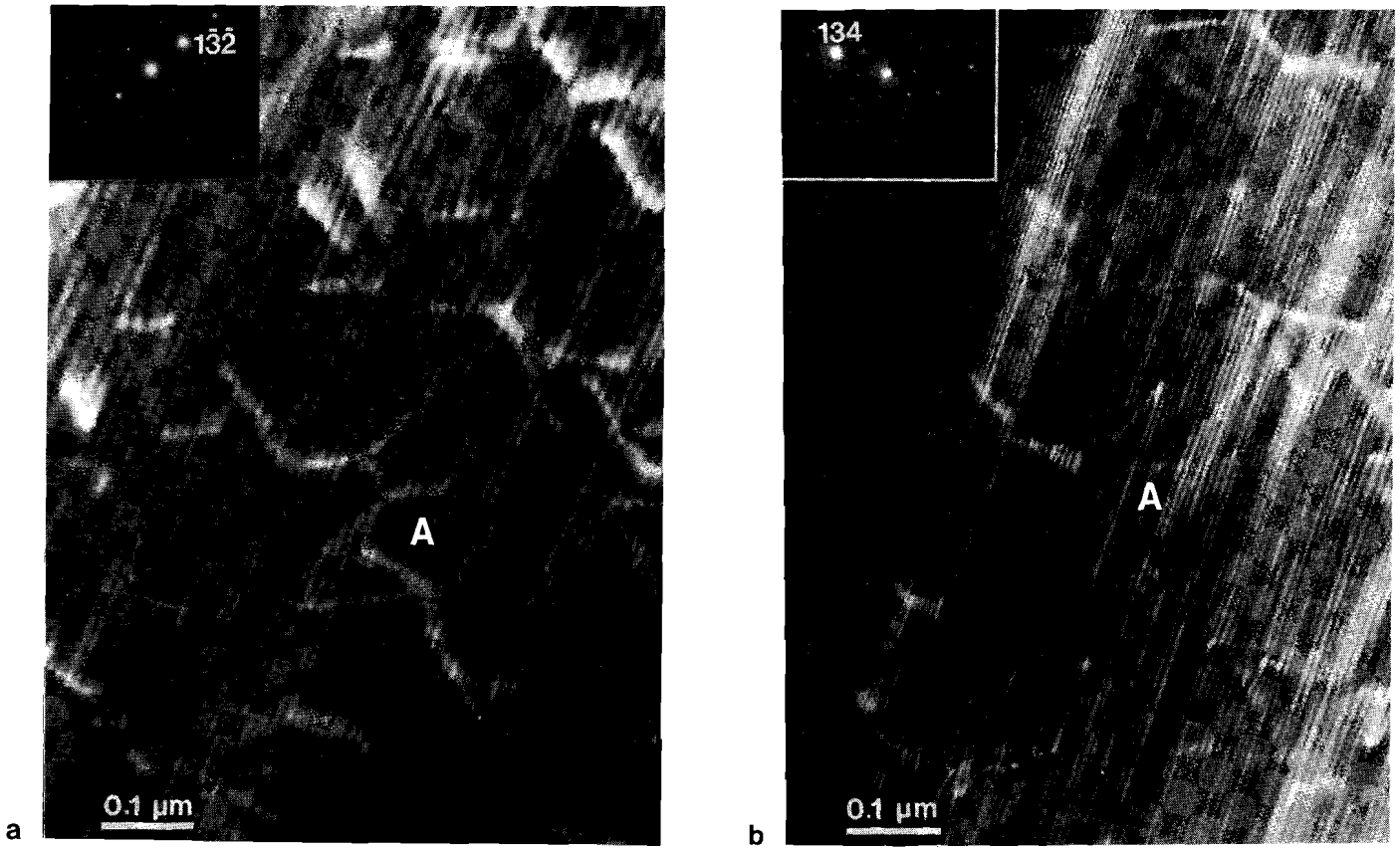

FIGURE 6.15. Example of a contrast analysis of [uv0] dislocations.
a. $\mathbf{g}=[1\bar{3}\bar{2}]^*$*; several dislocations are visible, e.g. the cluster around A. b.* $\mathbf{g}=[134]^*$*; the dislocations around A are now out of contrast. The background fringe contrast is parallel to the (001) trace.*

a) *[uv0] dislocations*. In general the dislocation densities are low where the (001) planes are straight. Most of the dislocations in these areas are of the [*uv*0] type. When the foil is heated by concentrating the electron beam on a small area the [*uv*0] dislocations become mobile and start moving parallel to the (001) plane.

Although a complete Burgers vector analysis was not achieved, some general information on the Burgers vector directions could be obtained. In lattice fringe images of [*uv*0] dislocations the (001) fringes are continuous, indicating that these dislocations do not affect the (001) planes. Furthermore, these dislocations are always out of contrast if the operating reflections are of the form 00*l*. This indicates that the Burgers vectors have no component in the direction of the c-axis, and can therefore be written in a general form as $\boldsymbol{b}$=[*uv*0].

Figure 6.15 shows two DF-images of [*uv*0] dislocations taken under two-beam conditions. There are three groups of dislocations:
1. dislocations visible for both $\boldsymbol{g}$=[134]* and $\boldsymbol{g}$=[1$\bar{3}\bar{2}$]*
2. dislocations visible for $\boldsymbol{g}$=[134]* but invisible for $\boldsymbol{g}$=[1$\bar{3}\bar{2}$]*
3. dislocations visible for $\boldsymbol{g}$=[1$\bar{3}\bar{2}$]* but invisible for $\boldsymbol{g}$=[134]*

(where $\boldsymbol{g}$ is the vector normal to the reflecting plane). Using the invisiblity criterion

$$\boldsymbol{g} \cdot \boldsymbol{b} = 0$$

and taking into account that the Burgers vectors lie in the (001) plane, this means that there are at least three different Burgers vectors, with directions ±[310], ±[3$\bar{1}$0] and [*uv*0] (u≠±3v).

Sometimes the [*uv*0] dislocations are associated with planar defects; these planar defects are parallel to (001). Generally the nature of planar defects can be analysed using the fringe pattern which is visible when the defect plane is inclined to the beam (see e.g. Edington 1975). Unfortunately this was not possible in the chlorites, due to the high defect density (see section 6.2.1). These planar defects are usually not associated with deviating lattice fringe spacings, and are therefore different from the planar defects studied with HRTEM (section 6.2).

b) *[00w] dislocations*. The other type of dislocation is associated with terminating (001) lattice fringes, which indicates that their Burgers vector has a component in the direction of the c-axis. Under special conditions (dislocation parallel to the beam, axial illumination; see Edington, 1975) terminating lattice fringes may be

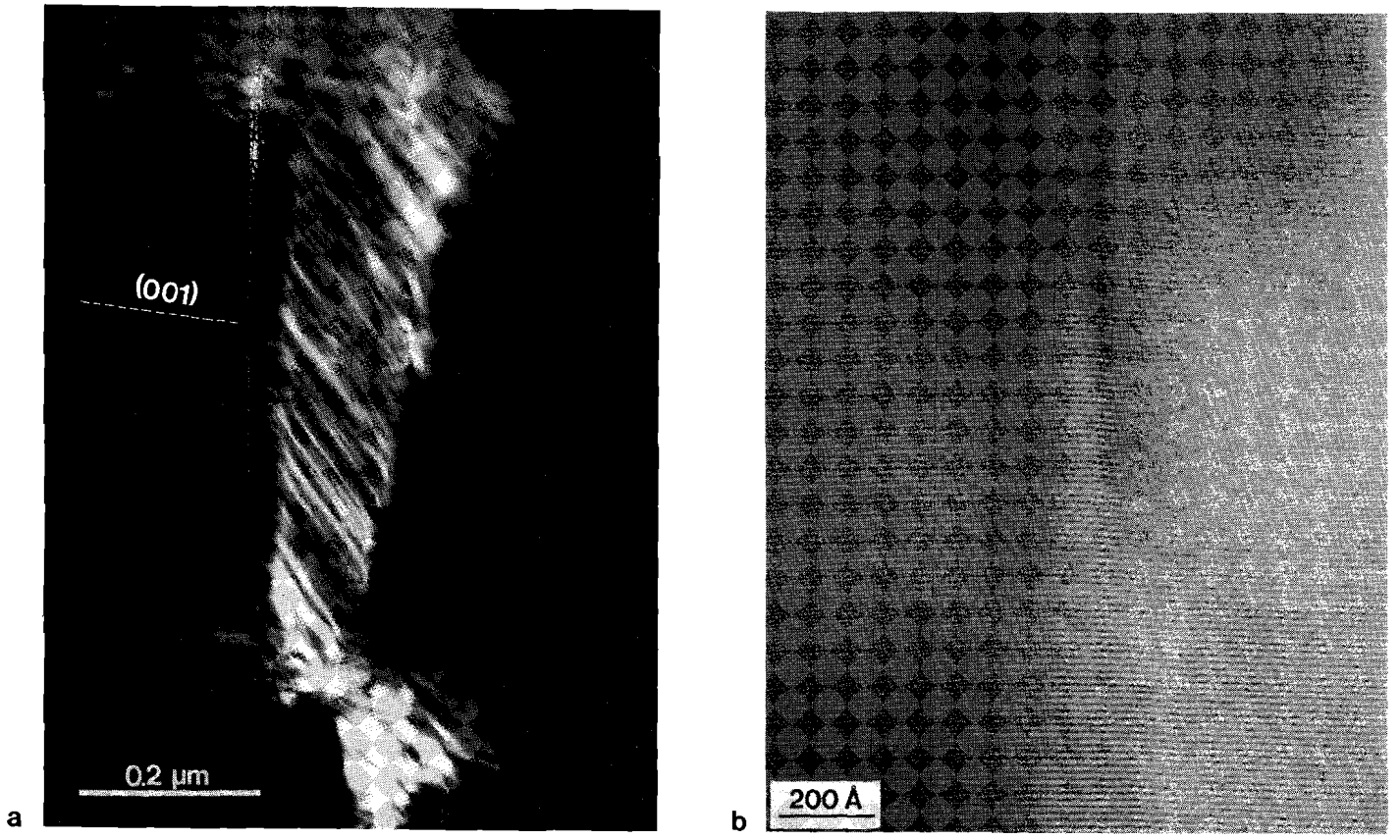

FIGURE 6.16. a. WB image of a tilt wall subnormal to (001); the dislocation lines are parallel to [110]. The spacing of the dislocations along the wall is variable. The (001) trace is indicated. b. HRTEM image of the boundary showing continuous (001) lattice fringes.

interpreted as terminating lattice planes; therefore these dislocations can be described as edge dislocations with a total Burgers vector $\boldsymbol{b}$=[001]. Similar dislocations have been described by Knipe (1981), Lee et al.(1984, 1986), Ahn and Peacor (1985) and Bell (1986).

Dislocation walls

At the subgrain boundaries the dislocations are so close to each other that they cannot be resolved using conventional BF or DF techniques. However, WB or HRTEM images show that these boundaries are formed by arrays of dislocations (Figs. 6.16 and 6.17).

One group of subgrain boundaries is oriented at a very high angle to (001) (Fig. 6.16). The misorientation across the walls is in the range of 1-3°. The dislocations that form the boundary are contained in the (001) plane and they are always parallel to [100], [010], and equivalent directions. Lattice fringe images show that the (001) planes are continuous across the boundaries (Fig. 6.16b), indicating that the dislocations are of the type [*uv*0]. Invisibility of the dislocations for (00*l*) reflections confirms this. Diffraction patterns (Fig. 6.14b) and lattice fringe images (Fig. 6.16b) show that the walls are pure tilt walls and that the rotation axes are parallel to the dislocation lines. This indicates that the dislocations are pure edge dislocations, and that their Burgers vectors are parallel to [010], [100], and equivalent directions.

The other group of subgrain boundaries is subparallel to (001) (Fig. 6.17). HRTEM images show that they are formed by a series of terminating crystal layers (Fig. 6.17b). These layer terminations can be described as edge dislocations with Burgers vector $\boldsymbol{b}$=[001]. If the boundary is inclined to the beam, the dislocations become visible (Fig. 6.17a). The spacing between the dislocations is very small. In the case of Fig. 6.17a the spacing is in the order of 100 Å. Measurements on lattice fringe images indicate an angle of misfit between 2 and 3°. Because the boundary is asymmetric, the equation

$$|\boldsymbol{b}| \; / \; d = \sin \Theta$$

applies (where $|\boldsymbol{b}|$=length of the Burgers vector, d=spacing between dislocations and Θ=angle of misfit, see Hull and Bacon 1984) indicating that the Burgers vector has a magnitude on the order of 3-4 Å, which is much smaller than the unit vector of 14 Å. The presence of partial

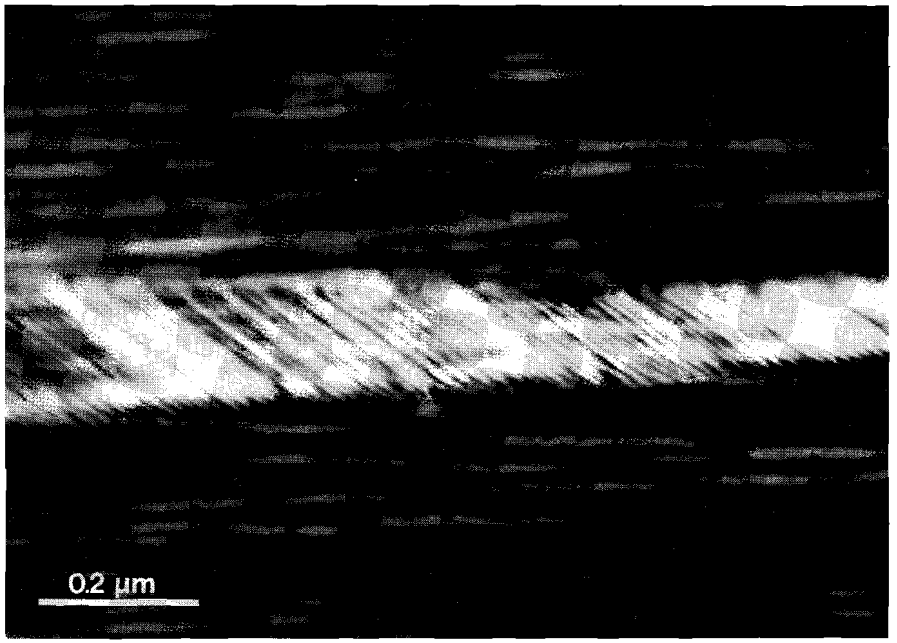

FIGURE 6.17. a. WB micrograph of a dislocation wall subparallel to (001). The spacing between the dislocation lines is on the order of 0.01 μm.

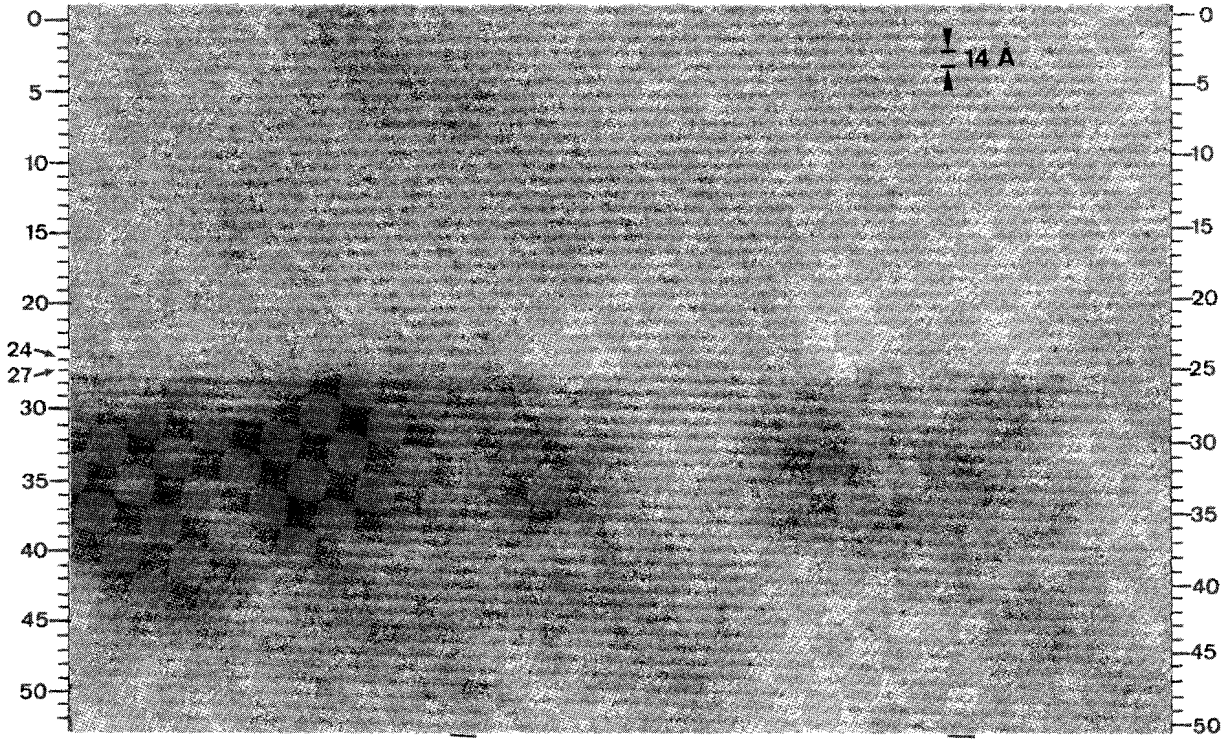

FIGURE 6.17 (continued). b. (001) lattice fringe image of the boundary. The bright fringes are numbered on both sides of the picture. Fringes 25 and 26 gradually wedge out from right to left; this can best be seen by viewing the page at a glancing angle in a direction parallel to the fringes.

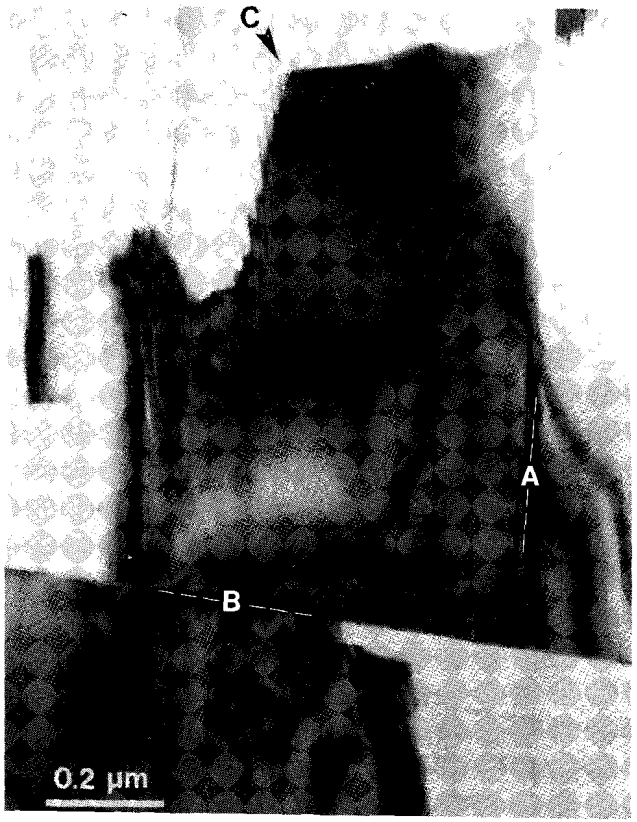

FIGURE 6.18. a. Subgrains in deformed chlorite; subgrain boundaries are subnormal (A) and subparallel (B) to (001). The arrow at C indicates the tip of a propagating boundary where there is a cluster of [00w] dislocations.

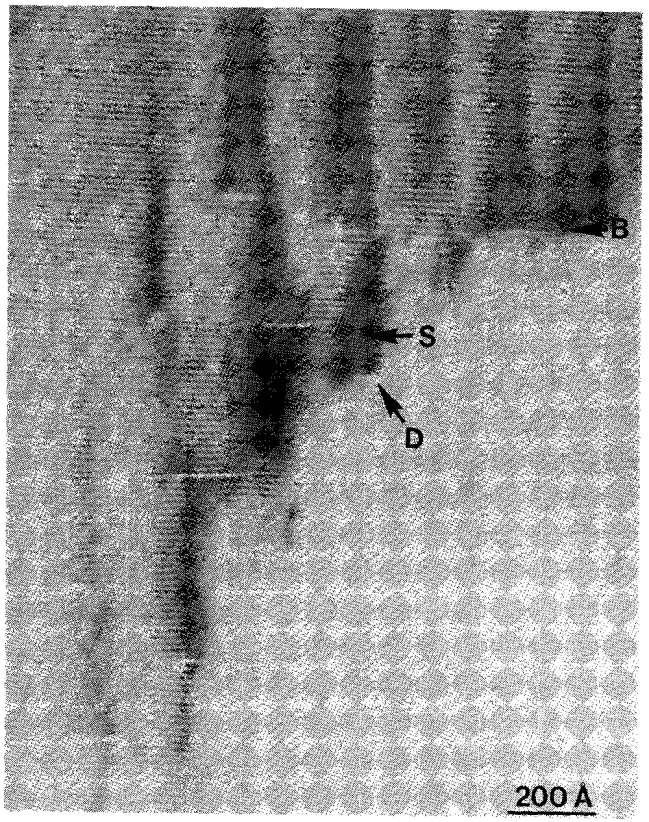

b. (001) lattice fringe image of the cluster of [00w] dislocations at the tip of the subgrain boundary; B = subgrain boundary, D = dislocation. The strain fields (S) of the dislocations are visible as regions with high contrast; the strain fields extend from one dislocation to another.

dislocations along these subgrain boundaries has been confirmed by HRTEM (Zwart and Bons, 1987; see section 6.6). The subgrain boundaries subparallel to (001) often terminate inside the crystal. Usually there is a cluster of [00w] dislocations just ahead of the tip of the boundary (Fig. 6.18).

Both types of subgrain boundaries can grade into high-angle boundaries. Along boundaries subparallel to (001) the misfit can increase within one micron from zero to more than 30° (Fig. 6.14a).

6.3.3 Discussion

In the previous section it has been shown that there are two groups of dislocations: [uv0] dislocations and [00w] dislocations. These two groups will be discussed separately.

a) *[uv0] dislocations.* Both the dislocation lines and the Burgers vectors of these dislocations are contained in the (001) plane. As in talc and mica, the Burgers vectors are parallel to [100], [010], and equivalent directions. The magnitude of the Burgers vectors is unknown. Regarding the magnitude of the unit displacement vectors, which vary from 5.2 Å for $\boldsymbol{b}$=[100] to 9.2 Å for $\boldsymbol{b}$=[010], it is unlikely that they are unit dislocations (although unit dislocations with $\boldsymbol{b}$=[100] (5.2 Å) do occur in the cation layer of micas; Silk and Barnes 1961, Amelinckx and Delavignette 1962, Demny 1963a). If they are partial dislocations, they would be expected to be associated with stacking faults. However, only a few of the dislocations are visibly associated with a planar defect.

In this context, it is necessary to consider the consequences of the stacking disorder. The stacking disorder itself is caused by displacements of b/3, which take place both within the 2:1 layer and at the interlayer (Spinnler et al. 1984; Bons and Schryvers, 1988a,b). Because most chlorites have disordered stacking sequences, displacements of 1/3<010> can apparently occur without any increase in energy. If, due to deformation, partial slip occurs along (001) over a distance b/3 in one of the appropriate directions, the resulting crystal would not have a higher energy state than before. The plane where the partial slip was induced would not differ from any other plane where the offset of b/3 was an original feature of the crystal (e.g. Fig. 6.19b), and it would therefore not show any additional contrast. In the case where slip

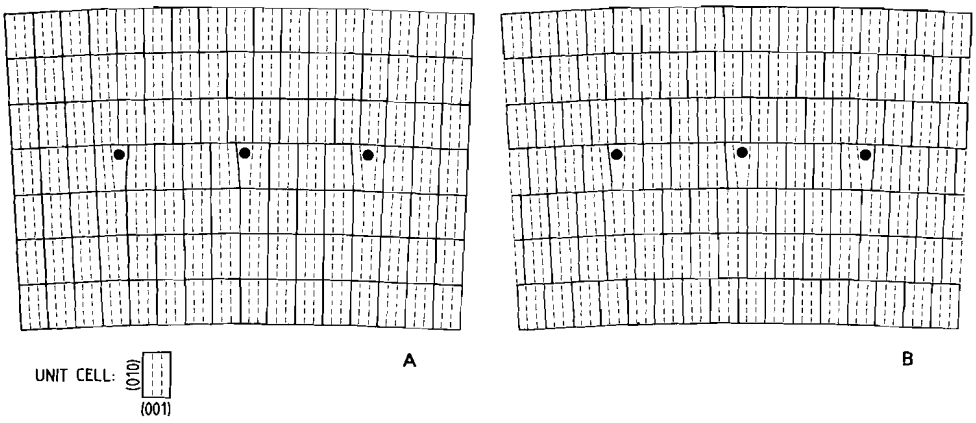

FIGURE 6.19. Schematic representation of partial dislocations with **b**=*1/3[010]. The black dots indicate dislocation cores. a. A crystal with a regular stacking sequence; there are stacking faults in between the dislocations. b. A crystal with stacking disorder; the crystal structure in between the partial dislocations does not differ from the overall crystal structure and no stacking faults will be visible.*

is restricted to a limited area within one (001) plane, the area of slip would be bounded by dislocations. Although these dislocations are partial dislocations, the surface in between can hardly be called a stacking fault. Also, the sum of the partial dislocations would not necessarily be a unit vector. Only those stacking faults which have a displacement vector other than b/3 will give rise to a visible planar defect, although the contrast will be obscured by the background contrast.

Most of the observed dislocations, including those of Fig. 6.15, are not visibly associated with stacking faults; often the Burgers vectors are parallel to <010>. In view of what was stated above these dislocations can be interpreted as partial dislocations with Burgers vectors $\boldsymbol{b}=\pm 1/3[010]$, $\boldsymbol{b}=\pm 1/6[310]$ and $\boldsymbol{b}=\pm 1/6[3\bar{1}0]$. The few dislocations which are visibly associated with stacking faults either have a displacement of b/3 in an area with a (short-range) regular stacking sequence, or have a totally different displacement vector, e.g. with direction <100>. The tilt walls with Burgers vector directions <100> are possibly formed by unit dislocations, because no stacking faults are visible on either side.

b) *[00w] dislocations.* Every chlorite crystal shows some free [00w] dislocations. In regions with straight (001) planes the dislocation density is low; if the crystal is bent the dislocation density is much higher and tiltwalls subparallel to (001) are formed.

The formation of dislocation walls requires the generation and/or movement of dislocations. Figure 6.20 shows two different models for the formation of a [00w] dislocation wall. In model A a number of [001] dislocations is distributed evenly throughout the undeformed crystal. Such dislocations have been observed frequently in phyllosilicates, especially in diagenetic and anchimetamorphic rocks (Knipe 1981; Lee et al. 1984, 1986; Ahn and Peacor 1985; Ahn et al. 1985; Bell 1986). If the crystal is strained the dislocations start to move and align themselves in a dislocation wall subparallel to (001). The movement of dislocations involves slip on (hk0) planes and climb along (001). In model B the dislocations nucleate at the edge of a perfect crystal, and move into the crystal by climb along (001). The surface of the crystal acts as a vacancy source. This process involves transport of material by diffusion along the boundary. In both models an increasing misfit across the boundary is accommodated by increasing the dislocation density along the boundary.

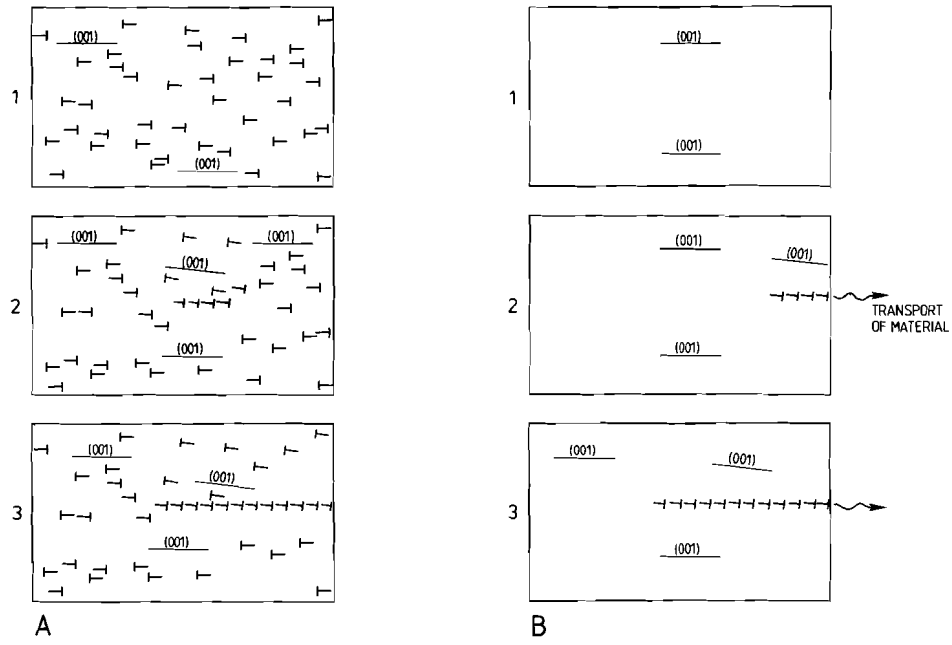

FIGURE 6.20. Two models for the formation of [00l] dislocation walls. Model A: dislocations which are originally evenly distributed throughout the crystal move towards the boundary by slip along (hk0) planes. Model B: dislocations nucleate at the grain boundary and move into the crystal by climb, which involves transfer of material. Most boundaries are formed by a combination of these two processes. ⊣ = edge dislocation; (001) = (001)-trace.

The TEM observations on chlorite indicate that both models for the formation of [00w]-dislocation walls may apply. Many boundaries, such as the boundaries in Fig. 6.14a, run from high-angle boundaries at the surface of the crystal into low-angle boundaries inside the crystal, and terminate somewhere inside the crystal. Apparently one section of the crystal is displaced relative to the rest of the crystal (cf. Gregg, 1986, fig. 2a); the strain is accommodated by the formation (and subsequent movement by climb) of [00w] dislocations (Model B).

Other subgrain boundaries do not reach the crystal surface (e.g. Fig. 6.18). At the tip of these boundaries there are often clusters of [00w] dislocations (Fig. 6.18b); this geometry can be interpreted in terms of dislocations moving towards the tip of the boundary. This involves dislocation glide along (hk0) planes. The absence of bands of [00w] dislocations along (hk0) planes indicates that it is not an easy slip plane. The strain contrast around the dislocations in Fig. 6.18b extends from one dislocation to another, indicating that not only the strain field, but also the stress field extends from one dislocation to the other. Apparently the stresses at the tip of the subgrain boundary are large enough to activate hard slip systems.

Most subgrain boundaries show characteristics of both models shown in Fig. 6.20; they have reached a high-angle stage at the crystal surface, grade into a low-angle boundary inside the crystal and terminate in a cluster of [00w] dislocations. Thus it can be concluded that usually both mechanisms of subgrain boundary formation operate simultaneously.

The fact that intermediate stages of the development of subgrain boundaries are preserved in these samples indicates that the propagation of a wall is relatively slow, even if the wall has developed into a high-angle boundary some distance away. The termination of a subgrain boundary inside a crystal leads to long-range stress fields at the tip of the boundary (Hull and Bacon 1984). In materials with multiple slip systems (e.g. metals, quartz, olivine) these stress fields are reduced by rapid propagation of the boundary by the attraction of free dislocations, and no intermediate stages are observed (e.g. White 1971, Boland et al. 1971, Takeuchi and Argon 1976, Hull and Bacon 1984). In chlorite the subgrain boundary can reach a relatively high angle of misfit before the stresses at the tip of the boundary are large enough to activate the hard (hk0) slip systems.

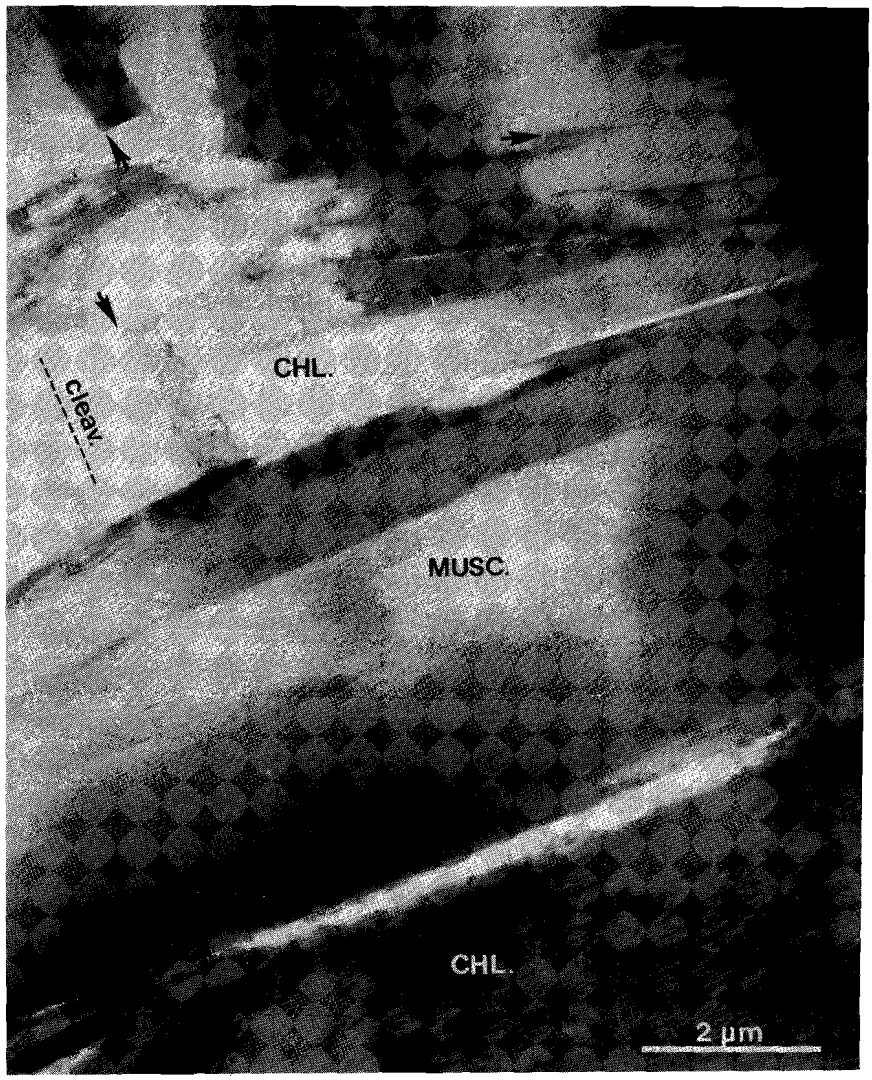

FIGURE 6.21. HVTEM image, taken at 0.9MV, of a chlorite-mica aggregate in a microlithon. The chlorite (CHL) is strongly curved and is full of dislocations and subgrains walls (arrows). The muscovite (MUSC) is almost straight and shows no defects, apart from some low-angle boundaries parallel to (001).

Both conventional TEM images and HRTEM images of [00w] tilt walls indicate that the magnitudes of the Burgers vectors are on the order of 3-4 Å (see above), which is a fraction of the unit vector of 14 Å. This could be explained by the termination of the 14 Å unit layer being divided into steps of the size of one tetrahedral or octahedral sheet (Zwart and Bons, 1987), thus minimizing the core energy of the dislocation. This process is called climb dissociation (Poirier, 1985).

Kinks can only be produced without creating voids between the layers if slip along the layers is possible; therefore the kinks in chlorite indicate slip along (001). In the example of Fig. 6.13 the rotation axis is parallel to <100>, which indicates slip in the <010> direction. The kink bands in the chlorites are relatively narrow and widely spaced (Fig. 6.12), so it can be assumed that most of the slip took place inside the kink band. This slip leads to the development of a high [uv0] dislocation density, while outside the kinkband, where the amount of slip is limited, dislocation density is much lower. Thus it is clear that slip along (001) is accommodated by the generation and movement of [uv0] dislocations. Due to the short Burgers vectors and the low stacking fault energy, movement of these partial dislocations should be relatively easy. This inference is supported by the observed mobility of the dislocations in the microscope; unit dislocations in muscovite are not mobile under these conditions (Silk and Barnes 1961). In contrast to mica and talc, where the dislocations occur either within the 2:1 layer or at the cation layer, the dislocations in chlorite can occur simultaneously at various levels in the unit layer. Thus higher dislocation densities (and therefore higher strains) can be reached, before the dislocations interfere with each other.

A slight curvature of the lattice, as is observed inside the subgrains, is usually associated with moderately high dislocation densities, on the order of $5 \cdot 10^9$ cm^{-2}. Apparently the bending is accommodated by some slip along (001) (flexural slip). If the bending increases, the dislocations pile up in dislocation walls subnormal to (001), thus concentrating the misorientation in a discrete subgrain boundary (glide polygonization).

If the amount of rotation varies in a direction normal to (001), as is often the case because the deforming grain is constrained by its neighbours, the misorientation has to be compensated in some way. In the deformed chlorites the misorientation is accommodated by the

formation of subgrain walls subparallel to (001), which is achieved by the generation and/or accumulation of [00w] dislocations, as has been shown above. By a combination of dislocation glide along (hk0) planes and climb along (001) these dislocation walls can accommodate any amount of misorientation.

If a crystal is to deform plastically while it is constrained by the surrounding grains, at least five independent slip systems are required; this is the Von Mises criterion (see Paterson 1969). If there are insufficient slip systems available, the stresses will finally exceed the strength of the bonds between the crystal layers and cleavage cracks will occur (Nicolas and Poirier 1976, p. 44), unless other mechanisms such as diffusion and extensive kinking are active (Paterson 1969).

In the case of phyllosilicates, there are several easy slip directions in the (001) plane, thus providing two independent slip systems. Other mechanisms are clearly necessary to allow a general plastic deformation. Most phyllosilicates show extensive kinking, which can increase the number of effective slip systems to a total of four (Paterson 1969). However, many phyllosilicates cannot provide the required five slip systems and cleavage cracks are common (Bell et al. 1986). No cleavage cracks have been observed in chlorites, indicating that completely plastic deformation is achieved. There are several mechanisms that either reduce the required number of slip sytems or add to the two slip systems that are always present.

The Von Mises criterion applies strictly to homogeneous, constant volume deformation. Pressure solution, although of minor importance in this case, combined with the diffusion processes associated with dislocation climb, will cause volume changes. Furthermore, the deformation is clearly inhomogeneous in all chlorites observed. Therefore less than five slip systems may be sufficient for plastic deformation.

In chlorite there are several mechanisms which add to the two slip systems to achieve plastic deformation. One mechanism is kinking, which is observed in the samples from the Alps, but which is only of minor importance in the slates. Another process is the movement of [00l] dislocations along (hk0) planes at high local stresses. Although this system is only activated locally, it is important because it is essential in the formation of subgrain boundaries subparallel to (001). As these boundaries are formed by very closely spaced parallel dislocation lines,

they provide easy paths for diffusion, possibly facilitating dislocation climb.

Thus, although there are only two easily activated independent slip systems, chlorite can deform plastically; this apparently occurs by a combination of dislocation glide, kinking and diffusion. The two types of chlorite investigated here show essentially the same deformation and polygonization mechanisms, despite the fact that the penninite was deformed under greenschist facies conditions, and the ripidolite was deformed under anchizone (sub-greenschist facies) conditions.

6.3.4 Conclusions

Intracrystalline deformation in chlorite involves a complex polygonisation mechanism, which divides the crystal into subgrains bounded by dislocation walls subnormal and subparallel to the (001) plane. As in other phyllosilicates, the deformation of chlorite is dominated by the (001) slip plane. Slip along this plane is very easy through the generation and movement of (partial) dislocations with $\boldsymbol{b}=[uv0]$. After initial bending of the (001) planes through a flexural slip mechanism, accommodated by slip along (001), the misorientation is concentrated in tiltwalls subnormal to (001). These tiltwalls are formed by (partial) dislocations with $\boldsymbol{b}=[uv0]$. Tiltwalls subparallel to (001) are formed by arrays of dislocations with a total Burgers vector [001]. These dislocations either nucleate at the grain boundary and move inwards by dislocation climb, or move towards the tip of propagating boundaries by glide along planes inclined to (001); once a boundary is formed the increasing misfit is accommodated by climb of these dislocations along (001). Due to the combination of very easy slip along (001) and the ability to form subgrain boundaries subparallel to (001) by dislocation climb and the activation of hard slip systems, chlorite deforms plastically even at temperatures as low as 250-350 °C.

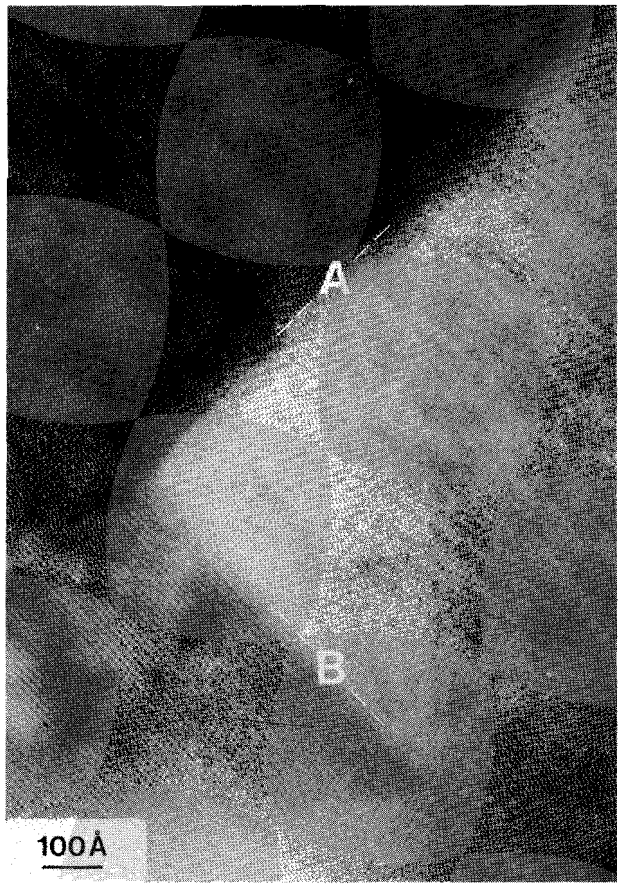

FIGURE 6.22. (001) lattice fringe image of a subgrain in muscovite. Subgrain bondaries are subnormal (A) and subparallel (B) to (001).

6.4 DEFORMATION OF MUSCOVITE

6.4.1 Observations

In general the muscovites show very few crystal defects. Even in chlorite-mica aggregates, which consist of alternating layers of chlorite and muscovite, the chlorite is full of dislocations and subgrains, while the muscovite is almost strain-free (Fig 6.21). Small-scale lattice defects, such as individual dislocations and stacking faults, could have been invisible due to beam damage, but larger defect structures such as subgrains should still be visible. Instead, the muscovites show a gentle curvature, usually without subgrains.

The fast radiation damage rate of the muscovites seriously hampers the observation of lattice defects. However, lattice defects in muscovite have been observed, e.g. with the 1MV microscope in Apeldoorn; at high voltages the radiation damage rate is low enough to allow time for rotation towards orientations which give good contrast. These dislocations are contained in the (001) plane. Any more information on dislocation line orientation and Burgers vectors could not be obtained.

Occasionally subgrains have been observed (Fig 6.22). The orientation of the subgrain boundaries is very similar to those in chlorite: subgrain boundaries are subparallel and subnormal to (001).

Small strain-free muscovite crystals are frequently observed in strongly deformed crystals in the microlithons. Usually there is no relation between the crystallographic orientations of the two crystals, and most small muscovites are oriented with the (001) planes more or less parallel to the cleavage lamellae (Fig. 6.23).

6.4.2 Discussion

Due to the fast beam damage of the muscovite very little information about the intracrystalline deformation processes could be obtained. In general it seems that polygonization in muscovite occurs in a way similar to chlorite, by the formation of subgrains with boundaries subnormal and subvertical to (001). However, the clusters of [00w] dislocations at subgrain boundary terminations, which are observed in chlorite, have never been observed in muscovite, suggesting that

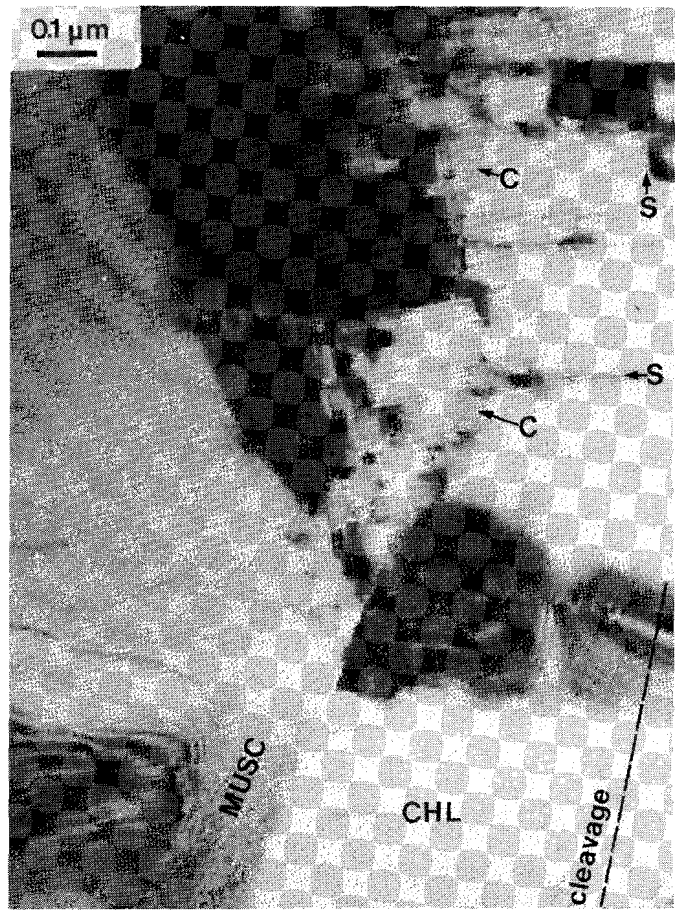

FIGURE 6.23. Small muscovite grain (MUSC) growing into highly deformed chlorite (CHL). Subgrain walls are indicated by S; clusters of [00w] dislocations by C. The orientation of the slaty cleavage is indicated. (BF HVTEM micrograph taken at 0.9 MV)

non-basal slip is not possible in muscovite, as has been suggested by many authors (see section 6.1.2). Apparently the formation of subgrains in muscovite takes place by the generation and accumulation of [uv0] dislocations (as has also been described by Bell and Wilson, 1981, 1986), and by climb of [00w] dislocations.

The most striking difference between chlorite and muscovite in the slate samples is the very low internal strain of muscovite relative to chlorite, see e.g. Fig. 6.21. As these crystals are deformed under exactly the same circumstances, suffering exactly the same amount of deformation, there clearly is a difference in the deformational behaviour between chlorite and muscovite.

The small muscovite grains which are found in deformed chlorites and muscovites (e.g. Fig. 6.23) can be interpreted as new grains growing into the deformed phyllosilicates, in analogy with the optical evidence (section 5.5.3). New chlorite, replacing muscovite, has never been observed. These observations suggest that deformation of muscovite under anchizone metamorphic conditions leads to grain boundary migration. There is some evidence for polygonization, but this mechanism is of secondary importance.

The large amount of dislocation creep in chlorite is possible due to the crystal structure which allows very high densities of stacking faults and dislocations (see section 6.3.3). This is not the case in muscovite. Dislocations do occur in the cation interlayer, but they are not very mobile (Silk and Barnes, 1961; Olives et al., 1983) in contrast to dislocations in chlorite (see section 6.3.2). According to Bell and Wilson (1977, 1981, 1986) partial slip and the formation of stacking faults is possible in the octahedral sheet of the 2:1 layer. However, the introduction of stacking faults will increase the energy state of the crystal, in contrast to chlorite. Therefore it is likely that the yield stress of muscovite is higher than that of chlorite; deformation will initially lead to elastic strain in muscovite concurrent with plastic strain in chlorite. If plastic strain occurs in muscovite, the stored plastic strain energy could be higher than in chlorite. As the stored strain energy is one of the driving forces for recrystallisation (Etheridge and Hobbs, 1974; Urai et al. 1986), this might be a reason for the early recrystallisation of muscovite relative to chlorite. The stored strain energy also increases the diffusivity and solubility and therefore enhances mass transfer, which is necessary for the crystallisation of new muscovite.

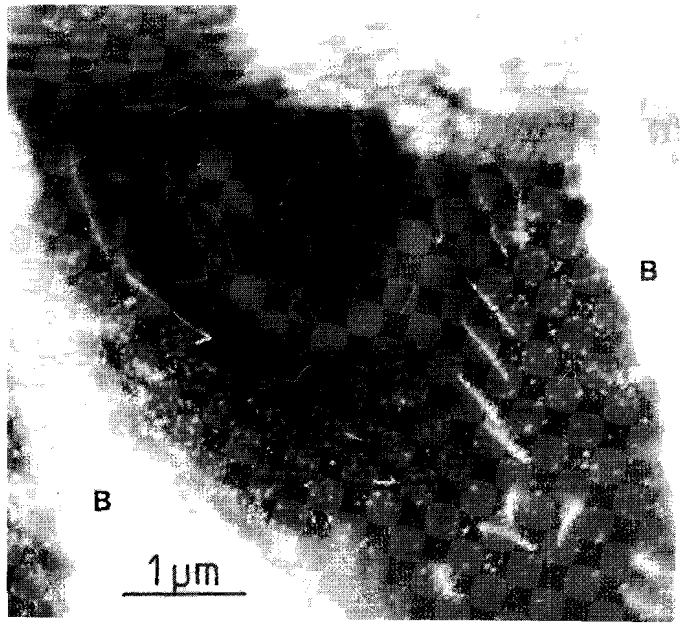

FIGURE 6.24. DF micrograph of dislocations in quartz in a microlithon. The white bands B are bend contours.

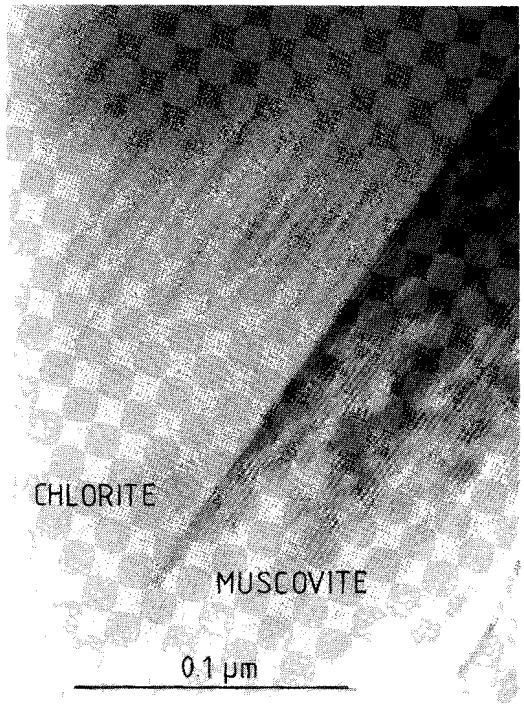

FIGURE 6.25. (001) lattice fringe image of a coherent boundary between chlorite and muscovite.

The argument presented above is only based on qualitative observations, and should be checked by deformation experiments of chlorite single crystals, and by theoretical calculations of dislocation core energies and stacking fault energies. Unfortunately, to the author's knowledge no elasticconstants or other mechanical data of chlorite are available, and this remains a subject for future research.

Previous authors have demonstrated that chemical driving forces are important during recrystallisation of phyllosilicates (Etheridge and Hobbs, 1974; Knipe, 1979, 1981). The prograde reaction Mg-poor chlorite → Mg-rich chlorite (see sections 5.3.8 and 5.5.3) indicates that chemical driving forces play a role in the recrystallisation of chlorite. The growth of muscovite into chlorite (e.g. Fig. 6.23) requires mass transport and must involve chemical driving forces because of the large chemical differences. In addition, the reaction of chlorite into muscovite involves a volume decrease and is therefore sensitive to the normal stress (Cosgrove, 1976). It is clear that both chemical and strain related driving forces contribute to the driving force for recrystallisation, but without means of calculating the magnitude of the individual forces it is not possible to determine which is dominant.

6.4.3 Conclusions

The deformation of muscovite under anchizone metamorphic conditions is dominated by grain boundary migration, while polygonization is of minor importance. This is in contrast to the behaviour of chlorite, where polygonization is very important under the same conditions. The difference may be caused by the difference in stored strain energy (both elastic and plastic), which is probably higher in muscovite than in chlorite for the same amount of strain.

6.5 DEFORMATION OF QUARTZ

Dislocations have been observed in all quartz crystals (e.g. Fig. 5.2). Dislocation densities up to $1 \cdot 10^9$ cm^{-2} have been observed. These densities are similar to those observed in some mylonites (White, 1976; Ord and Christie, 1984; Behrmann, 1985).

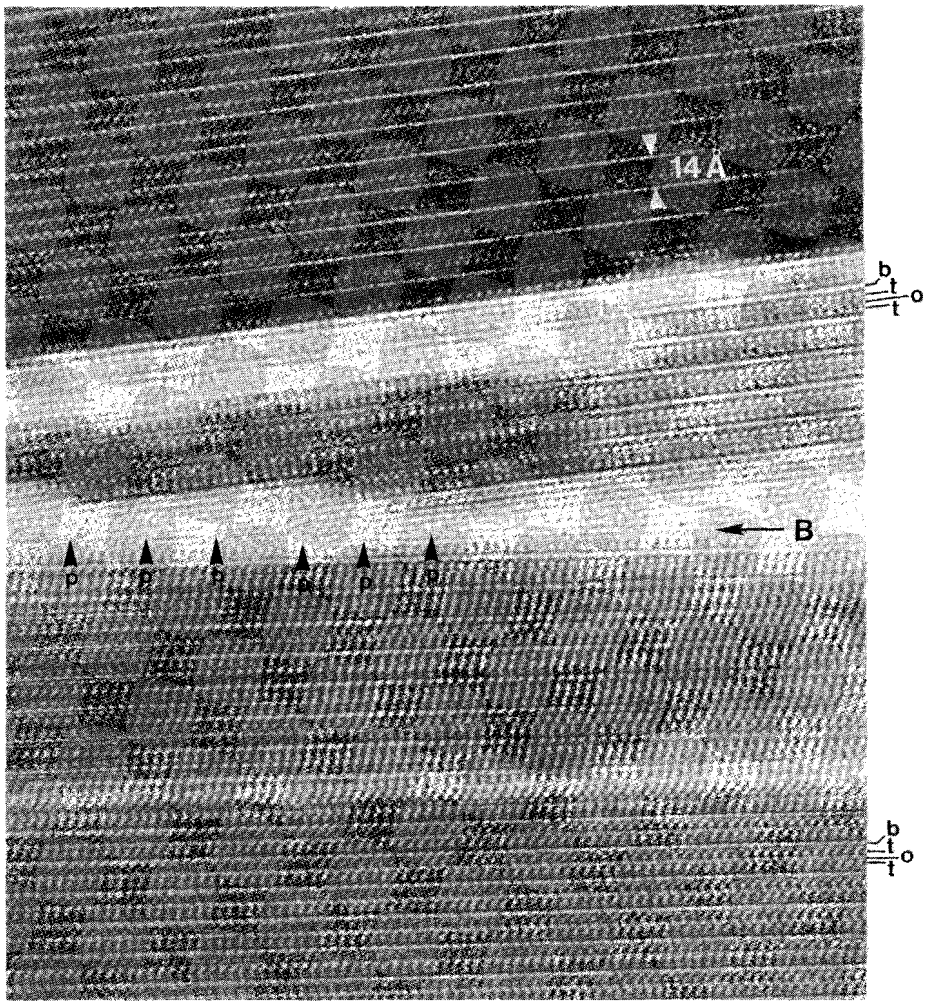

FIGURE 6.26. HRTEM image of a grain boundary in chlorite, viewed along a <100> direction. The angle between the two lattices is ca. 10°. The image shows structure up to a few Ångstroms from the interface, indicating that the crystal structure is continuous up to a few Ångstroms from the interface. The imaging code (b=brucite interlayer, t=tetrahedral sheet, o=octahedral sheet) is based on observations on a thinner part of the same crystal. Small amorphous patches (P) mark the terminations of individual interlayers or sheets, and can be interpreted as partial dislocations.

Optical microscopy observations have shown that deformation of quartz takes place mainly by mass transfer processes (see chapter 5). Furthermore, no crystallographic preferred orientation of the quartz has been observed. X-ray texture goniometry of anchizonal slates from the Alps (Siddans, 1980) has also shown that quartz has no crystallographic preferred orientation. Therefore it seems likely that intracrystalline deformation of quartz did not occur during slaty cleavage development, and the high dislocation densities may be inherited from the high-grade source area of the detrital quartz; such a high-grade hinterland has also been indicated by the high IC-indices of detrital micas and the high Th-content of detrital monazite (see chapter 4).

6.6 THE STRUCTURE OF GRAIN BOUNDARIES

6.6.1 Observations

All the intracrystalline deformation processes described above involve the generation and movement of grain boundaries. The structure of grain boundaries influences the mass transfer processes (e.g. White and White, 1981), which also contribute to the cleavage formation (see section 5.5). Therefore the intracrystalline deformation processes will affect the mass transfer processes indirectly. This section reports some TEM observations on the structures of the grain boundaries, and some preliminary remarks on the relationship with mass transfer processes will be made; the interactions between various processes during cleavage development will be discussed in more detail in chapter 7.

Several types of grain boundaries have been observed in between phyllosilicates:

1. completely coherent boundaries, where the crystal structure is continuous across the boundary, occur at twin interfaces and at chlorite/muscovite interfaces (Fig. 6.25).
2. semi-coherent boundaries are characterised by dislocations; in between the dislocations the crystal structure is continuous. Such boundaries have been observed frequently in between subgrains (Figs. 6.16, 6.17). Figure 6.26 shows a HRTEM micrograph of a semicoherent boundary in chlorite: the structure in the image is present within a few Ångstroms from the boundary, indicating that the crystal structure is

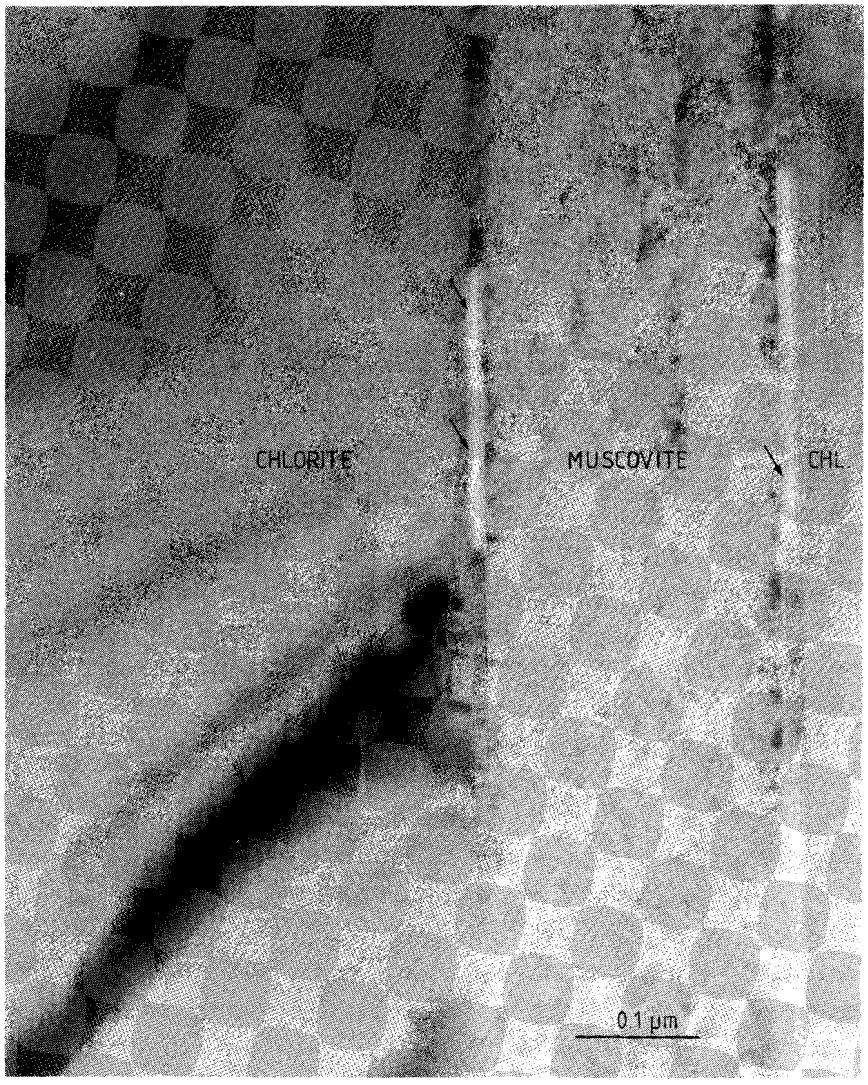

FIGURE 6.27. BF image of double-interface boundaries between chlorite and muscovite. The grain boundary layers show transparant areas due to electron beam damage (arrows)

continuous up to a few Ångstroms from the boundary. Such narrow boundaries in chlorite have been reported previously by Wirth (1986).
3. incoherent boundaries, where the crystal structure is not continuous across the boundary, are often associated with a layer of another phase along the boundary. As these boundaries are characterised by two interfaces (phyllosilicate - grain boundary layer - phyllosilicate) they will be termed *double-interface boundaries*. These double-interface boundaries occur in all microstructural positions, i.e. both in cleavage domains and in microlithons. The angle between the basal planes of the phyllosilicates at both sides of the boundary can vary from 0 to 90°. The grain boundary layers have a width of 70-100 Å and are very rapidly damaged by the electron beam (Fig. 6.27). The exact nature of these boundary layers could not be determined. In one case a HRTEM-image of such a layer has been obtained (Fig. 6.28). The image of the layer clearly shows structure, indicating that the layer is crystalline; however, the exact nature of this intergranular phase could not be determined from the image. The HRTEM image also shows that the disturbed region at the interface between phyllosilicate and the boundary layer is very narrow.

Boundaries in quartz, and between quartz and phyllosilicates, are characterised by a zone of preferential electron beam damage a few nanometers wide. Due to this beam damage no detailed information on the grain boundary structure could be obtained. Occasionally voids are observed at quartz interfaces (Fig. 6.29).

6.6.2 Discussion

White and White (1981) report zones of preferential electron beam damage along grain boundaries in several rocks, and also the presence of voids at the interfaces. As the voids have presumably been filled with hydrous fluid, they suggest that the zones of preferential beam damage correspond to hydrated zones along the grain boundaries. White and White (1981) suggest that the effective grain boundary width, i.e. the width of the zone of enhanced diffusion rates due to the disturbed crystal structure, is much larger in geological materials (several nanometers) than in metals, where the boundaries are sharp (a few Ångstrom width at most). The present study shows that in phyllosilicates the crystal structure is undisturbed up to a few Ångstrom from the interface; similar observations have been reported by Wirth (1986). Therefore it seems

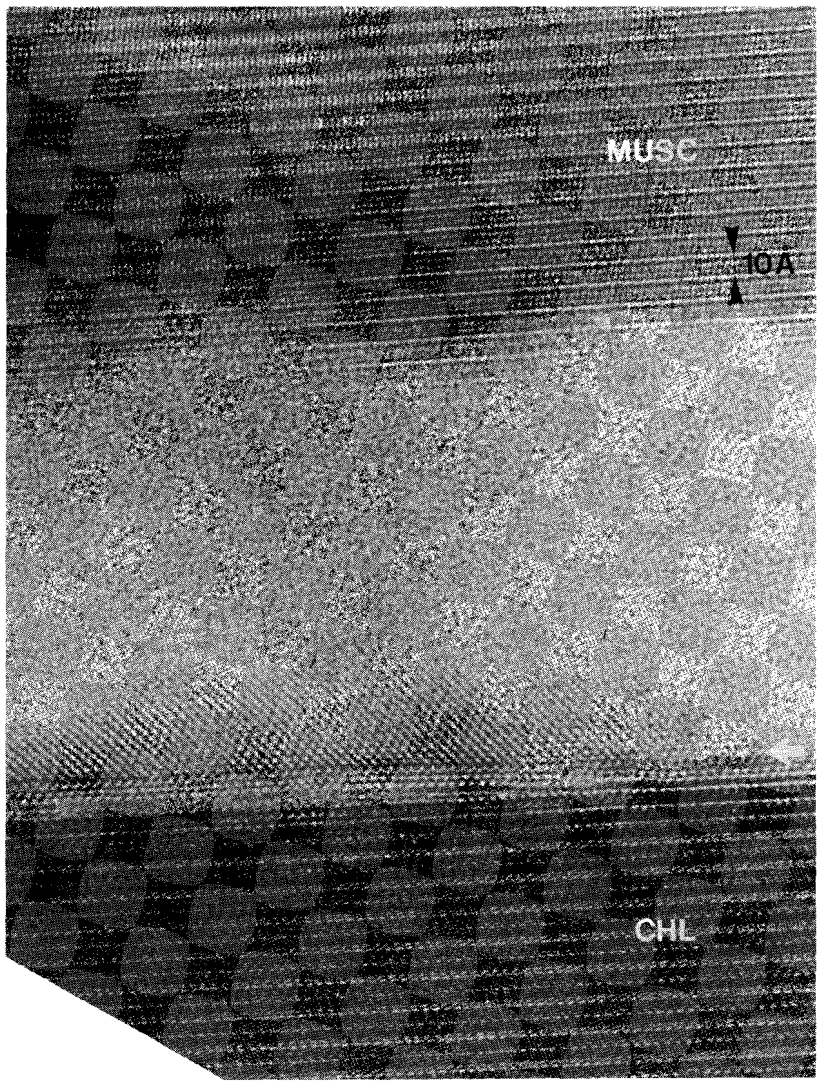

FIGURE 6.28. HRTEM image of a grain boundary layer between chlorite and muscovite, viewed along a <100> direction of the chlorite. The interface between the chlorite and the intergranular phase is indicated by the arrow.

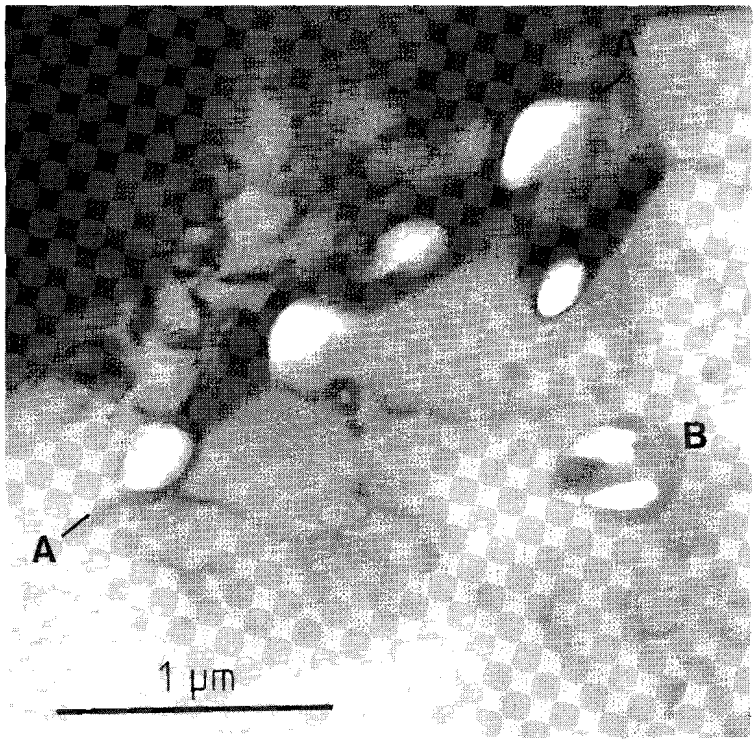

FIGURE 6.29. BF image of an interface in quartz (A-A) showing a series of voids along the boundary. Some isolated voids inside the quartz are also indicated (B).

likely that the effective grain boundary width in phyllosilicates is limited to a few Ångstroms. However, the observations on quartz interfaces do agree with those of White and White (1981).

It has been demonstrated in chapter 5 that extensive pressure solution has occurred in the slates of the Orri Dome. This means that fluid has been present at the grain boundaries. It seems likely that the hydrated zones and voids along quartz interfaces are remnants of these fluids. Although fluids have probably been present along some of the phyllosilicate interfaces, no such remnants have been observed at these interfaces.

Many of the phyllosilicate interfaces, especially in chlorite, are the result of dislocation creep processes. It is not likely that fluid has

been present along these boundaries, as they have developed from a more-or-less perfect crystal. Nevertheless, TEM-observations have shown that these boundaries are formed by closely spaced straight parallel dislocations (Figs. 6.16 and 6.17), and solid-state diffusion rates can be very high along such dislocation arrays (Le Claire and Rabinovitch, 1984) and may be significant at lower temperatures (e.g. Yund et al., 1983). Therefore it is possible that dislocation-enhanced solid-state diffusion contributed to other mass transfer processes such as pressure solution.

6.7 CONCLUSIONS

Polygonization dominates the deformation of chlorite during slaty cleavage development under anchizone conditions. Plastic deformation of chlorite involves a complex mechanism, in which the crystal is divided into subgrains with subgrain walls subnormal and subparallel to (001). Basal slip is very easy through the generation and movement of $[uv0]$ dislocations, which finally leads to the formation of subgrain boundaries subnormal to (001). Under special circumstances non-basal slip of $[00w]$ dislocations is possible. In combination with climb of $[00w]$ dilsocations this accounts for the formation of subgrain boundaries subnormal to (001).

Deformation of muscovite during slaty cleavage development is dominated by grain boundary migration. Some polygonization does occur, but this is of minor importance. No plastic deformation of quartz occurred during anchizonal cleavage development.

The (sub)grain boundaries formed by polygoniziation in the phyllosilicates contribute to the mass transfer process by dislocation enhanced diffusion. There are indications that fluid films have been present at the quartz interfaces.

Chapter 7
CONCLUSIONS: THE INTERACTION BETWEEN CLEAVAGE FORMING PROCESSES AND THE ROLE OF INTRACRYSTALLINE DEFORMATION

7.1 INTRODUCTION

In the previous chapters it has been demonstrated that many processes have been active during cleavage development in the Orri Dome and the Pallaresa Anticlinorium. All these processes have operated simultaneously, although their relative importance may have varied in space and time. It is not possible to separate the effects of each of the processes, as they influenced each other continuously. Several aspects of these interactions have already been mentioned in the previous sections. This chapter is an attempt to evaluate the effects of each process on the development of the slate, and the mutual interaction of the processes.

When a pelitic rock changes from a shale into a slate, three major aspects of the rock are changed: its mineralogy (metamorphism), its shape (deformation) and its fabric (the actual cleavage development). It is convenient to discuss these three changes separately.

7.2 METAMORPHISM

Many studies have shown significant differences between the mineralogy of shales and slates (Weaver, 1984; Lee and Peacor, 1983, 1985; Lee et al., 1984, 1986). In general shales contain a mixture of clay minerals such as chlorite, 1Md-illite, smectite and vermiculite, often forming irregular interstratifications; slates consist mainly of 2M-micas and chlorite in relatively regular interstratifications. Although metamorphism and deformation often occur synchronously during an orogeny, metamorphism is not a necessity for cleavage development, as is demonstrated by the observations of slaty cleavage in diagenetic rocks (Kubler, 1967b; Dunoyer de Segonzac, 1969; Artru et al., 1969). Chapter 4 also shows that the shale of the Orri Dome had a mature mineralogy of ordered intergrowths of chlorite and mica prior to cleavage development.

Nevertheless, Knipe (1979, 1981) has clearly shown that several prograde metamorphic reactions were associated with the formation of cleavage domains, and also in the present study some indications of prograde reactions (Mg-enrichment of chlorite in microlithons) have been found. Apparently there is an interaction between metamorphism and cleavage development.

At the metamorphic grades characteristic for slaty cleavage formation (lower greenschist facies at most), chemical reaction rates are very low, and many minerals do not reach chemical equilibrium (Kisch, 1983). For example, a shale exposed to anchizone metamorphic conditions can have a mineralogy which still reflects diagenetic conditions. However, when the rock is stressed, several processes are activated which affect the reaction rates. Due to locally increased normal stresses pressure solution will dissolve material which would otherwise be insoluble. When this material is redeposited in regions with low normal stresses the new phase will be in equilibrium with the current physical and chemical conditions. Solid state diffusion, which is important for the re-equilibration of an existing crystal, is normally negligable at low temperatures. When dislocations are induced by deformation, diffusion rates are enhanced; this effect is even greater when the dislocations are arranged in arrays of straight and parallel arrays. Thus deformation-enhanced solid-state diffusion may become significant and facilitate chemical re-equilibration of the deformed crystal. High dislocation densities will also increase the solubility of the crystal, thus adding to the effects of pressure solution.

These processes may explain the increase in Mg-content in chlorites in the microlithons, which is a prograde reaction (see section 5.3.8): these chlorites show the highest dislocation densities, and many extension sites (i.e. low normal stress) occur due to splitting of the crystal layers. The prograde reactions described by Knipe (1979, 1981) are also associated with deformation. The slates described by Knipe (1979, 1981) have a much more diverse mineralogy than the slates of the present study, and metamorphic reactions can be monitored in more detail: at the transition from microlithon to cleavage domain the following reactions take place: illite $\rightarrow$ phengite + paragonite, and Fe-rich chlorite $\rightarrow$ Fe-poor chlorite. Along the border between the microlithon and the cleavage domain Knipe (1979, 1981) and White and Knipe (1978)

observed a zone with a reduced grain size, which they call the *reaction zone*. As the grain size reduction will shorten the mass transfer paths, it will also enhance the reaction rates. However, this fine-grained reaction zone has not been observed in the slates of the Orri Dome.

In general it is clear that, although metamorphism and cleavage development are not necessarily associated with each other, the deformation responsible for the cleavage development will also enhance metamorphic reaction rates. The most important processes which will affect the reaction rates are pressure solution, intracrystalline deformation by dislocation creep and polygonization, and grain size reduction (which can also be the result of polygonization).

7.3 DEFORMATION

Cleavage development is inseparably linked with deformation. Numerous studies have demonstrated that slaty cleavage development is associated mainly with flattening perpendicular to the cleavage planes and extension parallel to the cleavage planes (see section 2.2.2). The main process responsible for the change in shape of the slate is pressure solution. Material is removed from the sides of grains facing the cleavage planes, and is redeposited elsewhere, mostly in veins and to a lesser extent in extension sites at grain faces at high angles to the cleavage (see section 5.5.3). This results in a reduction of the volume of the grains, shortening of the grains in a direction perpendicular to the cleavage, and some extension parallel to the cleavage. As a consequence, a shape preferred orientation is developed. As quartz and albite are preferentially dissolved, these minerals show the strongest shape preferred orientation (e.g. Fig. 5.12). The same shape change applies to the rock as a whole: pressure solution leads to a shortening of the rock perpendicular to the cleavage and an extension parallel to the cleavage.

Another process is the flattening of grains by plastic deformation; this is evident in the chlorite-mica aggregates. Most aggregates show evidence of shortening in a direction normal to the cleavage, and elongation parallel to the cleavage (e.g. Fig. 5.16). This leads to complex internal deformation structures, including folds, kinks, subgrains etc. (section 5.3.6), which are developed by the intracrystalline

deformation mechanisms described in chapter 5 and 6. The other processes, such as rigid-body rotation and recrystallisation are a consequence of deformation, but do not cause a shape change themselves.

7.4 FABRIC DEVELOPMENT

In a shale the quartz grains are usually equidimensional; the phyllosilicates are elongated parallel to the basal planes and form both a shape preferred orientation and a crystallographic preferred orientation parallel to the bedding. Sometimes dark seams are developed parallel to bedding as the result of compaction. Upon the transition to a slate existing fabric elements are re-oriented and new fabric elements are developed.

Pressure solution leads to an elongation of grains parallel to the cleavage, and a shape preferred orientation is developed. Plastic deformation of the phyllosilicates, assisted by pressure solution, also leads to a shape preferred orientation parallel to the cleavage. As the framework grains are flattened, either by pressure solution or by plastic deformation, other grains are re-oriented passively. The grains can rotate as a whole (rigid-body rotation) or in part (bending). The final result will be a shape preferred orientation parallel to the cleavage. Only grains with the long dimension perpendicular to the shortening direction will not rotate.

In chapter 6 it has been shown that both chlorite and muscovite have only one easy slip plane, the basal plane. In chlorite non-basal slip is possible under special circumstances, but this only occurs after extensive basal slip has led to significant stress concentrations (see section 6.3.3). The resolved shear stress along the basal planes will be zero if the principal compressive stress direction (σ_1) is parallel or normal to the basal planes, and in those cases no basal slip will occur. In practice this means that phyllosilicates which have their basal planes either parallel or normal to the cleavage planes will not deform plastically. However, if the basal planes are parallel to σ_1, buckling can rotate the planes locally, leading to a non-zero resolved shear stress. If the critical resolved shear stress (CRSS) is exceeded, basal slip is possible. Thus, only those grains which have their basal planes

perpendicular to σ_1, i.e. parallel to the cleavage, have a true stable orientation with respect to deformation by crystalline slip. Grains in other orientations can deform by crystalline slip. Therefore, plastic deformation by crystalline slip will result in a crystallographic preferred orientation of phyllosilicates parallel to the cleavage.

Due to the strong elastic anisotropy of muscovite (Alexandrov and Ryzhova, 1961) its thermodynamically stable orientation will be with the basal planes perpendicular to σ_1 (Kamb, 1959). When muscovite growth is facilitated, e.g. by changes in chemical potential or stored strain energy, it will grow preferentially in an orientation perpendicular to σ_1. This is observed in the slates of the Orri Dome: muscovites grow preferentially parallel to the cleavage (Figs. 5.19, 5.22). As chlorite is elastically more isotropic (Alexandrov and Ryzhova, 1961), this effect is less for chlorite.

7.5 THE INTERACTION BETWEEN THE PROCESSES

In the preceding sections it has been shown that pressure solution and plastic deformation are the main mechanisms responsible for the deformation of the rock. These processes also result in a shape fabric and a crystallographic fabric, aided by rotation, bending and grain growth. The development of a new fabric involves the formation of a new distribution of grain boundaries and crystal lattice orientations, which will then affect the geometry of the mass transfer system, and which will also influence the deformation by crystalline slip mechanisms.

In the original shale most phyllosilicates are oriented with their long axes and their basal planes parallel to the bedding. If the rock is shortened in a direction at a low angle to bedding, most of the phyllosilicates have an unstable orientation and crystalline slip will occur. This will take place immediately if the CRSS is high enough; if the basal planes are parallel to σ_1 slip will only occur after buckling of the crystal layers. Thus, the contribution of crystalline slip to the overall deformation will increase initially as more and more grains have their basal planes inclined to σ_1. In the course of cleavage development the number of grains in an orientation parallel to the cleavage will increase due to the mechanisms mentioned in section 7.4, and the contribution of crystalline

slip will decrease. Finally, when a continuous fabric *s.s.* is developed, all the grains have a stable orientation and no crystalline slip can occur. In a similar way the development of preferred orientation influences rotation and bending.

The rate of mass transfer is controlled by the geometry of the mass transfer paths, i.e. by the distribution of the grain boundaries. In the shale most grain boundaries are horizontal, and mass transfer is most rapid in horizontal directions. This is reflected in the shape of the monazite porphyroblasts, which have grown most rapidly in a direction parallel to the pre-cleavage fabric, regardless of the crystallographic orientation of the monazite. During cleavage development a new fabric is developed, which is characterised by long straight parallel grain boundaries in the cleavage domains. If, after the initial stages of cleavage development, all the cleavage domains become interconnecting, the new distribution of grain boundaries will facilitate rapid mass transfer along the cleavage domains. In the microlithons intracrystalline deformation will lead to the formation of dislocations and dislocation walls, which will facilitate solid-state diffusion towards the fluid along grain boundaries. Thus, the mass transfer processes will become increasingly efficient as the development of the cleavage fabric proceeds, thereby favouring processes like recrystallisation and pressure solution.

Summarizing, all the processes interact, deformation processes leading to fabric development, which will in turn influence the deformation processes. With increasing fabric development rotation and crystalline slip processes will decrease in importance, while pressure solution and recrystallisation will increase. As deformation often occurs simultaneous with prograde metamorphism, the temperatures may increase in the course of cleavage development. This will influence the stability of the existing phases and increase the rate of the reactions, thus favouring recrystallisation processes.

7.6 THE ROLE OF INTRACRYSTALLINE DEFORMATION DURING SLATY CLEAVAGE DEVELOPMENT

In the preceding sections intracrystalline deformation has been mentioned repeatedly. In the early stages of cleavage development plastic deformation of phyllosilicates contributes to the deformation of the rock as a whole, and also contributes to the development of a preferred orientation. Bending, folding and kinking of grains always involves intracrystalline deformation.

Intracrystalline deformation leads to the formation or movement of dislocations, dislocation walls (subgrain boundaries) and grain boundaries. Dislocations and dislocation walls will affect the solid state diffusion system by dislocation enhanced diffusion. The formation and movement of grain boundaries will influence the geometry of the paths for pressure solution. Intracrystalline deformation is therefore an essential factor in the deformation of the rock and in the development of the slaty cleavage fabric. In the later stages of cleavage development, when most of the grains have a stable orientation parallel to the cleavage, the importance of intracrystalline deformation diminishes; pressure solution and recrystallisation become the main deformation and fabric-forming processes

Intracrystalline deformation of chlorite takes place mainly by crystalline slip; dislocations are aligned into dislocation walls and subgrains are developed; the subgrains rotate with progressive deformation, leading to the formation of new high-angle boundaries and new orientations of the crystal lattice. Some crystalline slip and polygonization does occur in muscovite, but plastic and elastic deformation soon results in grain boundary migration and grain growth. This difference in deformational behaviour between chlorite and muscovite may be explained from crystallographic considerations (see section 6.4), but further research on this subject is necessary.

REFERENCES

Ahn, J.H., and Peacor, D.R., 1985. Transmission electron microscope study of diagenetic chlorite in Gulf Coast argillaceous sediments. Clays Clay Miner. 33: 228-236.

Ahn, J.H., Peacor, D.R., and Essene, E.J., 1985. Coexisting paragonite-phengite in blueschist eclogite: a TEM study. Am. Mineral. 70, 1193-1204

Ahn, J.H., Peacor, D.R., and Essene, E.J., 1986. Cation-diffusion-induced characteristic beam damage in transmission electron microscope images of micas. Ultramicroscopy 19: 375-382.

Alexandrov, K.S., and Ryzhova, T.V., 1961. Elastic properties of rock-forming minerals: II. Layered silicates. Bull (Izv.) Acad. Sci. USSR, Geophys. Ser. 12, 1165

Amelinckx, S. and Delavignette, P., 1962. Dislocations in layer structures. In: J.B. Newkirk and J.H. Wernick (Editors), Direct observation of imperfections in crystals. Interscience, New York, pp. 295-356.

Amelinckx, S. and Van Landuyt, J., 1976. Vlakke kristaldefekten, niet- stoichiometrie en polytypie. Chem. Weekblad 1976: m313-320.

Anthony, J.W., 1957. Hydrothermal synthesis of monazite. Am. Mineral. 42, 904

Artru, Ph., Dunoyer de Segonzac, G., Combaz, A., and Giraud, A., 1969. Variations d'origine sédimentaire et évolution diagénétique des caractères palynologiques et géochimiques des Terres Noires jurassiques en direction de l'Arc Alpine (France, sud-est). Bull. Centre Rech. Pau-SNPA 3, 357-376

Bailey, S.W., 1975. Chlorites. In: J.E. Gieseking (Editor), Soil components, Volume II: Inorganic components, Springer, New York, N.Y., pp. 191-263.

Bailey, S.W., 1980a. Summary of recommendations of AIPEA nomenclature committee on clay minerals. Am. Mineral. 65: 1-7.

Bailey, S.W., 1980b. Structure of layer silicates. In: Crystal structures of clay minerals and their X-ray identification. Mineral. Soc. Monogr. No 5, 1-124

Bailey, S.W., (ed.), 1984. Micas. Rev. Mineral. Vol. 13, 584 pp.

Bakewell, R., 1815. An introduction to geology. Harding, London, 2nd ed., 492 pp

Baronnet, A., and Olives, J., 1983. The geometry of micas around kink band boundaries I. A crystallographic model. Tectonophysics 91: 359-373.

Becker, G.F., 1896. Schistosity and slaty cleavage. J. Geol. 4, 429-448

Behrmann, J.H., 1985. Crystal plasticity and superplasticity in quartzite; a natural example. Tectonophysics 115, 101-129

Bell, A.M., 1985. Strain paths during slaty cleavage development - the role of volume loss. J. Struct Geol. 7, 563-568

Bell, I.A., and Wilson, C.J.L., 1977. Growth defects in metamorphic biotite. Phys. Chem. Miner. 2: 153-169.

Bell, I.A., and Wilson, C.J.L, 1981. Deformation of biotite and muscovite: TEM microstructure and deformation model. Tectonophysics 78: 201-229.

Bell, I.A., and Wilson, C.J.L., 1986. TEM observations of defects in biotite and their relationship to polytypism. Bull. Minéral. 109, 163-170

Bell, I.A., Wilson, C.J.L., McLaren, A.C., and Etheridge, M.A., 1986. Kinks in mica: role of dislocations and (001) cleavage. Tectonophysics 127: 49-65.

Bell, T.E., 1986. Microstructure in mixed-layer illite/smectite and its relationship to the reaction of smectite to illite. Clays Clay Miner. 34, 146-154

Bell, T.H., 1978. Syntectonic nucleation of new grains in deformed mica. Tectonophysics 51: T31-T37.

Beutner, E.C., 1978. Slaty cleavage and related strain in the Martinsburg Slate, Delaware Water Gap, New Jersey. Am. J. Sci. 278, 1-23

Boland, J.N., McLaren, A.C., and Hobbs, B.E., 1971. Dislocations associated with optical features in naturally deformed olivine. Contrib. Mineral. Petrol. 30: 53-63.

Bons, A.J., 1988. Deformation of chlorite in naturally deformed low-graderocks. Tectonophysics 155, in press.

Bons, A.J., and Schryvers, D., 1988a. High-resolution EM of stacking irregularities in chlorite crystals. Ultramicroscopy 24, 426

Bons, A.J., and Schryvers, D., 1988b. High-resolution electron microscopy of stacking irregularities in ripidolite chlorite. Submitted to Am. Mineral.

Borg, I. and Handin, J., 1966. Experimental deformation of crystalline rocks. Tectonophysics 3: 249-368.

Borradaile, G.J., 1978. Transected folds - study illustrated with examples from Canada and Scotland. Bull. Geol. Soc. Am. 89, 481-493

Borradaile, G.J., Bayly, M.B., and Powell, C.McA., 1982. Atlas of deformational and metamorphic rock fabrics. Springer, Berlin, 1982, 551 pp

Boulter, C.A., 1986. Strain paths during slaty cleavage formation - the role of volume loss: Discussion. J. Struct. Geol. 8, 719-720

Brindley, G.W., 1980. Order-disorder in clay mineral structures. In: Crystal structures of clay minerals and their X-ray identification. Mineral. Soc. Monogr. No 5, 125-195

Brown, B.E., and Bailey, S.W., 1962. Chlorite polytypism: I. Regular and semi-random one-layer structures. Am. Mineral. 47: 819-850.

Brown, G., and Brindley, G.W., 1980. X-ray diffraction procedures for clay-mineral identification. In: Crystal structures of clay minerals and their X-ray identification. Mineral. Soc. Monogr. No. 5, 305-359

Cloos, E., 1947. Oolite deformation in South Mountain Fold Maryland. Geol. Soc. Am. Bull. 58, 843-917

Coene, W., and Van Dyck, D., 1984a. The Real Space method for dynamical electron diffraction calculations in high resolution electron microscopy. II. Critical analysis of the dependency on the input parameters. Ultramicroscopy 15, 41-50

Coene, W., and Van Dyck, D., 1984b. The Real Space method for dynamical electron diffraction calculations in high resolution electron microscopy. III. A computational algorithm for the electron propagation with its practical applications. Ultramicroscopy 15, 287-300.

Cosgrove, J.W., 1976. The formation of crenulation cleavage. J. Geol. Soc. London. 132, 155

Craig, J., Fitches, W.R., and Maltman, A.J., 1982. Chlorite-mica stacks in low-strain rocks from Central Wales. Geol. Mag. 119, 243-256

Dal Piaz, G.V., Hunziker, J.C., and Martinotti, G., 1972. La Zona Sesia Lanzo e l'evoluzione tettonico-metamorfica delle Alpi Nord-occidentali interne. Mem. Soc. Geol. Ital. 11, 433-466.

De Boer, R.B., 1977. Pressure solution: theory and experiments. Tectonophysics 39, 287-301

Deer, W.A., Howie, R.A., and Zussman, J., 1962. Rock-forming Minerals, Vol. 5: Non-silicates. Longman, London, 371 pp.

Deer, W.A., Howie, R.A., and Zussman J., 1966. An introduction to the rock-forming minerals. Longman, London, 528 pp.

Deer, W.A., Howie, R.A., and Zussman, J., 1986. Rock-forming minerals, Vol. 1B, 2nd edition. Disilicates and ring silicates. Longman, London, 629 pp.

De Sitter, L.U., and Zwart, H.J., 1959. Geological map of the Paleazoic of the Central Pyrenees, sheet 3, Ariège, France, 1:50,000. Leidse Geol. Meded. 22, 351-418

Demny, J., 1963a. Elektronenmikroskopische Untersuchungen an sehr dünnen Glimmerfolien I. Versetzungen in Glimmer und ihre Kontraste. Z. Naturforsch. A18: 1088-1096.

Demny, J., 1963b. Elektronenmikroskopische Untersuchungen an sehr dünnen Glimmerfolien. II. Das Verhalten der Glimmers bei stärkeren Elektronenbestrahlung. Z. Naturforsch. A18: 1097-1101.

Dimberline, A.J., 1986. Electron microscope en microprobe analysis of chlorite-mica stacks in the Wenlock turbidites, mid Wales, UK. Geol. Mag. 123, 299-306

Donnot, M., Guigues, J., Lulzac, Y., Magnien, A., Parfenoff, A. and Picot, P, 1973. Un nouveau type de gisement d'europium: la monazite grise à l'europium en nodules dans les schistes palozoiques de Bretagne. Mineralium Deposita 8, 7-18

Drury, M.R., Hoogerduijn Strating, E., and Vissers, R.L.M., 1988. The microstructures and deformation history in mantle peridotites from the Voltri Massif, Ligurian Alps, N.W. Italy. To be submitted to Geol. Mijnbouw.

Duncan, A.C., 1985. Transected folds: a re-evaluation, with examples from the 'type area' at Sulphur Creek, Tasmania. J. Struct. Geol., 7, 409-420

Dunoyer de Segonzac, G., 1970. The transformation of clay minerals during diagenesis and low-grade metamorphism: a review. Sedimentology 15, 281-346

Dunoyer de Segonzac, G., and Heddebaut, C., 1971. Paléozoique anchi-métamorphique à illite, chlorite, pyrophyllite, allevardite, et paragonite dans les Pyrénées Basques. Bull. Serv. Carte Géol. Alsace Lorraine 24, 277-290

Edington, J.W., 1975. Interpretation of transmission electron micrographs. Monographs in Practical Electron Microscopy in Materials Science No. 3, Philips Technical Library, MacMillan, London, 112 pp.

Eichentopf, H., and Greiling, R.O., 1987. Arcuate hinge cleavage associated with welded contacts: an example. J. Struct. Geol. 9, 905-910

Engelder, T., and Marshak, S., 1985. Disjunctive cleavage formed at shallow depths in sedimentary rocks. J. Struct. Geol. 7, 327-344

Etheridge, M.A., and Hobbs, B.E., 1974. Chemical and deformational controls on recrystallization of mica. Contrib. Mineral. Petrol., 43: 111-124

Etheridge, M.A., Hobbs, B.E., and Paterson, M.S., 1973. Experimental deformation of single crystals of biotite. Contrib. Mineral. Petrol., 38: 21-36.

Etheridge, M.A., Paterson, M.S., and Hobbs, B.E., 1974. Experimentally produced preferred orientation in synthetic mica aggregates. Contrib. Mineral. Petrol., 44: 275-295.

Fairbain, H.L., 1949. Structural petrology of deformed rocks. Cambridge, Mass.: Addison-Wesley Press

Frey, M., 1978. Progressive low-grade metamorphism of a black shale formation, Central Swiss Alps, with special reference to pyrophyllite and margarite assemblages. J. Petrol. 19, 95-135

Ghosh, S.K., 1982. The problem of shearing along axial plane foliations. J. Struct. Geol. 4, 63-67

Goodman, P., and Moodie, A.F., 1974. Numerical evaluation of *N*-beam wavefunctions in electron scattering by the multislice method. Acta. Cryst. A30, 280-290.

Gratier, J.P., 1983. Estimation of volume changes by comparative chemical analysis in heterogeneously deformed rocks (folds with mass transfer). J. Struct. Geol. 5, 329-339

Gray, D.R., 1981. Cleavage-fold relationships and their implications for transsected folds: an example from southeast Virginia, U.S.A.. J. Struct. Geol. 3, 265-277

Gregg, W.J., 1986. Deformation of chlorite-mica aggregates in cleaved psammitic rocks from Islesboro, Maine. U.S.A.. J. Struct. Geol., 8: 59-68.

Griggs, D.T., Turner, F.J., and Heard, H.C., 1960. Deformation of rocks at 500-800 °C. In: D.T. Griggs and J. Handin (Editors), Rock deformation. Geol. Soc. Am. Mem. 79, 39-104.

Hall, M.G., and Lloyd, G.E., 1981. The SEM examination of geological samples with a semiconductor back-scattered electron detector. Am. Mineral. 66, 362-368

Harker, A., 1885. The cause of slaty cleavage: compression v. shearing. Geol. Mag. 2, 15-17

Harker, A., 1886. On slaty cleavage and allied rock structures. Rep. Brit. Assoc. Advan. Sci. 1885, 813-852

Hartevelt, J.J.A., 1970. Geology of the Upper Segre and Valira Valleys, Central Pyrenees, Andorra/Spain. Leidse Geol. Meded. 45: 167-236.

Haskin, M.A., and Haskin, L.A., 1966. Rare earths in European shales: a redetermination. Science, 154, 507-509.

Heling, D., 1970. Microfabrics of shales and their rearrangement by compaction. Sedimentology 15, 247-260

Hey, M.H., 1954. A new review of the chlorites. Mineral. Mag. 30: 277-292.

Hills, F.W., 1945. Example of the interpretation of folding. J. Geol. 53, 47-57

Hobbs, B.E., Means, W.E., and Williams, P.F., 1976. An outline of structural geology. Wiley, New York, N.Y., 571 pp.

Holeywell, R.C., and Tullis, T.E., 1975. Mineral reorientation and slaty cleavage in the Martinsburg formation, Lehigh Gap, Pennsylvania. Bull. Geol. Soc. Am. 86, 1296-1304

Holst, T.B., 1985. Implications of a large flattening strain for the origin of a bedding-parallel foliation in the Early Proterozoic Thomson Formation, Minnesota. J. Struct. Geol. 7, 375-384

Hörz, F., 1970. Static and dynamic origin of kink bands in micas. J. Geophys. Res. 75: 965-977.

Hörz, F., and Ahrens, T.J., 1969. Deformation of experimentally shocked biotite. Am. J. Sci. 276: 1213-1229.

Hull, D., and Bacon, D.J., 1984. Introduction to dislocations, 3rd edition. Int. Ser. Mater. Sci. Technol. Vol. 37, Pergamon, Oxford, 257 pp.

Izrailev, L.M., and Solov'eva, N.A., 1974. Accessory authigenic monazite in the upper paleozoic deposits of northern Verkhoyan'e. Lithol. Mineral. Resources 9, 624-628

Jahren, J., 1988. High resolution imaging of chlorites and illites. A compara tive study of calculated and experimental images. Ultramicroscopy, 24: 70.

Kamb, W.B., 1959. Theory of preferred orientation developed by crystallization under stress. J. Geol. 67, 153-170

Kisch, H.J., 1980a. Incipient metamorphism of Cambro-Silurian clastic rocks from the Jåmtland Supergroup, Central Scandinavian Caledonides, Western Sweden: illite crystallinity and "vitrinite" reflectance. J. Geol. Soc. London, 137: 271-288.

Kisch, H.J., 1980b. Illite crystallinity and coal rank associated with lowest-grade metamorphism of the Taveyyanne greywacke in the Helvetic zone of the Swiss Alps. Ecl. geol. Helv. 73, 753-777

Kisch, H.J., 1981. Coal rank and illite crystallinity associated with the zeolite facies of Southland and the Pumpellyite-bearing facies of Otago, southern New Zealand. New Zealand J. Geol. Geophys. 24, 349-360

Kisch, H.J., 1983. Mineralogy and petrology of burial diagenesis (burial metamorphism) and incipient metamorphism in clastic rocks. In: G. Larsen and G.V. Chilingar (Editors), Diagenesis in sediments and sedimentary rocks, Vol. 2. Develop. Sedimentol. 25B: 289-493.

Kligfield, R., Owens, W.H., and Lowrie, W., 1981. Magnetic susceptibility anisotropy, strain and progressive deformation in Permian sediments from the Maritime Alps (France). Earth Planet. Sci. Lett. 55, 181-189

Knipe, R.J., 1979. Chemical changes during slaty cleavage development. Bull. Mineral. 102, 206-209

Knipe, R.J., 1981. The interaction of deformation and metamorphism in slates. Tectonophysics 78, 249-272

Knipe, R.J., and White, S.H., 1977. Microstructural variation of an axial plane cleavage around a fold - a H.V.E.M. study. Tectonophysics 39, 355-381

Kossovskaya, A.G., and Shutov, V.D., 1970. Main aspects of the epigenesis problem. Sedimentology 15, 11-40

Kubler, B., 1964. Les argiles, indicateurs de métamorphisme. Revue Inst. fr. Pétrole 19, 1093-1113

Kubler, B., 1967a. La crystallinité de l'illite et les zones tout a fait supérieures du métamorphisme. Etages Tectoniques, Coll. NeuchÉtel, 1967, 105-122

Kubler, B., 1967b. Anchimétamorphisme et schistosité. Bull. Centre Rech. Pau- SNPA, 1: 259-278

Kubler, B., 1968. Evaluation quantitative du métamorphisme par lacristallinité de l'illite. Bull. Centre Rech. Pau - SNPA 2, 385-397

Laugel, A., 1855. Du clivage de roches. C.R. Acad. Sci. 40:182, 185, 978-980

Le Claire, A.D., and Rabinovitch, A., 1984. The mathematical analysis of diffusion in dislocations. In: Diffusion in crystalline solids (G.E. Murch and A.S. Nowick, Eds.), Acad. Press, 1984, p. 257-318

Le Corre, C., 1979. L'évolution typologique et texturale des roches argilo-siltueses au cours de la schistogenèse. Notion de la trajectoire de fabrique. Bull. Minéral. 102, 273-281

Lee, J.H., and Peacor, D.R., 1983. Intralayer transitions in phyllosilicates ofMartinsburg shale. Nature, 303: 608-609

Lee, J.H., and Peacor, D.R., 1985. Ordered 1:1 interstratification of illiteand chlorite: a transmission and analytical electron microscopy study. Clays Clay Miner. 33: 463-467

Lee, J.H., Peacor, D.R., Lewis, D.D., and Wintsch, R.P., 1984. Chlorite-illite/muscovite interlayered and interstratified crystals: a TEM/STEM study. Contrib. Mineral. Petrol., 88: 372-385.

Lee, J.H., Peacor, D.R., Lewis, D.D., and Wintsch, R.P., 1986. Evidence for syntectonic crystallization for the mudstone to slate transition at Lehigh Gap, Pennsylvania, U.S.A.. J. Struct. Geol., 8: 767-780.

March, A., 1932. Mathematische Theorie der Regelung nach der Korngestalt bei affiner Deformation. Z. Krist. 81, 285-297

Marshak, S., and Engelder, T., 1985. Development of cleavage in limestones in a fold-thrust belt in eastern New York. J. Struct. Geol. 7, 345-360

Mattauer, M., and Henry, J., 1974. The Pyrenees. in: Mesozoic-Cenozoic orogenic belts. Data for orogenic studies. A.M. Spencer, ed. Geol. Soc. London, Spec. Publ. 4, 3-23

Maxwell, J., 1962. Origin of slaty and fracture cleavage in the Delaware Water Gap area, New Jersey and Pennsylvania. in: Petrologic Studies: A.F. Buddington Volume (A. Engel, H. James and B. Leonard, eds), Geol. Soc. Am., Boulder, Co. 281-311

Mey, P.H.W., 1967. The geology of the Upper Ribargorzana and Baliera Valleys, Central Pyrenees, Spain. Leidse Geol. meded. 41, 153-220

Miller, R.B., 1988. Fluid flow, metasomatism and amphibole deformation in an imbricated ophiolite, North Cascades, Washington. J. Struct. Geol. 10, 283-296

Mohr, D.W., 1983. An occurrence of monazite porphyroblasts in black metashale, western North Carolina. Geol. Soc. Am., Abstr. Progr. 15,2, p 55.

Mohr, D.W., 1984. Zoned porphyroblasts of metamorphic monazite in the Anakeesta Formation, Great Smokey Mountains, North Carolina. Am. Mineral. 69, 98-103

Moore, J.C., and Geigle, J.E., 1974. Slaty cleavage: incipient occurrences in the deep sea. Science 183, 509-510.

Morad, S., and AlDahan, A.A., 1986. Diagenetic alteration of detrital biotite in proterozoic sedimentary rocks from Sweden. Sed. Geol. 47, 95-107

Mügge, O., 1898. Ueber Translationen und verwandte Erscheinungen in Krystallen. Neues. Jahrb. Mineral., Geol., Paläontol. 71-158.

Naha, K., and Ray, S.K., 1972. Structural evolution of the Simla Klippe in the lower Himalayas. Geol. Rndsch. 61, 1050-1086

Nance, W.B., and Taylor, S.R., 1976. Rare earth element patterns and crustal evolution I: Australian Post-Archaean sedimentary rocks. Geochim. Cosmochim. Acta 40, 1539-1551

Nicolas, A., and Poirier, J.P., 1976. Crystalline plasticity and solid state flow in metamorphic rocks. Wiley, New York, 444 pp.

Norris, R.J., and Rupke, N.A., 1986. Development of slaty cleavage in a mudstone unit from the Canabrian Mountains, northern Spain. J. Struct. Geol. 8, 871-878

O'Brien, N.S., 1970. The fabric of shale - an electron microscope study. Sedimentology 15, 229-246.

Oertel, G., 1970. Deformation of a slaty, lapillar tuff in the Lake District, England. Geol. Soc. Am. Bull. 81, 1173-1188

Olives, J., 1985a. Interlayer energy for partial slip and cleavage in muscovite. Phil. Mag. A52: 145-152.

Olives, J., 1985b. Biotites and chlorites as interlayered biotite-chloritecrystals. Bull. Minéral. 108, 635-641.

Olives, J., Amouric, M., De Fouquet, C., and Baronnet, A., 1983. Interlayering and interlayer slip in biotite as seen by HRTEM. Am. Mineral., 68: 754-758.

Ord, A., and Christie, J.M., 1984. Flow stresses from microstructures in mylonitic quartzites of the Moine thrustzone, Assynt area, Scotland. J. Struct. Geol. 6, 639-654

Overstreet, W.C., 1967. The geological occurrence of monazite. U.S. Geol. Surv. Prof. Paper No. 530, 327 pp

Paterson, M.S., 1969. Ductility of rocks. In: A.S. Argon (Editor), Physics of strength and plasticity. M.I.T. Press, Cambridge (Mass.), pp. 377-392.

Piqué, A., 1982. Relations between stages of diagenetic and metamorphic evolution and the development of a primary cleavage in the northwestern Moroccan Meseta. J. Struct. Geol. 4, 491-500.

Poirier, J.P., 1985. Creep of crystals: high-temperature deformationprocesses in metals, ceramics and minerals. Cambridge University Press, Cambridge, 260 pp.

Powell, C. McA., 1979. A morphological classification of rock cleavage. Tectonophysics 58, 21-34

Powell, C.McA., 1974. Timing of slaty cleavage during folding of Precambrian rocks, northwest Tasmania. Bull. Geol. Soc. Am. 85, 1043-1060

Ramsay, J.G., 1967. Folding and fracturing of rocks. McGraw-Hill, New York, 568 pp.

Ramsay, J.G., and Huber, M.I., 1983. The techniques of modern structural geology. Volume 1: Strain analysis. Academic Press London, 307 pp.

Ramsay, J.G., and Huber, M.I., 1987. The techniques of modern structural geology. Volume 2: folds and fractures. Academic Press, London, 391 pp.

Reks, I.J., and Gray, D.R., 1982. Pencil structures and strain in weakly deformed mudstone and siltstone. J. Struct. Geol. 4, 161-176

Roberts, D., 1971. Abnormal cleavage patterns in fold hinge zones from Varanger Peninsula, Northern Norway. Am. J. Sci. 271, 170-180

Roy, A., 1978. Evolution of slaty cleavage in relation to diagenesis and metamorphism: a study from the Hunsrückschiefer. Bull. geol. Soc. Am. 89, 1775-1789

Rutter, E.H., 1976. The kinetics of rock deformation by pressure solution. Phil. Trans. R. Soc. London A 283, 203-219

Rutter, E.H., 1983. Pressure solution in nature, theory and experiment. J. geol. Soc. London 140, 725-740

Sander, B., 1930. Gefügekunde der Gesteine. Springer Verlag Berlin, 352 pp.

Savage, J.F., 1965. Terrestrial photogrammetry for geological purposes. ITC Publ., Delft Spec. Publ. 2, 41-53

Schneider, M., 1972. Shock-induced mechanical deformations in biotite from crystalline rocks of the Ries crater (Southern Germany). Contributions to Mineralogy and Petrology, 37: 75-85.

Schramm, J.-M., 1981. Ueber den Einfluss der Verwitterung auf die Illitkristallinität. Karenthin 84, 238-249

Self, P.G., Glaisher, R.W., and Spargo, A.E.C., 1985. Interpreting high-resolution transmission electron micrographs. Ultramicroscopy 18, 49-62

Serdyuchenko, D.P., and Kochetkov, O.S., 1974. Metasedimentary monazite in Riphean schists of the Timans. Doklady; Earth Sci. Section (Acad. Sci. USSR) 218, 124-125

Sharp, D., 1846. On slaty cleavage. Quart. Journ. 3, 74-104

Shirozu, H., and Bailey, S.W., 1965. Chlorite polytypism: III Crystal structureof an orthohexagonal iron chlorite. Am. Mineral. 50, 868-885

Siddans, A.W.B., 1972. Slaty cleavage - a review of research since 1815. Earth Sci. Rev. 8, 205-232

Siddans, A.W.B., 1977. The development of slaty cleavage in a part of the French Alps. Tectonophysics 39, 533-557

Siddans, A.W.B., 1979. Deformation, metamorphism and texture development in Permian mudstones of the Glarus Alps. Ecl. geol. Helv. 72, 601-021

Siddans, A.W.B., 1980. Compaction, métamorphisne et structurologie des argilites permiennes dans les Alpes-Maritimes (France). Rev. géol. dyn. géogr. phys. 22: 279-292.

Silk, E.C.H., and Barnes, R.S., 1961. The observation of dislocations in mica. Acta Metall. 9: 558-562.

Sorby, H.C., 1853. On the origin of slaty cleavage. New. Philos. J. (Edinburgh) 55, 137-148

Sorby, H.C., 1879. Structure and origin of limestone. Quart. J. Geol. Soc. London, 35, 39-95

Soula, J.C., 1982. Characteristics and mode of emplacement of gneiss domes and plutonic domes in the Central Eastern Pyrenees. J. Struct. Geol. 4, 313-342

Southwick, D.L., 1987. Bundled slaty cleavage in laminated argillite, north-central Minnesota. J. Struct. Geol. 9, 985-994

Speksnijder, A., 1985. Anatomy of a strike-slip fault controlled sedimentarybasin, Permian of the southern Pyrenees, Spain. Sediment. Geol. 44, 179-223

Speksnijder, A., 1986. Geological analysis of paleozoic large-scale faulting in the South-Central Pyrenees. Geol. Ultraiectina 43, 210 pp

Speksnijder, A., 1987a. The detection and significance of early deformation in the southern Variscan Pyrenees, Spain; implications for regional Paleozoic structural evolution. Geol. Rndsch. 76, 451-476

Speksnijder, A., 1987b. The structural development of the Orri Dome, southernVariscan Pyrenees, Spain. Eclogae geol. Helv. 80, 697-733

Spence, J.C.H., 1981. Experimental high-resolution electron microscopy. Monographs on the physics and chemistry of materials. Clarendon Press, Oxford, 370 pp.

Spinnler, G.E., Self, P.G., Iijima, S., and Buseck, P.R., 1984. Stacking disorder in clinochlore chlorite. Am. Mineral., 69: 256-263.

Starkey, J., 1968. The geometry of kink bands in crystals - a simple model. Contrib. Mineral. Petrol., 19: 133-141.

Stenn, K., and Bahr, G.F., 1970. Specimen damage caused by the beam of the transmission electron microscope, a correlative reconsideration. J. Ultrastruct. Res. 31: 526-550.

Takeuchi, S., and Argon, A.S., 1976. Steady-state creep of single phase crystalline matter at high temperatures. J. Mater. Sci. 11: 1542-1566

Teichmüller M., and Teichmüller R., 1981. The significance of coalification studies to geology - a review. Bull. Centre Rech. Explor.-Prod. Elf-Aquitaine 5, 491-534

Teichmüller M., Teichmüller R., and Weber, K., 1979. Inkohlung und Illit Kristallinität, vergleichende Untersuchungen im Mesozoikum und Paläozoikum von Westfalen. Fortschr. Geol. Rheinlnd. u. Westf. 27, 201-276

Tullis, T.E., and Wood, D.S, 1972. The relationship between preferred orientation and finite strain for three slates. Geol. Soc. Am. Abstr. and Progr. 4, 694

Tullis, T.E., and Wood, D.S., 1975. Correlation of finite strain from both reduction bodies and preferred orientation of mica in slate from Wales. Geol. Soc. Am. Bull. 86, 632-638

Turner, H.J., 1948. Mineralogical and structural evolution of the metamorphic rocks. Geol. Soc. Am. Mem. 30, 1-342

Urai, J.L., Means, W.D., and Lister, G.S., 1986. Dynamic recrystallisation of minerals. In:B.E. Hobbs and H.C. Heard (Editors): Mineral and Rock Deformation: Laboratory Studies. The Paterson Volume. Geophysical Monograph 36, p. 161-199.

Van den Eeckhout, B., 1986. A case study of a mantled gneiss antiform, the Hospitalet Massif, Pyrenees (Andorra, France). Geol. Ultraiectina 45, 193 pp.

Van der Pluijm, B.A., and Kaars Sijpesteijn, C.H., 1984. Chlorite-mica aggregates: morphology, development and bearing on cleavage formation in very low-grade rocks. J. Struct. Geol. 6, 399-407

Van der Pluijm, B.A., Lee, J.H., and Peacor, D.R., 1988. Diffusion of K and other elements during analytical electron microscopy. In prep.

Van Dyck, D., and Coene, W., 1984. The Real Space method for dynamical electron diffraction calculations in high resolution electron microscopy. I. Principles of the method. Ultramicroscopy 15, 29-40

Van Dyck, D., Van Tendeloo G., and Amelinckx, S. 1982. Direct interpretation of high resolution electron images of substitutional alloy systems with a column structure. Ultramicroscopy, 10, 263-280

Verhoef, P.N.W., Vissers, R.L.M., and Zwart, H.J., 1984. A new interpretation of the structural and metamorphic history of the western Aston Massif (Central Pyrenees, France). Geol. Mijnb. 63, 399-410

Voll, G., 1960. New work on petrofabrics. Lpool. Mnchr. geol. J. 2, 503-567

Waldron, H.M., and Sandiford, M., 1988. Deformation volume and cleavage development in meta-sedimentary rocks from the Ballarat slate belt. J. Struct. Geol. 10, 53-62.

Weaver, C.E., 1960. Possible uses of clay minerals in search for oil. Clays Clay Min. 8, 214-227

Weaver, C.E., 1984. Shale-slate metamorphism in southern Appalachians. Developm. Petrol. 10, 239 pp.

Weber, K., 1972a. Notes on the determination of illite crystallinity. N. Jb. Min. Mh. 6, 267-276

Weber, K., 1972b. Kristallinität des Illits in Tonschiefern und andere Kriterien schwacher Metamorphose in nordöstlichen Rheinischen Schiefergebirge. N. Jb. Geol. Paläont. Abh., 141: 333-363

Weber, K., 1976. Gefügeuntersuchungen am transversalgeschieferten Gesteine aus dem östlichem Rheinischem Schiefergebirge (Ein Beitrag zu Genese der transversale Schieferung). Geol. Jb. ser. D, 15, 3-98

Weber, K., 1981. Kinematic and metamorphic aspects of cleavage formation in very low-grade metamorphic slates. Tectonophysics 78, 291-306

White, J.C., and White, S.H., 1981. On the structure of grain boundaries in tectonites. Tectonophysics 78, 613-628.

White, S.H., 1971. Natural creep deformation of quartzites. Nature Phys. Sci. 234: 175-177

White, S.H., 1976. The effect of strain on the microstructures, fabrics and deformation mechanisms in quartzites. Phil. Trans. R. Soc. London A283, 69-86

White, S.H., Huggett, J.M., and Shaw, H.F., 1985. Electron-optical studies of phyllosilicate intergrowths in sedimentary and metamorphic rocks. Mineral. Mag. 49, 413-423

White, S.H., and Johnston, D.C., 1981. A microstructural and microchemical study of cleavage lamellae in a slate. J. Struct. Geol. 3, 279-290

White, S.H., and Knipe, R.J., 1978. Microstructure and cleavage development in selected slates. Contrib. Mineral. Petrol. 66, 165-174

Williams, P.F., 1972. Development of metamorphic layering and cleavage in low grade metamorphic rocks at Bermagui, Australia. Am. J. Sci. 272, 1-47

Williams, P.F., 1977. Foliation: a review and discussion. Tectonophysics 39, 305-328

Williams, P.F., Collins, A.R., and Wiltshire, R.G., 1969. Cleavage and penecontemporaneous deformation structures in sedimentary rocks. J. Geol. 77, 415-425

Wilson, C.J.L., and Bell, I.A., 1979. Deformation of biotite and muscovite: optical microstructure. Tectonophysics, 58: 179-200.

Winkler, H.G.F., 1979. Petrogenesis of metamorphic rocks. 5th ed. Springer, New York, 348 pp.

Wirth, R., 1986. High-angle grain boundaries in sheet silicates (biotite/chlorite): a TEM-study. J. Mater. Sci. Lett. 5, 105-106.

Wood, D.S., 1974. Current views of the development of slaty cleavage. Ann. rev. Earth. Planet. Sci. 2, 369-401

Woodland, B.G., 1982. Gradational development of domainal slaty cleavage, its origin and relation to chlorite porphyroblasts in the Martinsburg Formation. Tectonophysics 82, 89-124

Woodland, B.G., 1985. Relationship of concretions and chlorite-muscovite porphyroblasts to the development of domainal cleavage in low-grade metamorphic deformed rocks from north-central Wales, Great Britain. J. Struct. Geol. 7, 205-215.

Wunderlich, H.G., 1959. Erzeugung engständiger Scherflächen in plastischem Material. N. Jb. Geol. Paläont. Abh. 1, 34-44

Yund, R.A., Smith, B.M., and Tullis, J., 1983. Dislocation-assisted diffusion of oxygen in albite. Phys. Chem. Minerals, 7: 185-189.

Zwart, H.J., 1959. On the occurrence of chloritoid in the Pyrenees. Geol. Mijnb. 21, 119-122

Zwart, H.J., 1962. On the determination of polymetamorphic mineral associations, and its application to the Bosost area (Central Pyrenees). Geol. Rndsch. 52, 38-65

Zwart, H.J., 1965. Geological map of the Paleozoic of the Central Pyrenees, sheet 6, Aston, France, Andorra, Spain, 1:50,000. Leidse Geol. Meded. 33, 191-254

Zwart, H.J., 1979. The geology of the Central Pyrenees. Leidse Geol. Meded. 50, 1-74

Zwart, H.J., 1981. Three profiles through the Central Pyrenees. Geol. Mijnb. 60, 97-104

Zwart, H.J., 1986. Structural Geology of the Central Pyrenees. Tectonophysics 129, 9-27

Zwart, H.J., and Bons, A.J., 1987. The structure of grain boundaries in slates. EOS, Transactions, Am. Geophys. Union, 68, 1454.

CURRICULUM VITAE

Anton-Jan Bons werd geboren op 8 juli 1959 in De Lemmer, Friesland. Van zijn tweede tot zijn twaalfde jaar woonde hij in Indonesië, waar zijn belangstelling voor de geologie gewekt werd. Hij behaalde in 1977 het diploma Gymnasium B aan het Chr. Lyceum Dr. W.A. Visser 't Hooft in Leiden en ging in hetzelfde jaar geologie studeren aan de Rijksuniversiteit te Leiden en later aan de Rijksuniversiteit te Utrecht. Het kandidaatsexamen G3 werd afgelegd in 1980. In 1984 studeerde hij af in de structurele en toegepaste geologie, met het bijvak exploratiegeofysica. Tijdens de doctoraalstudie vervulde hij verschillende student-assistentschappen bij de vakgroep Structurele en Toegepaste Geologie. Van 1984 tot 1988 was hij als wetenschappelijk assistent verbonden aan diezelfde vakgroep; in die tijd werd het onderzoek voor dit proefschrift gedaan. Momenteel is hij verbonden aan de Technische Universiteit te Delft, bij de vakgroep Fysische en Chemische Materiaalkunde, waar hij electrononenmicroscopisch onderzoek doet aan halfgeleidermaterialen.